QUANTIFYING ZONAL PATTERNS OF CLIMATE FEEDBACKS AND THEIR ROLE IN POLAR AMPLIFICATION

Julia Anne Crook

Submitted in accordance with the requirements for the degree of
Doctor of Philosophy

The University of Leeds
School of Earth and Environment

October, 2011

Intellectual Property and Publication Statements

The candidate confirms that the work submitted is her own, except where work which has formed part of jointly-authored publications has been included. The contribution of the candidate and the other authors to this work has been explicitly indicated below. The candidate confirms that appropriate credit has been given within the thesis where reference has been made to the work of others.

Publications

Chapter 3 is based on the work published in J.A. Crook, P.M. Forster and N. Stuber (2011), Spatial Patterns of Modeled Climate Feedback and Contributions to Temperature Response and Polar Amplification, *J. Climate*, *24*, 3575-3592. N. Stuber provided climate model data for HadSM3 simulations under different forcings which she had run, P.M. Forster provided advice on the work as the candidate's supervisor, and the candidate performed all the analysis and wrote the paper.

Chapter 4 is based on the work published in J.A. Crook and P.M. Forster, (2011), A balance between radiative forcing and climate feedback in the modeled 20th century temperature response, *J. Geophys. Res*., *116*, D17108. P.M. Forster provided advice on the work as the candidate's supervisor and the candidate performed all the analysis and wrote the paper.

Acknowledgements

I wish to thank my supervisor Piers Forster for his invaluable advice and encouragement throughout this project. I would also like to thank Nicola Stuber and Gaby Rädel (Department of Meteorology, University of Reading, UK) for providing the data for the HadSM3 experiments used in Chapter 3, and Lawrence Jackson (University of Leeds, UK) for advice on regression statistics. I thank Nathan Gillett (Canadian Centre for Climate Modelling and Analysis, Victoria, BC) and Daithi Stone (Climate Systems Analysis Group, University of Cape Town, SA) for their invaluable advice on the use of the attribution/detection code and interpretation of its output (Chapter 4), and the authors of the attribution code Myles Allen (Climate Dynamics Group, University of Oxford, UK) and Daithi Stone for allowing me to use the code. I thank Mark Flanner (Department of Atmospheric, Oceanic and Space Sciences, University of Michigan, USA) for his re-gridded MODIS albedo data used in Chapter 5. I also thank several anonymous reviewers for their helpful comments in the production of published papers resulting from the work described in Chapters 3 and 4. Finally I thank my husband, Rolf, for support throughout and suggestions for improvements to some of the text.

I acknowledge the modelling groups, the Program for Climate Model Diagnosis and Intercomparison (PCMDI) and the WCRP's Working Group on Coupled Modelling (WGCM) for their roles in making available the WCRP CMIP3 multi-model dataset. Support of this dataset is provided by the Office of Science, U.S. Department of Energy. I also acknowledge the following centres for provision of their data sets: CRU, University of East Anglia for the HadCRUT3 dataset, the European Centre for Medium-Range Weather Forecasts (ECMWF) for the ERA-40 and Interim temperature reanalyses which have been obtained from the ECMWF Data Server, the International Satellite Cloud Climatology Program for the ISCCP albedo data held by NASA Goddard Institute for Space Studies, NASA for the MODIS albedo data products, and the Space Science and Engineering Centre, University of Wisconsin for the use of the APP-x albedo data.

This work was funded by NERC grant NE/E016189/1, “An Observationally-Based Quantification of Climate Feedbacks”.

Abstract

The significant climate warming seen over the 20th century has been largely attributed to anthropogenic emissions of greenhouse gases. Spatial patterns of likely future warming are dependent on patterns of climate feedback, but current understanding of climate feedbacks is largely at the global mean or hemispheric scale. The aim of this project is to improve understanding of zonal mean climate feedbacks and their contribution to polar amplification using observations and models.

Zonal mean climate feedbacks and contributions to the equilibrium temperature response were determined for eight slab ocean GCMs forced by doubling CO_2 and for a single model under different forcing mechanisms. Relative contributions to polar amplification and the greatest inter-model differences in zonal mean feedbacks and temperature response contributions are presented.

Contributions to the temperature response of AOGCM simulations of the 20th century due to radiative forcing, climate feedback and heat storage/transport were analyzed to understand how well climate models reproduce the observed 20th century temperature record. They generally perform well despite large differences in feedback strength through compensating differences in forcing and heat storage/transport, but projected future warming trends are much more dependent on a model's feedback strength. The poor representation of tropical 20th century warming and Arctic amplification in some models are attributed to unrealistic forcing or feedback patterns. Over the whole of the 20th century, the feedback strength is likely to be underestimated by the multi-model mean.

Zonal patterns of surface albedo feedback were determined from AOGCMs and satellite observations in the seasonal cycle and long term climate change contexts. Observations show large changes in long term albedo feedback in regions outside the cryosphere, unlike models. Land use change or vegetation feedbacks and difficulties of measuring albedo under different cloud conditions may be to blame. The observed annual mean NH mid to high latitude feedback is greater than that for models. Models and observations agree in some regions in their seasonal cycle feedback but different satellite data sets show some significant differences.

Table of Contents

Table of Tables

Table of Figures

Glossary

APP-x	Extended Advanced Very High Resolution Radiometer Polar Pathfinder [*Wang and Key*, 2005a; 2005b]
AOGCM	Coupled atmosphere-ocean GCM
CMIP3	World Climate Research Program Climate Model Intercomparison Project phase 3 [*Meehl et al.*, 2007b]
CO_2	Carbon dioxide
ERA40	European Centre for Medium-Range Weather Forecasts (ECMWF) 40 year reanalysis data set [*Uppala et al*., 2005]
ERA Interim	ECMWF interim reanalysis data set [*Dee et al*., 2011]
ERBE	Earth Radiation Budget Experiment
GCM	General circulation model
HadCRUT3	Hadley Centre and University of East Anglia, Climate Research Unit surface temperature data sets: anomaly time series from 1850 [*Brohan et al*., 2006], absolute climatology [*Jones et al.*, 1999]
IPCC AR4	Intergovernmental Panel on Climate Change 4th Assessment Report (2007)
ISCCP	International Satellite Cloud Climatology Program [*Schiffer and Rossow*, 1983]
MODIS	Moderate Resolution Imaging Spectroradiometer
NH	Northern Hemisphere
SH	Southern Hemisphere
SRES	IPCC Special Report on Emissions Scenarios [*Nakicenovic and Swart*, 2000]
TOA	Top of atmosphere

1 Introduction

1.1 Context

There is now a very high level of certainty that man has had an influence on the Earth's climate in the last 150 years through the release of greenhouse gases and aerosols, through changes in both stratospheric and tropospheric ozone concentration, and through changing land use [*Hegerl et al.,* 2007]. Observations over the 20th century show two distinct periods of warming, up to 1940 and from the mid 1960's onwards, with a cooling period between. The global mean linear warming trend from 1906-2005 was 0.74±0.18 ºC, but the rate of warming over the last 50 years has been almost double that over the last 100 years. Since the mid-1970s, warming has been greater over land than ocean and greater in the Northern Hemisphere (NH) than the Southern Hemisphere (SH) [*Hegerl et al*., 2007], with particularly strong warming in the Arctic (see Section 1.3) leading to concerns that the Greenland ice sheet might collapse in future causing large sea level rises.

Understanding the response of the climate system to both anthropogenic and natural (solar radiation and volcanic eruptions) forcing mechanisms is an active area of research. The climate responds directly to the forcing mechanism, but also processes in the system can either amplify or dampen this response. These processes are referred to as climate feedbacks and include changes in water vapour and lapse rate, changes in ice and snow extent and thickness, and changes in cloud amount and properties.

Complex three-dimensional general circulation climate models (GCMs) are extensively used to make projections of temperature change due to various forcing mechanisms and to understand 20th century warming. Confidence in climate models is gained by the fact that they are based on fundamental physical laws, including the equations of conservation of energy, momentum and mass. They are assessed by their ability to reproduce current climatology and climate variability, and by comparing their feedback parameters with estimates from observations [*Randall et al*., 2007]. These models are also assessed by their ability to reproduce past climates (ancient and modern) and are used to investigate how much influence humans have had over the 20th century climate.

Numerous studies, using the optimal fingerprinting technique (see Appendix 1) and Bayesian methods, have shown that 20th century temperature changes can only be explained by both natural and anthropogenic forcing, but that the anthropogenic forcing has dominated in recent decades [*Hegerl et al*., 2007; *Stone et al*., 2009; *Min and Hense*, 2006]. These studies are based on global means (Figure 1.1) as well as distinct spatio-temporal patterns in warming; for example, the temporal pattern of the NH meridional temperature gradient has been used to constrain the relative impacts of greenhouse gas and aerosol forcing [*Stott et al*., 2006]. Although attribution of the last 50 years of warming to anthropogenic forcing is robust, the cause of the early 20th century warming remains uncertain, with the relative importance of solar forcing, volcanic forcing, greenhouse gases and internal variability being different for different models [*Stott et al*., 2000; *Hegerl et al*., 2003; *Meehl et al*., 2004; *Nozawa et al*., 2005; *Delworth and Knutson*, 2000; *Knutson et al.*, 2006; *Wang et al*., 2007].

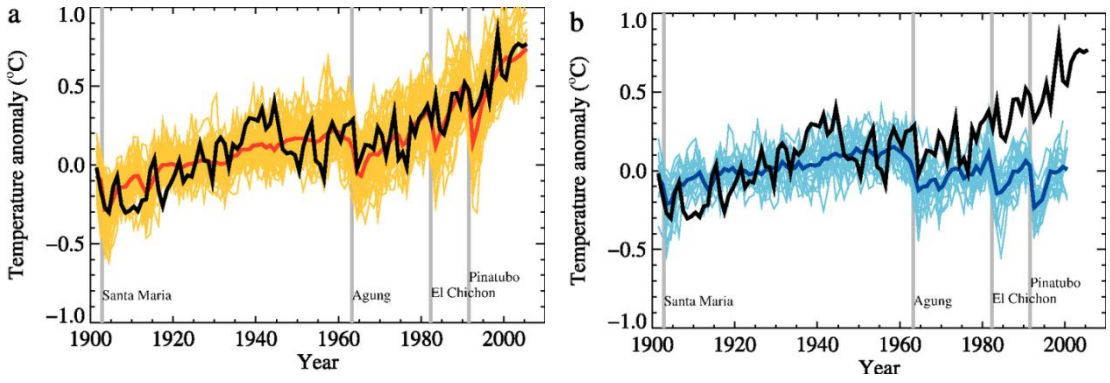

Figure 1.1: Comparison between global mean surface temperature anomalies (°C) from observations (black) and AOGCM simulations forced with (a) both anthropogenic and natural forcings and (b) natural forcings only. The multi-model ensemble mean is shown as a thick coloured curve and individual simulations are shown as thin coloured curves. From Hegerl et al. [2007].

Although different climate models reproduce 20th century warming quite well, they give a wide range of annual global mean equilibrium surface temperature responses due to a doubling of CO_2 (equilibrium climate sensitivity): 2 to 4.5 °C (with a best estimate of 3 °C). This range has little changed from the previous IPCC report to the latest [*Meehl et al*., 2007a] despite model improvements, and principally arises from the different strengths of the feedback mechanisms between models. Attempts have been made to constrain the estimated range of equilibrium

climate sensitivity using observations. The probability distribution functions (PDFs) of equilibrium climate sensitivity as determined by a number of such studies (Figure 1.2) indicate that the upper end of equilibrium climate sensitivity is still particularly poorly constrained.

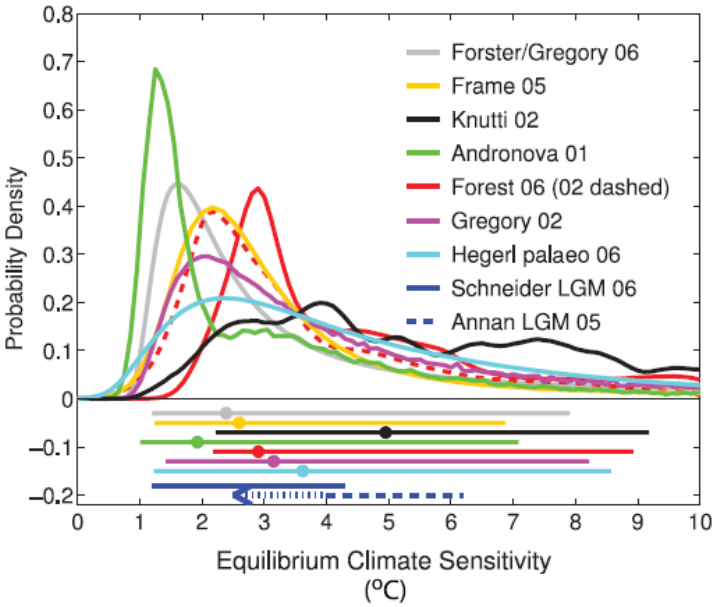

Figure 1.2: Different estimates of the PDF for climate sensitivity (°C) for a doubling of CO_2. All PDFs are scaled to integrate to unity between 0 °C and 10 °C. The bars show the respective 5 to 95% ranges, and the dots show the median estimate. Also shown are the 5 to 95% approximate ranges for two estimates from the Last Glacial Maximum. From Hegerl et al. [2007] which gives references and details.

Inter-model differences in climate sensitivity also result in considerable differences in projected warming over the next century. A good understanding of the roles of forcing and feedback in contemporary climate change is, therefore, of great importance for policy makers who are committed to stabilising greenhouse gas emissions to a level that would prevent dangerous anthropogenic climate change. The definition of dangerous climate change is subjective but it has been suggested that it would be around 2 ˚C of warming at which point certain tipping points (e.g. ice sheet collapse which leads to large sea level rise) would be reached making climate change irreversible and costly to biodiversity and humans [*Mann*, 2009]. Although the level of dangerous climate change is expressed as a global mean temperature change, it clearly depends on the extent of warming in high latitudes where ice sheets are susceptible to collapse. Therefore, it is important to understand

the pattern of future warming which will be dependent on the pattern of climate feedbacks and future radiative forcing. The overall aim of this project is to gain a better understanding of climate feedbacks in terms of their zonal patterns through the use of observations and models. The detailed aims of this project are given at the end of Chapter 2, after the presentation of the current literature on the subject to which I now turn.

1.2 The energy budget and the relationship between radiative forcing and climate feedback

The Earth maintains its temperature through a balance of incoming shortwave radiation from the Sun and outgoing longwave radiation from its surface and atmosphere. Greenhouse gases and clouds in the atmosphere trap some of the outgoing longwave radiation making the Earth's surface temperature around 30 K higher than it would be without the atmosphere. Figure 1.3 shows schematically the Earth's annual global mean energy budget.

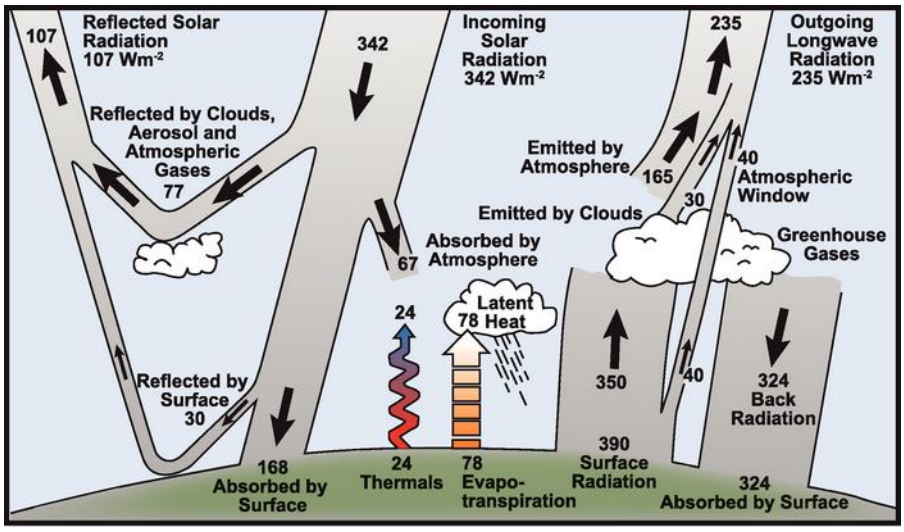

Figure 1.3: Earth's annual global mean energy budget. From Le Treut et al., [2007].

Changes in the concentration of atmospheric constituents (greenhouse gases, aerosols and ozone), and changes in solar radiation cause perturbations in the energy budget known as radiative forcings. A radiative forcing causes changes in temperature throughout the atmosphere. These temperature changes result in changes in black body emission, changes in surface albedo through melting of snow and sea

ice, changes in water vapour content of the atmosphere, changes in cloud amount and properties, and changes in the lapse rate. These cause further changes in the radiative flux and, therefore, temperature, and are known as radiative feedbacks. Other types of climate feedback include vegetation responses to temperature and carbon dioxide (CO_2) changes, release of methane from permafrost melt, the ability of the ocean to store carbon, and the disintegration of ice sheets [*Jansen et al.*, 2007]. These complex feedbacks become more important when considering climate change over geological timescales, such as comparing the Last Glacial Maximum (LGM) or the Mid-Holocene with today, and are not generally included in GCMs when studying contemporary climate change. It is only the radiative feedbacks which are the subject of this thesis. How these individual radiative feedbacks are analysed and how the feedback strengths compare in models and observations are discussed in detail in Chapter 2.

Radiative forcing is defined by the IPCC AR4 [*Forster et al.*, 2007] and earlier assessment reports as the change in net (down minus up) radiative flux (shortwave + longwave) at the tropopause after allowing for stratospheric adjustment to radiative equilibrium but with the surface and tropospheric states held fixed. The concept of radiative forcing arose from early studies of climate response to insolation and CO_2 changes using simple radiative-convective models [*Forster et al.*, 2007]. These studies have shown that the global mean equilibrium surface temperature response is approximately proportional to the global mean radiative forcing,

$$\overline{\Delta T_{s,eq}} = \lambda \bar{F} \qquad 1.1$$

where λ is the climate sensitivity parameter and overbar indicates a global mean. Unlike the temperature response, radiative forcing does not include the climate feedbacks which show considerable spread in models and are not well understood [*Forster et al.*, 2007]. Differences in radiative forcing are found even when the models are supposedly forced in the same way. However, the differences in feedbacks between models contribute about three times more to the range of climate sensitivity than differences in radiative forcing. Therefore, radiative forcing has been used as a simple measure for quantifying and ranking different forcing mechanisms to first order.

1.2.1 Alternative definitions of radiative forcing

A number of studies have attempted to ascertain how well the linear relationship between global mean surface temperature and the stratospherically adjusted radiative forcing holds for a variety of forcing mechanisms and for varying amounts of forcing. Although early studies [*Ramaswamy et al.*, 2001] suggested the climate sensitivity parameter for different CO_2 and solar forcings varies by less than 25%, more recent studies have shown that the climate sensitivity parameter varies considerably for other forcing mechanisms, particularly when the forcing pattern is geographically inhomogeneous, such as changes in ozone and absorbing aerosol [*Hansen et al.*, 1997; *Forster et al.*, 2000; *Joshi et al.*, 2003; *Shine et al.*, 2003; *Forster et al.*, 2007]. Aerosol forcing includes the direct effect of scattering and absorption of shortwave radiation and the indirect effect of altering cloud properties such as cloud droplet number concentration (CDNC), droplet size and cloud lifetime (Figure 1.4).

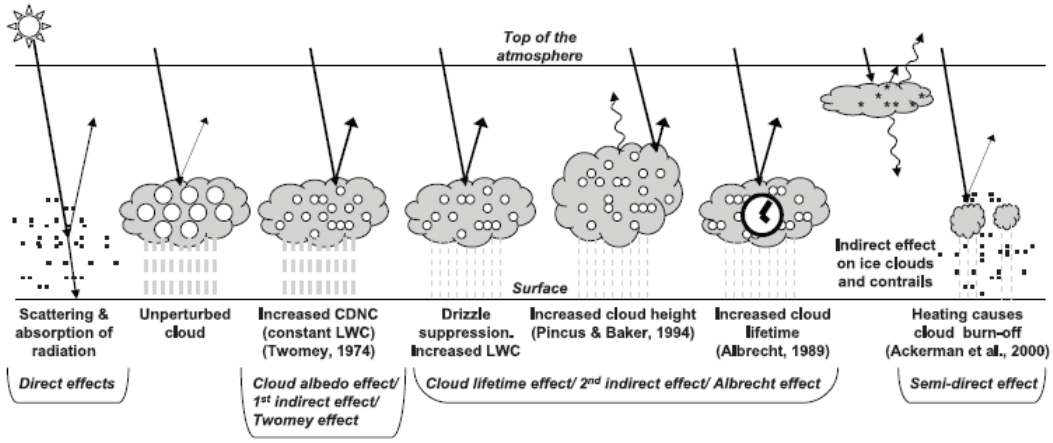

Figure 1.4: Aerosol direct and indirect effects. From Forster et al. [2007] which gives the references.

Absorption of radiation by absorbing aerosols leads to local heating, altering the vertical temperature, humidity and cloud profiles. These relatively rapid adjustments to the troposphere cause top of atmosphere (TOA) radiative flux adjustments before the surface temperature changes, which, therefore, may be considered part of the forcing rather than the feedback. This results in the stratospherically adjusted forcing

being unable to predict even the sign of the temperature change for some cases of partially absorbing aerosol [*Shine et al*., 2003].

Alternative definitions of radiative forcing have been used to find a better prediction of response (Figure 1.5). The stratospherically adjusted radiative forcing (Figure 1.5b) gives a better indication of response than the instantaneous radiative forcing (Figure 1.5a) particularly for stratospheric ozone forcing, and this became the IPCC standard. However, the zero-surface-temperature-change radiative forcing (Figure 1.5c and d), where all but the surface temperature is allowed to respond, gives an even better indication of response for absorbing aerosols, depending on precisely how it is calculated [*Shine et al*., 2003; *Hansen et al*., 2005].

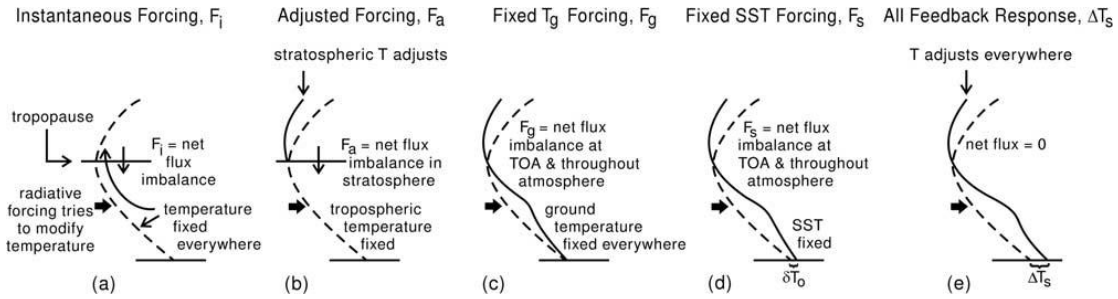

Figure 1.5: Alternative definitions of radiative forcing. From Hansen et al. [2005].

It is reasonable to allow fast feedback processes to operate as these are felt as forcings at the surface in long term climate change. Instantaneous and stratospherically adjusted radiative forcings can be calculated in offline radiation code, whereas those that allow some tropospheric response require GCM simulations. The troposphere-adjusted forcing can be calculated from fixed sea-surface temperature integrations [*Hansen et al*., 2005], fixed sea- and land- surface temperature integrations [*Shine et al*., 2003] or a regression method [*Gregory et al*., 2004]. Rapid tropospheric adjustments have also been found in CO_2 forcing [*Gregory and Webb*, 2008; *Andrews and Forster*, 2008], but these are much smaller than those seen for absorbing aerosols.

1.2.2 Transient climate change

To estimate the climate sensitivity parameter using equation 1.1 requires climate change experiments to be run to equilibrium. It is possible to run models with mixed-layer oceans to equilibrium, but very computationally costly to do so for full coupled atmosphere-ocean models (AOGCMs) because mixed-layer ocean models reach equilibrium within a few decades whereas full ocean models take thousands of years only to reach quasi-equilibrium. Therefore, estimating the climate sensitivity from transient experiments is advantageous. It is assumed in the transient case that the expected equilibrium temperature can be estimated because the climate sensitivity parameter does not change with time.

The vertically integrated energy budget at any time *t* and location *x* is given by:

$$\frac{d\Delta H}{dt}(x,t) = \Delta A(x,t) + \Delta R(x,t) \approx \Delta A(x,t) + F(x,t) + Y(x)\Delta T_s(x,t) \qquad 1.2$$

where $\frac{d\Delta H}{dt}$ is the rate of change of energy content of the column , i.e. heat storage, ΔA is the change in horizontal heat convergence, and ΔR is the change in TOA net downward radiative flux. ΔR is approximated as a forcing term, F, which may or may not vary with time, and a feedback term which in turn is approximated as a linear function of the surface temperature response, ΔT_s, with the proportionality constant being the "signed" climate feedback parameter, Y. The signed feedback parameter is a convention meaning feedbacks that amplify the temperature change are positive and those that dampen it are negative. Overall the global mean signed feedback is negative, allowing the radiative response to oppose the forcing and a new equilibrium to be reached. At time t=0, there is no temperature change and ΔR equals the initial radiative forcing. At equilibrium, sometime after the forcing has stopped changing, the heat storage term is zero, ΔA is equal to $-\Delta R$, and equation 1.2 becomes

$$-Y(x)\Delta T_{s,eq}(x) = -\Delta R_{eq}(x) + F_{eq}(x) \qquad 1.3$$

In the global mean, there is no transport of heat, and equations 1.2 and 1.3 respectively become

$$\overline{\frac{d\Delta H}{dt}}(t) = \overline{\Delta R}(t) \approx \bar{F}(t) + Y\overline{\Delta T_s}(t) \qquad 1.4$$

and

$$-Y\overline{\Delta T_{s,eq}} = \overline{F_{eq}} \qquad 1.5$$

The global mean feedback parameter, Y, which is the global mean of the temperature weighted local feedback parameter, $Y(x)$, is inversely proportional to the climate sensitivity parameter

$$-\frac{\overline{Y(x)\Delta T_{s,eq}(x)}}{\overline{\Delta T_{s,eq}}} = -Y = \frac{1}{\lambda} \qquad 1.6$$

such that equation 1.5 is the same as equation 1.1.

The climate sensitivity parameter may be estimated from transient experiments using equation 1.4 by regressing $\overline{\Delta R}(t) - \bar{F}(t)$ against $\Delta T_s(t)$. If the forcing is not changing with time, regressing $\overline{\Delta R}(t)$ against $\Delta T_s(t)$ gives an intercept on the ΔR axis of the troposphere-adjusted forcing [*Gregory et al*., 2004; *Hansen et al*., 2005; *Forster and Taylor*, 2006; *Gregory and Webb*, 2008; *Andrews and Forster*, 2008]. Changes in radiative flux due to internal mechanisms and not related to surface temperature changes are seen in the scatter of the regression plots.

Using conventional radiative forcings, the climate sensitivity during a transient run where CO_2 is increased at 1% per year to the 70th year ($2\times CO_2$) and then held constant may increase or decrease with time depending on the model [*Senior and Mitchell*, 2000; *Boer and Yu*, 2003a]. However, if the troposphere-adjusted forcing is used, the climate sensitivity shows little time/state dependence [*Williams et al*., 2008]. For mixed-layer ocean models the tropospheric adjustments take place within the first few years whereas for AOGCMs the adjustment takes a few decades. Unfortunately this means there is no clear timescale to separate forcing and feedback.

1.3 Polar amplification

IPCC AR4 climate models show greater warming at high latitudes than low latitudes when forced with increased greenhouse gases. However, the extent of this polar amplification varies considerably between models with the range of simulated Arctic warming being 1.5 to 4.5 times the global mean warming (Figure 1.6) [*Holland and Bitz*, 2003].

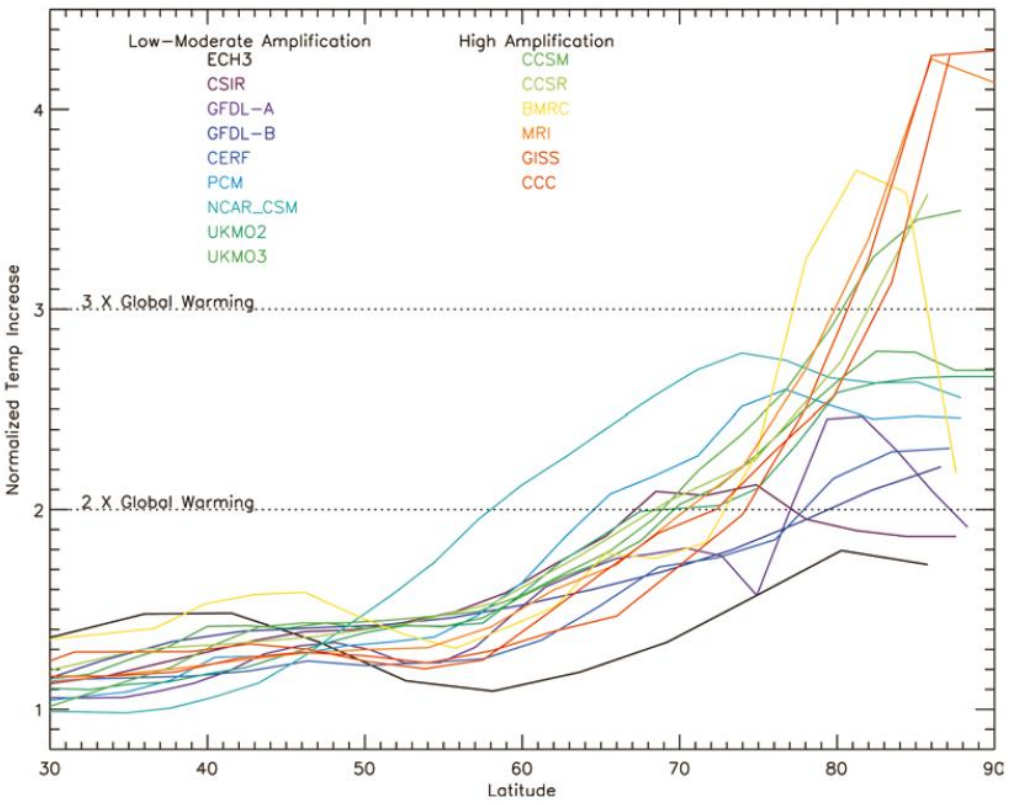

Figure 1.6: Annual zonal mean 2m air temperature response for 2×CO_2 normalized by the global mean response. From Holland and Bitz [2003].

The polar amplification is least in the summer in all models but the month of maximum warming varies from October to March. It has been projected that September Arctic sea ice will disappear completely by 2100 [*Boé et al.*, 2009] with implications for Arctic ecosystems and human activity in the region. The likely future extent of high latitude warming is also important in determining when the Greenland and Antarctic ice sheets might melt, causing large sea level rises, and therefore affects the definition of dangerous climate change.

Snow and ice radiative feedbacks have been widely accepted to play a major role in polar amplification. However, suppression of surface albedo feedback in models still leaves considerable polar amplification [*Forster et al.*, 2000; *Hall*, 2004], although ice insulation feedback is still active in these cases. When sea ice thins, more heat can be transferred from the ocean to the atmosphere and this can have a strong seasonal impact. Other studies suggest feedbacks due to atmospheric dynamics and heat transport, water vapour, lapse rate and clouds also contribute to

polar amplification [*Holland and Bitz*, 2003; *Vavrus*, 2004; *Alexeev et al*., 2005; *Cai*, 2006; *Winton*, 2006a; *Cai and Lu*, 2007, *Lu and Cai*, 2009a], although the relative importance of these contributions is not well understood. Significant correlation of polar amplification with the control climate sea ice thickness and ocean heat transport has been found, as has a significant correlation between the control climate sea ice extent and the latitude of maximum warming [*Holland and Bitz*, 2003].

Both box models [*Cai*, 2006] and GCMs [*Alexeev et al*., 2005] show that initial warming from a uniform forcing increases the poleward heat transport and warms the high latitude atmosphere leading to an enhanced surface warming. This high latitude warming will then weaken the poleward heat transport to some extent. When moist processes are included, the high latitude atmospheric specific humidity increases leading to an enhanced surface warming due to the local water vapour feedback. Poleward heat transport is also enhanced through latent heating of the upper atmosphere and cooling of the surface due to evaporation at low latitudes [*Cai and Lu*, 2007]. The extent of the polar amplification depends on the relative strengths of the control climate poleward heat transport, the hydrological cycle and the local water vapour and ice-albedo feedbacks. Increasing poleward heat transport is indicated by decreasing (increasing) net downward radiation at high (low) latitudes. This is seen in reanalysis data and in IPCC AR4 climate models $2\times CO_2$ experiments. Therefore both observations and GCMs support this "dynamical amplifier" theory [*Cai*, 2006].

Observations suggest that the Arctic has warmed at twice the rate of the global mean over the last 100 years [*Trenberth et al*., 2007]. Arctic sea ice extent at the end of the summer melt season in September has declined at a rate of -7.8 % decade^{-1} from 1953–2006 [*Stroeve et al*., 2007] with the rate increasing since 1979. Record low Arctic sea ice extent was recorded in September 2007 [*Comiso et al*., 2008], but the current summer 2011 sea ice extent is also well below the 1979-2000 average [*National Snow and Ice Data Centre*, 2011]. The link between observed Arctic warming and atmospheric circulation has been investigated using indices such as the Arctic Oscillation index [*Thomson and Wallace*, 1998]. High phases of these indices in the winter are associated with higher Arctic temperatures. Although these indices were in high phases from the 1970s to mid 1990s they have since become more neutral whereas Arctic warming has shown a persistent positive trend throughout.

Clear maxima found well above the surface in the recent Arctic winter and summer warming from the ERA40 reanalysis, are not consistent with surface albedo feedbacks being the main cause of polar amplification, but are consistent with the calculated increase in atmospheric northward energy transport [*Graversen et al*., 2008]. However, this vertical structure is strongly dependent on the reanalysis set used and therefore these conclusions have been contested [*Screen and Simmonds*, 2010]. It has also been suggested that the increase in black carbon deposited on snow reducing albedo [*Hansen and Nazarenko*, 2004; *Hansen et al*., 2007; *Flanner et al*., 2007] and the forcing caused by increasing black carbon (absorbing) aerosol [*Shindell and Faluvegi*, 2009] have contributed to Arctic warming.

Although observations in the Antarctic are particularly sparse over the whole of the 20th century, temperature trends have shown a small although insignificant warming over the 1958-2002 period [*Chapman and Walsh*, 2007]. Some central parts of the continent have seen a small insignificant cooling. However the Antarctic Peninsula and large parts of the Southern Ocean have seen significant warming, with the Antarctic Peninsula showing a significant warming trend of 0.3 °C decade^{-1}. This warming is much less than in the Arctic, partly due to the greater fraction of ocean (which has a higher heat capacity than land) in the SH. Over the last 30 years there has been a trend towards a high index Southern Annular Mode (SAM) which gives rise to a poleward shift and strengthening of the westerlies, resulting in warming at mid-latitudes and cooling in the polar-cap region, particularly aloft [*Thompson and Solomon*, 2002]. Modelling studies have suggested the SAM and Antarctic temperature trends can be attributed to a combination of greenhouse gas increases and Antarctic stratospheric ozone decreases [*Gillett and Thompson*, 2003; *Arblaster and Meehl*, 2006; *Cai and Cowan*, 2007]. With stratospheric ozone depletion expected to recover over the coming century, the SAM is expected to weaken and substantial warming (2 ˚C to 3 ˚C) could be seen throughout Antarctica [*Shindell and Schmidt*, 2004].

1.4 Outline of the thesis

This chapter has placed this thesis in the context of contemporary climate change and highlighted the need to reduce uncertainties in climate feedbacks to make better projections of future climate change required for good policy decisions. It has

introduced the concepts of climate feedbacks and radiative forcing, equilibrium and transient climate change, and has pointed out the distinct latitudinal patterns of warming seen over the 20th century and predicted by climate models.

Chapter 2 describes the individual radiative feedbacks, how these feedbacks are analysed and how the feedback strengths compare in models and observations. This thesis does not cover the complex feedbacks involved with carbon cycle changes (e.g. vegetation, permafrost melting) or the collapse of ice sheets.

Chapters 3-5 present the work I have done for my PhD: Chapter 3 presents my comparison of zonal patterns of modelled climate feedbacks and their contributions to the temperature patterns and polar amplification; Chapter 4 presents my comparison of climate models' representation of 20th century surface temperature response with surface temperature observations; Chapter 5 presents my comparisons of surface albedo feedbacks in climate models and satellite observations.

Finally, Chapter 6 presents the overall conclusions from my work and recommendations for further research.

2 Climate Feedback Literature Review

This chapter describes the individual radiative feedbacks, how these feedbacks are analysed and how the feedback strengths compare in models and observations. It does not cover the complex feedbacks involved with carbon cycle changes (e.g. vegetation, permafrost melting) or the collapse of the Greenland and Antarctic ice sheets mentioned in Chapter 1. It concludes by setting the aims of this project in the light of current understanding of feedbacks.

2.1 Climate feedback mechanisms

2.1.1 Planck feedback

All bodies with a temperature above absolute zero emit radiation according to the Stefan-Boltzmann equation

$$R = \sigma \varepsilon T^4 \qquad 2.1$$

where R is the emitted longwave radiation, σ is the Stefan Boltzmann constant, and ε is the emissivity. For the Earth's climate system, R is the TOA outgoing longwave radiation, T is the surface temperature, and ε (although better described as a transmissivity in this case) is dependent on the atmospheric state including cloud amount and properties. By increasing the surface temperature, the Earth's radiative cooling is enhanced, counteracting the forcing that caused the warming. This is known as the Planck black body feedback. It is based on fundamental physics and is well represented in models, so is often not included in inter-model feedback comparisons. It is a strong negative feedback (the global mean value is about -3.3 W m^{-2} K^{-1} [*Cess et al.*, 1990]) and is the reason why the Earth reaches a new equilibrium temperature when a forcing is applied. Although the emitted longwave radiation is proportional to the fourth power of the temperature, this relationship approximates to linear over the relatively small range of temperature change expected under climate change.

2.1.2 Water vapour feedback

The relationship between water vapour and temperature is described by the Clausius-Clapeyron equation

$$\ln\left(\frac{e_s}{e_{s0}}\right) = \frac{\Delta H_{vap}}{R_{wv}}\left(\frac{1}{T_0} - \frac{1}{T}\right) \qquad 2.2$$

where e_s is the saturated vapour pressure at temperature T, ΔH_{vap} is the latent heat of vaporisation and R_{wv} is the gas constant for water vapour. Observations and models suggest relative humidity remains almost constant with climate change [*Bony et al*., 2006] so the specific humidity is proportional to e_s. Water vapour is a powerful greenhouse gas and, therefore, an increase in water vapour with temperature will trap more longwave radiation and cause a positive feedback. The radiative impact of a change in water vapour is approximately proportional to the logarithm of its concentration or specific humidity, which, from the right hand side of equation 2.2, is approximately linear with temperature over the relatively small range of temperature change expected under climate change. Humidity changes in the upper troposphere, where the unperturbed humidity is relatively low, have greater radiative effect than changes lower down [*Forster and Collins*, 2004]. Humidity is also dependent on the large-scale atmospheric circulation and on detrainment of moisture from convective systems which itself is dependent on the penetration height of convective cells, on cloud microphysical properties affecting inter-conversion between cloud water, precipitation and water vapour, and on turbulent mixing between cloud-saturated and environmental air [*Bony et al*., 2006].

2.1.3 Lapse rate feedback

The troposphere has a negative lapse rate, i.e. cools with height. The lapse rate affects the emission of TOA longwave radiation, a greater lapse rate having a greater greenhouse effect. Therefore, when warming is greater in the upper troposphere than at lower levels, the lapse rate decreases, producing a negative feedback. Lapse rate is controlled by radiative, convective and dynamical processes [*Bony et al*., 2006].

2.1.4 Ice and snow feedbacks

The cryosphere provides three types of feedback, snow albedo feedback, sea ice albedo feedback and sea ice insulation feedback. Snow and ice are highly reflective so as snow and ice retreat polewards with increased temperature, less shortwave radiation is reflected to space producing a positive feedback. Sea ice

forms an insulating layer between the underlying ocean and overlying atmosphere. Typically in summer heat is transferred from atmosphere to ocean whereas in winter the reverse is true. The thicker (thinner) the sea ice the greater (lesser) the insulation between the sea and the air. Therefore thinning sea ice will tend to have a warming effect in winter but a cooling effect in summer.

Snow albedo is dependent on depth of snow but also on age because snow crystals change shape and bond together with time [*Bony et al*., 2006]. GCMs parameterise these relationships, but may miss out other important ones such as snow-vegetation canopy interactions, where, in tree-covered areas, snow may fall through the canopy or be held within the canopy.

Most GCMs have dynamic sea ice but do not represent well the complex sea ice surface state of the real world where snow-covered ice, surface meltwater ponds and drainage channels, ridged ice and leads, which all have different albedos, coexist in a sub GCM grid area [*Bony et al*., 2006]. GCMs may also parameterise the dependence of albedo on solar zenith angle [*Curry et al*., 2001].

GCMs generally prescribe the Greenland and Antarctic ice sheets so that although they allow fresh snow to fall on the ice sheet surface, the ice sheet itself does not disintegrate dynamically. To study the disintegration of ice sheets under climate change, AOGCMs must be incorporated with ice sheet models [e.g. *Ridley et al*., 2010].

The effect of surface albedo on planetary albedo is dependent on the effective albedo of the atmosphere and on clouds [*Winton*, 2006b]. These attenuate the surface albedo such that its effect on planetary albedo is approximately halved [*Qu and Hall*, 2006].

2.1.5 Cloud feedback

Clouds reflect shortwave and trap longwave radiation. The relative strengths of these effects depend on their height and optical depth. There is a large spectrum of cloud types from low level boundary layer clouds to deep convective clouds each with their own optical properties and effects on the radiation budget. Therefore understanding cloud feedback requires an understanding of how climate change alters the distribution of different cloud types. The occurrence of cloud types is controlled by atmospheric dynamics as well as temperature, atmospheric stability

and wind shear and therefore cloud feedback depends on changes in all these properties [*Bony et al*., 2006].

2.2 Climate feedback analysis methods

By definition, a feedback parameter for a particular feedback is the change in radiative flux, *R*, (often at the TOA) caused by the change in the feedback property, *x*, per unit surface temperature change:

$$Y_x = \frac{\partial R}{\partial x}\frac{\partial x}{\partial T_s} \qquad 2.3$$

It is also assumed that the radiative effect of the different feedbacks are additive such that $Y = Y_0 + Y_\Gamma + Y_q + Y_\alpha + Y_c$, where Y_0, Y_Γ, Y_q, Y_α and Y_c are the radiative feedback parameters associated with homogeneous temperature change (the Planck black body feedback), lapse rate changes, water vapour changes, surface albedo changes and cloud changes respectively. The different approaches that have been used to diagnose feedbacks are now described.

2.2.1 Partial radiative perturbation method

The partial radiative perturbation (PRP) method [*Wetherald and Manabe*, 1988] uses equation 2.3 to determine the feedback parameter for each type of feedback, *x*. Partial derivatives of TOA radiative flux with respect to changes in parameter *x* (temperature or water vapour or albedo or some cloud property) are evaluated by running the model radiation code offline using control values of all parameters except *x*. *R* thus produced using the value of *x* from a forced run is compared with *R* produced using the value of *x* from the control run to obtain the first term of the right-hand side of equation 2.3. The second term is obtained from differences in surface temperature and *x* at equilibrium for a forced simulation compared to a control simulation. The lapse rate feedback is calculated as a residual from the total temperature feedback and the Planck black body feedback. Forward and reverse calculations are sometimes performed to account for correlation between fields such as water vapour and cloud. This two-sided PRP method involves taking the average of the change in TOA radiative flux due to the change in *x* calculated using the forced climate state and the control climate state. Although the PRP

method allows separate evaluation of the impact of different feedbacks it does require considerable computation and access to radiative code not accessible to all.

2.2.2 Kernel method

The kernel method is similar to the PRP method except that instead of using the forced and control values of x and T_s, the radiative effect of a small spatially uniform change in x is determined as a function of latitude, longitude, altitude and month to produce a "radiative kernel", K^x. The radiative kernel can then be multiplied by $\frac{\Delta x}{\Delta T_s}$ from forced simulations and integrated vertically to give the feedback parameter. This method avoids the correlation issue described above. *Soden et al*. [2008] have shown that radiative kernels from different models are very similar and therefore comparison of models using one set of kernels is both adequate and computationally efficient. Radiative kernels can be determined for temperature, T, water vapour, q, and surface albedo, α. However, due to the non-linearity of feedback from overlapping cloud, the cloud feedback, Y_c, can only be calculated as a residual:

$$Y_c = \frac{1}{\Delta T_s}\left[\Delta R - F - \sum_i \left(K_i^T \Delta T_i + K_i^q \Delta q_i + K_i^\alpha \Delta \alpha_i\right)\right] \qquad 2.4$$

where ΔR is the total TOA change in radiative flux, F is the radiative forcing, and $K^x \Delta x$ is the radiative effect of feedback x (integrated over each level i).

2.2.3 Cloud radiative forcing method

As introduced in Section 1.2.2, the total TOA net downward radiative flux change is related to the total feedback parameter by

$$\Delta R \approx F + Y \Delta T_s \qquad 2.5$$

where F is the radiative forcing. The cloud radiative forcing (CRF) method [*Cess et al*., 1990; 1996] diagnoses feedback parameters by breaking down equation 2.5 into clear-sky (CS) and cloud radiative forcing (CRF) components where cloud radiative forcing is the difference between all-sky and clear-sky radiative fluxes. This may further be decomposed into shortwave (SW) and longwave (LW) components [see *Gregory and Webb*, 2008] such that

$$\Delta R_{SWCS} + \Delta R_{SWCRF} + \Delta R_{LWCS} + \Delta R_{LWCRF} \approx$$
$$F_{SWCS} + F_{SWCRF} + F_{LWCS} + F_{LWCRF} + \qquad 2.6$$
$$(Y_{SWCS} + Y_{SWCRF} + Y_{LWCS} + Y_{LWCRF})\Delta T_s$$

Given that lapse rate and water vapour predominantly affect longwave and surface albedo affects shortwave, the decomposition into shortwave and longwave allows some assignment to feedback processes. The cloud feedback diagnosed by this method is a contrast between all-sky and clear-sky, and therefore includes cloud masking effects which should strictly be included in the other feedback terms [*Zhang et al*., 1994; *Colman*, 2003; *Soden et al*., 2004]. For example, changes in surface albedo will have less effect under cloudy conditions than under clear sky. The feedback may be diagnosed using equilibrium changes in radiative fluxes and surface temperature [*Boer and Yu*, 2003b], or by regression of radiative flux changes against surface temperature changes before equilibrium is reached [*Gregory et al*., 2004]. This method is much more computationally efficient than the PRP method and also has the advantage that the method is applicable for observations, but feedback parameters diagnosed using these two methods cannot be directly compared.

2.2.4 Winton's albedo feedback

Winton [2005] devised an optical model to relate the upward and downward shortwave fluxes at the surface and TOA to the optical properties of the atmosphere (upward and downward transmissivity and albedo) and surface (albedo) in order to determine contributions to changes in the shortwave fluxes from changes in these optical properties. The model is based on the assumption that the atmosphere reduces the shortwave flux reaching the surface by reflection and absorption, that multiple reflections occur between the surface and the atmosphere, and that the atmosphere absorbs some of the upward shortwave radiation before it can escape to space. Solving the equations of the full four-parameter model for the optical properties requires upward ($\uparrow$) and downward ($\downarrow$) shortwave fluxes at the TOA and surface, and upward TOA shortwave flux and downward surface shortwave flux when the surface albedo is zero. The former four diagnostics are commonly available from climate models, but the latter two require extra calculations in the climate model. The net

downward surface shortwave radiative flux, or surface shortwave absorption, (S_B) is given by

$$S_B = S_{B\downarrow} - S_{B\uparrow} = \frac{S_{B\downarrow}(1-\alpha_s)(1-\frac{\alpha_\uparrow S_{B\uparrow}}{S_{B\downarrow}})}{1-\alpha_\uparrow \alpha_s} \qquad 2.7$$

where α_s is the surface albedo and $\alpha_\uparrow$ is the upward atmospheric albedo. By parameterising the upward atmospheric albedo as

$$\alpha_\uparrow = 0.05 + 0.85(1-\frac{S_{B\downarrow}}{S_{B\downarrow CLR}}) \qquad 2.8$$

where $S_{B\downarrow CLR}$ is the clear-sky downward shortwave flux at the surface, it is possible to calculate the surface shortwave absorption using only those diagnostics readily available from climate models. *Winton* [2005] showed that by using this simplified version of the model, the root mean square error on the surface shortwave absorption is increased by only about 1% compared to the full four-parameter model, and that the impact of the surface albedo on the TOA budget is typically reduced by less than 10% from its impact on the surface. Therefore the surface albedo feedback parameter may be estimated from the change in surface shortwave absorption by using the forced and control surface albedos with all other parameters remaining constant. The change in surface shortwave absorption depends on whether those other parameters are from the forced or control climate simulation and so an average is taken:

$$\begin{aligned}\Delta S_{\alpha_s \to \alpha_{s'}} = \frac{1}{2}[&S_B(S_{B\downarrow}, S_{B\uparrow}, \alpha_\uparrow, \alpha_{s'}) - S_B(S_{B\downarrow}, S_{B\uparrow}, \alpha_\uparrow, \alpha_s) \\ &+ S_B(S_{B\downarrow'}, S_{B\uparrow'}, \alpha_{\uparrow'}, \alpha_{s'}) - S_B(S_{B\downarrow'}, S_{B\uparrow'}, \alpha_{\uparrow'}, \alpha_s)]\end{aligned} \qquad 2.9$$

Winton [2006b] used this method on the transient CO_2 warming simulations of IPCC AR4 climate models and found comparable values of global mean surface albedo feedback to previous studies using the PRP method.

2.2.5 Online feedback suppression

Although this method does not quantify the feedback parameter, the impact of a particular feedback may be assessed by suppressing that feedback mechanism in a model and then comparing the response of that model to the standard model [*Hall and Manabe*, 1999; *Hall*, 2004; *Graversen and Wang*, 2009]. This is known as the online feedback suppression method. However, by removing one of the feedback

mechanisms the strength of the others may be affected, for example multiple positive feedbacks may amplify each other [*Hall and Manabe*, 1999].

2.3 Modelled climate feedbacks

Feedback studies have mostly concentrated on quantifying the global mean feedbacks due to changes in water vapour, clouds, surface albedo, and lapse rate [e.g. *Bony et al*. 2006]. Comparisons (Figure 2.1) suggest water vapour feedback is the strongest positive feedback, followed by cloud feedback and surface albedo feedback, with the lapse rate feedback being most likely negative [*Bony et al*., 2006; *Soden and Held*, 2006; *Colman*, 2003].

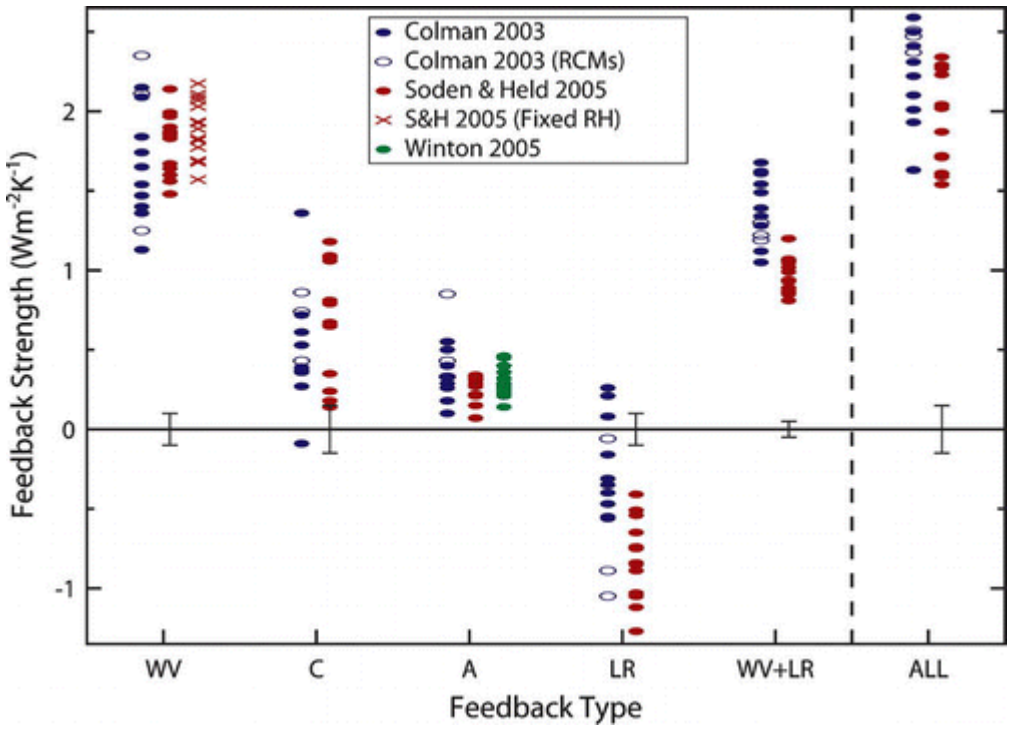

Figure 2.1: Comparison of GCM climate feedback parameters (in $Wm^{-2}K^{-1}$) for water vapour (WV), cloud (C), surface albedo (A), lapse rate (LR), and the combined water vapour + lapse rate (WV+LR). ALL represents the sum of all feedbacks. Vertical bars depict the estimated uncertainty in the calculation of the feedbacks. From Bony et al. [2006].

Cloud feedbacks show considerable inter-model differences. Studies have shown that deep convective clouds and low-level clouds respond in different ways in different models but low level cloud differences, especially in the tropics, give the greatest inter-model difference [*Bony et al*., 2006].

Due to the differences in the convective and dynamical processes in the tropics and high latitudes GCMs predict greater warming in the upper atmosphere than at the surface in the tropics, whereas at high and mid latitudes the reverse is true. The lapse rate feedback is therefore positive at mid and high latitudes but negative in the tropics. In the global mean the tropical lapse rate response dominates giving an overall negative lapse rate feedback. The large inter-model differences in lapse rate feedback are primarily due to differing meridional warming patterns [*Bony et al*., 2006].

Temperature and water vapour are tightly coupled in models so that they exhibit almost constant relative humidity in the global mean, and lapse rate and water vapour feedbacks of models show a strong anti-correlation. Therefore, the inter-model spread of the combined water vapour and lapse rate feedbacks is considerably less than that of the individual water vapour and lapse rate feedbacks, leaving cloud feedback as the main culprit in inter-model spread.

A number of studies have looked at the spatial pattern of feedback strength, but these have generally been either an assessment of multiple feedbacks in one model [e.g. *Colman*, 2002; *Boer and Yu*, 2003b], an assessment of one feedback in multiple models [e.g. *Winton*, 2006b], and/or application of a new method to estimate feedback patterns [e.g. *Soden et al*., 2008; *Winton*, 2006b]. They also usually assess the local contribution to the global mean feedback rather than the local feedback itself. The multi model ensemble mean feedback patterns expressed as the local contribution to the global mean feedback calculated by *Soden et al*. [2008] are shown in Figure 2.2. These were calculated using the radiative kernel method for IPCC AR4 models forced with the SRES A1B scenario. The cloud feedback is calculated as a residual using a forcing that is assumed to be uniform which is clearly a simplification. Maxima for temperature and water vapour feedbacks occur in the tropics and there is a clear anti-correlation between the two. The surface albedo feedback is of course largest over the snow and ice covered regions.

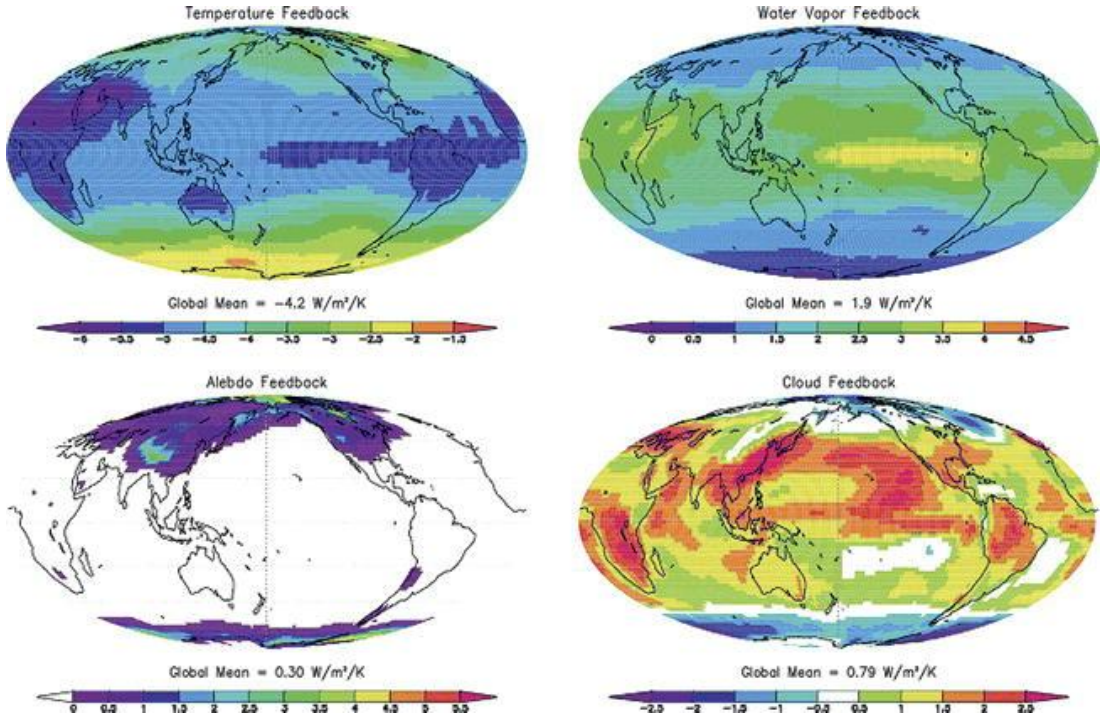

Figure 2.2: Multi model ensemble mean maps of the temperature, water vapour, albedo, and cloud feedback computed using climate response patterns from the IPCC AR4 models and the GFDL radiative kernel. From Soden et al. [2008].

2.3.1 Modelled surface albedo feedback

Although inter-model differences in the surface albedo feedback are smaller than those of other feedbacks in the global mean [*Bony et al*., 2006], surface albedo feedback is important at high latitudes where the divergence of temperature response between models is greatest [*Randall et al*., 2007; *Lu and Cai*, 2009a]. GCMs suggest that in the NH, where there is more land, the snow albedo feedback is equally as important as sea ice albedo feedback, whereas in the SH the sea ice albedo feedback is strongest [*Hall*, 2004; *Winton*, 2006b] because snow on the Antarctic ice sheet remains frozen most of the year.

High latitude warming is found to be greatest in winter and least in summer despite the surface albedo feedback being strongest in summer. In summer the extra absorbed surface energy from the decrease in surface albedo is used to warm the ocean and melt further ice and snow resulting in a small atmospheric temperature change. In the winter the resulting thinner sea ice allows more sensible heat transfer from the ocean to the atmosphere and, because of the very stable atmosphere at that time of year, the warming is concentrated near the surface [*Hall*, 2004].

Surface albedo feedback is commonly defined as the net downward change in top of atmosphere (TOA) shortwave radiative flux, S_α, per unit surface air temperature (SAT) change caused by changes in surface albedo:

$$Y_\alpha = \frac{\partial S_\alpha}{\partial T_s} = -I \frac{\partial \alpha_p}{\partial \alpha_s} \frac{\partial \alpha_s}{\partial T_s} \qquad 2.10$$

where I is the incoming surface shortwave radiative flux, α_p is the planetary albedo, α_s is the surface albedo and T_s is the surface air temperature. The sensitivity of surface albedo to SAT, $\frac{\partial \alpha_s}{\partial T_s}$, in the internal variability context can be determined by regressing surface albedo against SAT values from a control run. A comparison of $\frac{\partial \alpha_s}{\partial T_s}$ in the internal variability and climate change contexts ($2\times CO_2$) for the GFDL model found that for the SH the surface albedo feedback was greater in the internal variability case in all seasons, whereas for the NH the surface albedo feedback was quite similar in both contexts [*Hall*, 2004]. In the climate change context the changes in SAT and sea ice thickness and extent are considerably greater than in the internal variability context resulting in a much stronger sea ice insulation feedback. This greater feedback in the climate change context causes greater SAT change for the same amount of surface albedo change. In much of the NH snow albedo feedback dominates over sea ice albedo feedback, and $\frac{\partial \alpha_s}{\partial T_s}$ for land only points was found to be much more similar in the two contexts. *Hall* [2004] suggested, therefore, that it would not be possible to determine SH surface albedo feedback in the climate change context from a time series dominated by internal variability, but for the NH this would be less of an issue. This was demonstrated by calculating $\frac{\partial \alpha_s}{\partial T_s}$ in a climate simulation with forcing representative of past, present and future using different time periods in the regression. For the earlier periods, little climate change has occurred and the data is dominated by internal variability, whereas for later time periods climate change is greater. *Hall* [2004] therefore concluded that observations of surface albedo and temperature would be required well into the 21st century before a reliable estimate of SH surface albedo feedback could be determined (Figure 2.3).

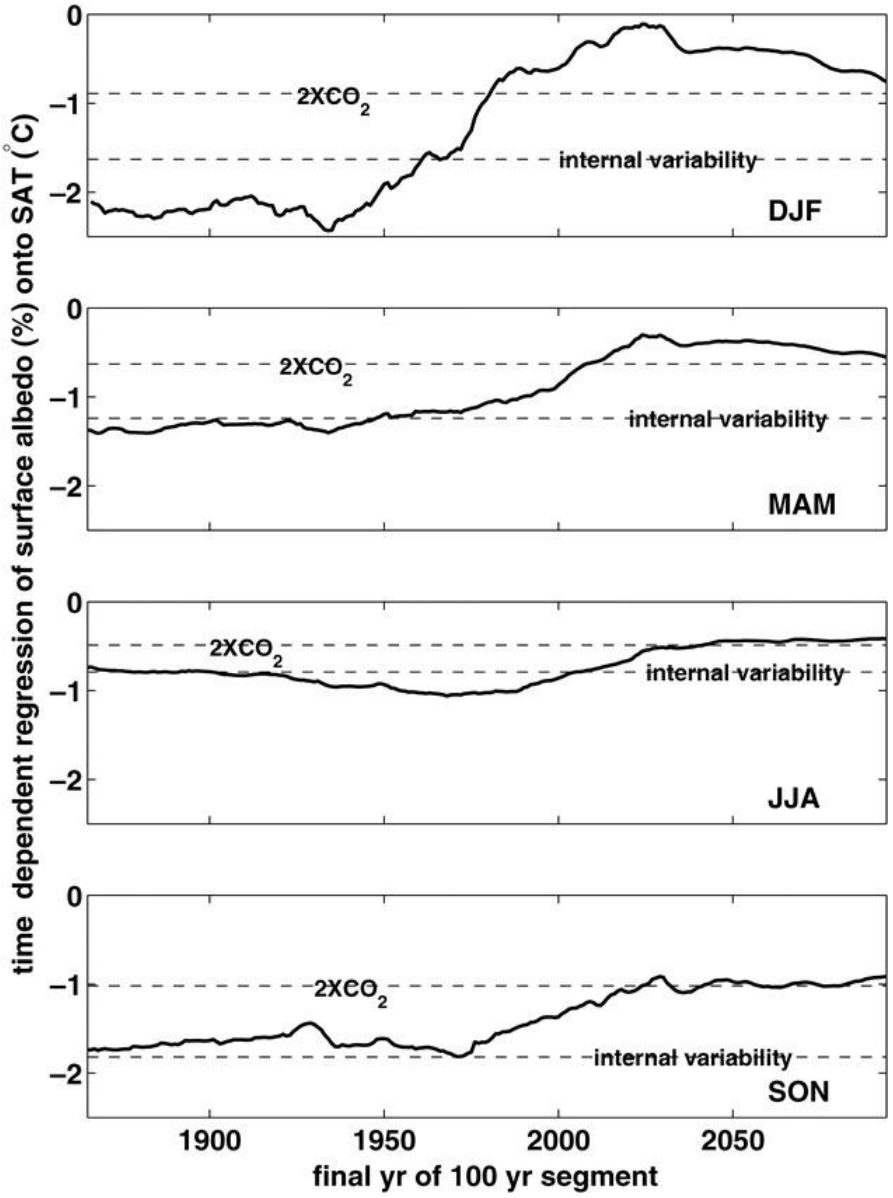

Figure 2.3: Time-dependent regression of seasonal mean surface albedo averaged over 30°S - 90°S onto seasonal mean SAT averaged over the same region in the scenario run using 100-year segments for the regressions. From Hall [2004].

Hall and Qu [2006] assessed the value of the two partial derivatives in equation 2.10 and found that the inter-model differences in extratropical NH mean springtime snow albedo feedback stem largely from the $\frac{\partial \alpha_s}{\partial T_s}$ term, and the $\frac{\partial \alpha_p}{\partial \alpha_s}$ term is similar across models and observations (~0.5). They also showed that this $\frac{\partial \alpha_s}{\partial T_s}$ term in the current seasonal cycle is highly correlated ($r^2 = 0.92$) to that from long term climate change for IPCC AR4 climate models by comparing the change in snow albedo and SAT from April to May in 20th century simulations (seasonal cycle

context) with the change in April snow albedo and SAT over the 21st century of SRES A1B simulations (Figure 2.4).

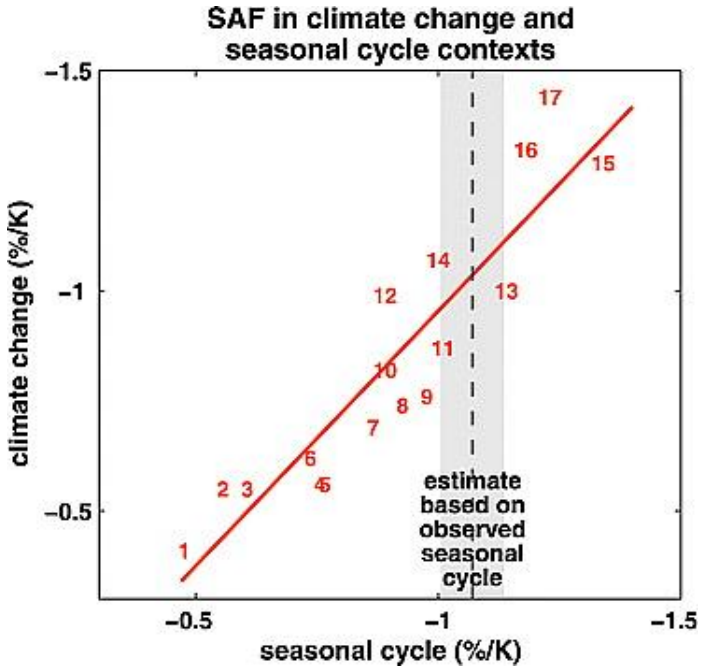

Figure 2.4: Scatterplot of simulated springtime extratropical NH $\Delta\alpha_s/\Delta T_s$ values in climate change (ordinate) vs. $\Delta\alpha_s/\Delta T_s$ values in the seasonal cycle (abscissa). A least-squares fit regression line for simulations is also shown. The observed springtime seasonal cycle $\Delta\alpha_s/\Delta T_s$ value based on ISCCP surface albedo and ERA40 SAT is plotted as a vertical dashed line with the grey bar representing an estimate of the uncertainty at the 95% level. From Hall and Qu [2006].

Although it is unknown how the sea ice albedo feedback behaves in these two contexts, the observed seasonal cycle may have great potential for estimating the surface albedo feedback under climate change.

In a warming world the extent of snow cover decreases and changes in the optical properties of the remaining snow due to ageing (snow metamorphosis) also occur. Both affect the snow albedo feedback. A study by *Qu and Hall* [2007] suggests that the strength and inter-model spread of snow albedo feedback in transient climate change simulations is dominated by the decrease in snow cover. Models with large mean effective snow albedo tend to have large surface albedo contrast between snow-covered and snow-free land and large snow albedo feedback. Therefore, high quality observations of surface albedo of snow-covered surfaces would be very useful in constraining the parameterisations of albedo used in climate models and their snow albedo feedback.

2.4 Constraining climate feedbacks from observations

Due to the large differences in feedback between models, attempts have been made to constrain feedbacks using observations. However, observations have their limitations. Observed variability of the climate system may not be representative of long term anthropogenic global warming. Natural forcings due to the seasonal solar cycle and volcanic eruptions operate in the shortwave domain whereas greenhouse gas forcing acts primarily in the longwave domain. Natural and anthropogenic forcings differ in their geographical structures, and fluctuations in temperature and circulation on short timescales are not comparable to those on long time scales [*Bony et al*., 2006].

The total climate feedback parameter (and climate sensitivity) has been estimated from TOA radiative fluxes from ERBE satellite data from 1985-1996 and observed temperature anomalies using best estimates of radiative forcing over the time period [*Forster and Gregory*, 2006]. The total feedback parameter (non-signed, i.e. -*Y*) was found to be 2.3 ± 1.4 W m^{-2} K^{-1}, which equates to a climate sensitivity of 1.0–4.1 K assuming Gaussian errors in the measured parameters. The ERBE data does not extend poleward of 60º so this feedback parameter does not fully include contributions from high latitude feedbacks. Comparisons of modelled feedback with and without including the polar regions suggested the impact of the reduced global coverage is small and that the feedback measured over this relatively short timescale is still representative of the long term climate change feedback. A more recent study of the Earth's energy budget using satellite estimates of TOA radiative fluxes from 1985-2005 suggested a smaller feedback parameter and hence higher climate sensitivity with a much greater upper limit [*Murphy et al.*, 2009].

2.4.1 Observed water vapour feedback

Relationships between water vapour and temperature over different timescales are not necessarily comparable, making it difficult to infer the magnitude of the water vapour feedback from observations of internal variability [*Bony et al*., 2006]. However, observations can be used to assess how well a model reproduces seasonal, inter-annual and decadal variations of relative humidity distributions for the current climate. The response to volcanic aerosol forcing is measurable for events such as the eruption of Mt. Pinatubo and this has been used to quantify the

water vapour feedback [*Soden et al*., 2002; *Forster and Collins*, 2004], although natural variations contaminate the cooling. In the global mean, reasonable agreement in the water vapour changes between the model and observations was found, whereas height-latitude distributions varied considerably between simulations and did not match observations well. The observed global mean water vapour feedback parameter was found to be consistent with the modelled water vapour feedback for the Pinatubo event and was also consistent with previously reported water vapour feedback due to long term climate change from multiple models. It has been estimated that the water vapour feedback takes 4-7 years to be fully operational [*Hallegatte et al*., 2006] which suggests this feedback is not at full strength following a short term event such as a volcanic eruption.

Observed water vapour feedback has also been determined using observations of specific humidity in the internal variability context where changes were largely due to the El Niño Southern Oscillation (ENSO) [*Dessler et al*., 2008; *Dessler and Wong*, 2009]. The observed global mean water vapour feedback was consistent with that from ENSO variability in IPCC AR4 climate models, but these studies gave a slightly larger global mean water vapour feedback than that of *Forster and Collins* [2004], particularly for the water vapour feedback determined from reanalysis data [*Dessler and Wong*, 2009] rather than satellite data. It was also found that the modelled feedback from ENSO variability was larger and had a greater inter-model spread than that from long term climate change. Under ENSO variability, the water vapour feedback was caused mostly by tropical water vapour changes. The tropical temperature change was reasonably consistent between models but the extratropical temperature change, and therefore global mean temperature change, varied considerably.

2.4.2 Observed surface albedo feedback

Recent studies have suggested that the observed NH snow albedo feedback is positive. Modelled surface air temperature anomalies associated with ENSO in North America agreed well with observations when snow albedo feedback was present but were halved when the snow albedo feedback was suppressed [*Yang et al*., 2001].

As described in Section 2.3.1, *Hall and Qu* [2006] showed that the current seasonal cycle over springtime has great potential for estimating NH mean

springtime snow albedo feedback. A comparison of the value of $\frac{\Delta\alpha_s}{\Delta T_s}$ obtained from the observed seasonal cycle using ISCCP surface reflectance and ERA40 surface temperature with that from IPCC AR4 climate models suggested many models have an unrealistic springtime NH mean snow albedo feedback in the seasonal cycle context (Figure 2.4). The uncertainty estimate for the observed $\frac{\Delta\alpha_s}{\Delta T_s}$ term only included statistical uncertainty and not measurement error. The ISCCP surface reflectance is based on satellite measurements at a single visible channel although converted to a broadband value based on seven visible and near-infrared channels from ERBE data. The actual uncertainty would be larger than that shown but is very unlikely to cover the range of modelled $\frac{\Delta\alpha_s}{\Delta T_s}$.

Flanner et al. [2011] used satellite measurements of snow and ice coverage from 1979 to 2008 to quantify the NH mean cryospheric radiative impact of changing surface albedo and to constrain the associated surface albedo feedback. The surface albedo over this time period was determined from the snow and ice coverage data by calibration with coincident MODIS and APP-x albedo products, taking into account first-year and multi-year ice. By using snow and ice coverage data and converting it to surface albedo, a longer time period can be used than if albedo data were used directly. The more recent MODIS data is also considered more accurate than older satellite data such as ISCCP. The radiative kernel method (Section 2.2.2) was then used to convert surface albedo changes to TOA radiative flux changes and hence surface albedo feedback. The NH mean surface albedo feedback was found to be 0.62 W m^{-2} K^{-1} (range of 0.33 to 1.07 W m^{-2} K^{-1}) which is considerably higher than that from IPCC AR4 climate models.

2.4.3 Observed cloud feedback

Cloud feedback is complex, with dependencies on optical properties, as well as cloud amount and height, which in turn are dependent on atmospheric circulation as well as temperature. A number of studies assessing the relationships between cloud type, atmospheric dynamics, atmospheric stability, wind shear and temperature, as well as compositing or clustering techniques (sorting into cloud type and dynamic regimes) have been used to compare modelled and observed cloudiness and cloud radiative forcing [*Bony et al*., 2006]. Considerable differences have been found in

the cloud fraction, optical thickness and cloud-top height between ISCCP satellite observations and models, although models have improved. Clouds are usually of sub-grid size in GCMs and are, therefore, highly parameterised. There has been limited evaluation of these parameterisations in GCMs [*Stephens*, 2005].

Most of the estimates of cloud feedback from observations have concentrated on just part of the problem, such as evaluation only in the tropics [*Spencer et al*., 2007] or only of low clouds [*Clement et al*., 2009], resulting in the feedback differing even in sign. *Spencer at al*. [2007] found a negative tropical cloud feedback from intra-seasonal variability and this was caused mainly by changes in cirrus cloud. They suggested this supports the controversial "adaptive iris hypothesis" [*Lindzen et al*. 2001], which, based on observations from the western tropical Pacific, states that tropical cirroform cloud coverage opens and closes like the iris of an eye in response to warm and cool anomalies producing a negative feedback. However, it is not clear that these short term responses would apply over the long time scales of global warming.

Dessler [2010] determined global mean cloud feedback caused by ENSO variability and found it to be positive, although the large uncertainties did not exclude the possibility of a small negative feedback. This observed feedback was found to be consistent with the cloud feedback determined for IPCC AR4 climate models in response to both ENSO and long term climate change, but no correlation was found between modelled cloud feedback in the ENSO and long term climate change contexts.

2.5 Quantifying temperature response contributions of feedbacks

Quantifying the temperature response contributions (partial temperature responses) due to each feedback allows comparison of their impacts with other non-feedback processes such as heat storage. *Dufresne and Bony* [2008] decomposed the global mean temperature response by using the special nature of the Planck feedback, Y_0 and the additivity of feedback parameters and partial temperature responses. Expressing the feedback gain for each non-Planck feedback, *x*, as $g_x = -\frac{Y_x}{Y_0}$, the partial temperature response for each non-Planck feedback, *x*, is

$$\Delta T_x = g_x \Delta T \qquad 2.11$$

and the partial temperature response due to the Planck feedback, i.e. the response that would be obtained if there were no other feedbacks active is

$$\Delta T_0 = (1 - \sum_{x \neq 0} g_x)\Delta T \qquad 2.12$$

This equation applies to equilibrium temperature responses but heat storage can be modelled as an ocean heat uptake efficiency, κ, for transient climate responses and treated as another feedback parameter. Using this decomposition, *Dufresne and Bony* [2008] found that for transient climate change in IPCC AR4 AOGCMs the partial temperature responses due to cloud feedback, water vapour plus lapse rate feedback and the ocean heat uptake were comparable, but the inter-model differences were primarily due to cloud feedback.

An alternative method for decomposing temperature responses at any point in space or time and more accurately handling heat storage as well as heat transport comes from the energy balance equation 1.2 [see also *Lu and Cai*, 2009b]. The radiative impact of the Planck feedback ($Y_0 \Delta T_s$) is separated out to the left hand side and the energy budget equation rearranged to give

$$\Delta T_s = \frac{-1}{Y_0}\left[\frac{-d\Delta H}{dt} + \Delta A + F + \sum_{x \neq 0} Y_x \Delta T_s\right] \qquad 2.13$$

where the terms on the right-hand side therefore give the partial temperature responses due to the release of heat stored, the change in horizontal heat transport, the forcing, and the non-Planck feedbacks. As long as the Planck feedback can be separated the remaining feedback parameters may be analysed using any of the methods described in Section 2.2. At equilibrium in the annual mean $\frac{d\Delta H}{dt}$ goes to zero and the change in horizontal heat transport is equal to the net downward change in TOA radiative flux, ΔR.

2.6 Summary and aims of this project

This chapter has described the different radiative feedbacks and the methods used to analyse them. It has shown the large inter-model spread in global mean feedback parameters, particularly for cloud feedback. Observed feedback parameters have been measured in the global mean and for large regions. Generally they have

been found to have a similar magnitude to feedback parameters of IPCC AR4 GCMs, but they have quite large uncertainties and provide little constraint to models. Very few studies have looked at observed feedback patterns and compared these to modelled feedback patterns. However, *Forster and Collins* [2004] showed there can be significant differences in latitude-height distributions of specific humidity changes in models and observations even though the global mean water vapour feedback was similar.

Chapter 1 highlighted the greater warming at high latitudes than low latitudes seen in climate models and 20th century observations in the NH. It also highlighted the greater inter-model differences in temperature response at high latitudes indicating the greater uncertainty in feedbacks there. The reasons for this polar amplification of warming may be attributable to a number of feedbacks but relative contributions are not well understood.

The aims of this project are to better understand the zonal pattern of feedbacks, the inter-model differences in these patterns, and how the modelled and observed patterns compare. Quantifying the zonal patterns of feedbacks will help understand the causes of polar amplification and could also help constrain modelled feedbacks. This project falls into three work packages concentrating on different aspects of these aims:

1. How do the zonal patterns of feedback compare in different models forced with CO_2? How do the zonal patterns of feedback compare in a single model with different forcing mechanisms? How do the feedbacks in different models contribute to polar amplification in both hemispheres? This work is presented in Chapter 3.
2. Can the observed and modelled 20th century temperature record be used to constrain total feedback? By separating modelled 20th century temperature responses into contributions from forcing, feedback and heat storage/transport I investigate why models do or do not reproduce the observed temperature response patterns. This work is presented in Chapter 4.
3. Surface albedo feedback has been shown to play an important role in polar amplification. Although snow and ice albedo feedback have been determined from observations in the NH, there have been no estimates of surface albedo feedback from observations globally, no estimates of zonal patterns of

surface albedo feedback, and no estimates of non-cryosphere surface albedo feedback. Although NH snow albedo feedback behaves similarly in the seasonal cycle and long term climate change in springtime, it is unknown whether this applies in all seasons, globally and also to sea ice albedo feedback. Chapter 5 presents my analysis of surface albedo feedback from satellite observations and models in the seasonal cycle and long term climate change contexts in order to address these shortcomings.

All three work packages make use of output from climate models taking part in the World Climate Research Program (WCRP) Climate Model Intercomparison Project phase 3 (CMIP3).

3 The Role of Climate Feedback in Polar Amplification

3.1 Introduction

Chapters 1 and 2 provided the background to this thesis with Chapter 2 concluding with the aims of this project, splitting the work into three work packages. This chapter describes the first of those work packages and addresses the following questions:

1. How do the zonal patterns of feedback compare in different models forced with CO_2?
2. How do the zonal patterns of feedback compare in a single model with different forcing mechanisms?
3. How do the feedbacks in different models contribute to polar amplification in both hemispheres?

In this study the spatial pattern of local feedback was determined using the regression method of *Gregory et al.* [2004] from eight slab ocean CMIP3 climate models, forced with doubled CO_2. The equilibrium surface temperature response pattern for each model was broken down into components due to each feedback, the horizontal transport of heat and the troposphere-adjusted forcing. The contribution of these components to polar amplification was then quantified. The same analysis was applied to the results from idealised aerosol perturbation experiments as well as $2\times CO_2$ and +2% solar constant experiments using the HadSM3 GCM to investigate how feedback patterns vary between forcing mechanisms. This work has been published in *Crook et al*. [2011].

The methods are described in Section 3.2. The data for the CMIP3 models and the HadSM3 experiments are presented in Sections 3.3.1 and 3.3.2 respectively. The results are described in Section 3.4 and conclusions are given in Section 3.5.

3.2 Methods

3.2.1 Determination of local feedback

The linear model of feedback (equation 2.5) was used to determine feedback parameters. The CRF method (see Section 2.2.3) was used to split the feedbacks into

longwave and shortwave clear-sky and CRF components (equation 2.6). An alternative way to split the shortwave feedback is to use the Winton method to determine the surface albedo feedback (see Section 2.2.4). Then assuming that water vapour feedback effects on shortwave radiation are minimal, the difference between the total shortwave radiative flux change and the surface albedo radiative flux change gives the shortwave forcing component plus the shortwave radiative flux change associated with cloud changes, and therefore, can be used to find a true shortwave cloud feedback.

$$\Delta R_{SW} - \Delta S_{\alpha} \approx F_{SW} + Y_{SWCL}\Delta T_s \qquad 3.1$$

The difference between the shortwave clear-sky feedback and the surface albedo feedback can be used to give a measure of the shortwave cloud masking effect (see Section 2.2.3).

The local feedback parameters and troposphere-adjusted forcing components were determined at different spatial scales by performing a linear regression of each local ΔR component against the local ΔT_s for the years before equilibrium is reached, following the method of *Gregory et al.* [2004]. Chapter 1 discussed the different definitions of radiative forcing and showed that allowing rapid tropospheric adjustments to be included in the forcing results in a better prediction of climate sensitivity and temperature response, particularly for absorbing aerosol forcing. Given that this study compares feedback patterns for different forcing mechanisms, including absorbing aerosol, the use of the regression method to determine feedback is appropriate. Regressions were performed on the global means, the polar regions (60ºN-90°N and 60ºS-90°S), the tropics (30°S-30°N) and the zonal means at the resolution of the model for both annual means and seasonal means, and on each 10˚×10˚ grid box for annual means. Regressions at all spatial scales were also performed on the total radiative flux change to find a total feedback parameter and total troposphere-adjusted forcing (equation 2.5) so that a check could be made that the total feedback and forcing were the same as the sum of the feedback and forcing components. Previous studies have applied the linear regression method to global means, and, therefore, the validity of this method at different spatial scales is discussed in detail in Section 3.4.1. Local feedback parameters were also calculated at equilibrium using the stratosphere-adjusted forcing components where they were available. The results from the two forcing definitions are compared in Section 3.4.2.

The longwave clear-sky feedback was further broken down into a Planck feedback term and a water vapour plus lapse rate feedback term:

$$\Delta R_{LWCS} = F_{LWCS} + (Y_{WV+LR} + Y_0)\Delta T_s \qquad 3.2$$

The Planck feedback term was determined using the Edwards Slingo radiative transfer code as employed in *Rap et al*. [2010]. Three-dimensional temperature and specific humidity profiles were obtained for each model using the climatological monthly mean from the control run and the equilibrium monthly mean from the $2\times CO_2$ run. For the control case the temperature was uniformly incremented by 1 K, 2 K, 3 K and 4 K and the corresponding change in longwave TOA radiative flux was obtained under clear-sky conditions. For the $2\times CO_2$ case the temperature was uniformly decremented by 1 K, 2 K, 3 K and 4 K and the corresponding change in longwave TOA radiative flux was obtained under clear-sky conditions. The Planck feedback parameters for the control and $2\times CO_2$ cases were determined by regressing the change in TOA radiative flux against the uniform temperature change. The mean of these two values was taken as the Planck feedback acting during the $2\times CO_2$ simulation. The regressions had very good straight line fits showing that the Planck feedback is constant over the range of temperature responses typically seen in the $2\times CO_2$ experiments. The Planck feedback for the $2\times CO_2$ case was slightly less negative than that for the control case. This is because in this method the temperature in the control case was incremented above the tropical equilibrium $2\times CO_2$ temperature and likewise the temperature in the equilibrium $2\times CO_2$ case was decremented below the tropical control temperature, and the Planck feedback would be expected to be more negative at higher temperatures. The greatest difference (0.1 W m^{-2} K^{-1}, i.e. ~2.5 %) was found in the tropics where the surface temperature response to $2\times CO_2$ is smallest.

3.2.2 Determination of equilibrium partial temperature responses

The equilibrium partial temperature responses for the feedbacks, forcing and heat transport were calculated using equation 2.13 with the forcing and the feedback terms as determined from the archived stratosphere-adjusted forcing (where available) as well as from regression. The standard deviations in the equilibrium partial temperature changes from regression were calculated from the standard deviation of the corresponding regression forcing, F_{regr}, component.

3.2.3 Determination of polar amplification contributions

Polar amplification was quantified by *Holland and Bitz* [2003] for the NH as the mean temperature response poleward of 75°N divided by the global mean temperature response. There is no strict definition of the "polar region"; different studies have used different equatorward boundaries. Given that in the SH the sea ice extends considerably further equatorward than 75°S, the NH and SH polar regions were defined in this study symmetrically as 60°N-90°N, and 60°S-90°S respectively (hence the choice of regressions in these regions). Some of the feedbacks have the effect of warming quite uniformly, whereas others cool in some places and warm in others, so only comparing the equilibrium partial temperature responses in the polar region does not give a full understanding of contributions to polar amplification. Therefore, partial polar amplification contributions, PA_x, were defined in this study as the normalised difference in the warming between polar and tropical regions for each partial temperature contribution, determined from the regressions in these regions, such that

$$PA^{NH} = \sum_x PA_x^{NH} = \sum_x \frac{\Delta T_x^{60N-90N} - \Delta T_x^{30N-30S}}{\overline{\Delta T}} \qquad 3.3$$

and

$$PA^{SH} = \sum_x PA_x^{SH} = \sum_x \frac{\Delta T_x^{60S-90S} - \Delta T_x^{30N-30S}}{\overline{\Delta T}} \qquad 3.4$$

This means when there is no partial polar amplification, PA_x will be zero.

3.3 Model data

3.3.1 2×CO_2 experiments

The eight slab ocean models from the CMIP3 multi-model dataset with results available for the whole of the integration from 2×CO_2 experiments were chosen. These models have equilibrium surface temperature changes across most of the range of equilibrium climate sensitivities given in *Meehl et al.* [2007] (see Table 3.1). The differences in seasonal and annual mean TOA radiative flux components and surface temperature data compared to those in the equivalent control run were determined at each grid box. The methods for determining local feedback

parameters, equilibrium partial temperature responses and contributions to polar amplification as described in Section 3.2 were applied.

Table 3.1: $2\times CO_2$ experiments equilibrium temperature response and polar amplification.

Model	**Equilibrium global mean ΔT (K)**	**Annual mean NH polar amp. (eqn. 3.3)**	**Annual mean SH polar amp. (eqn. 3.4)**
1. GISS ER	2.72	0.52	0.11
2. NCAR CCSM3.0	2.74	0.71	0.87
3. GFDL CM2.0	2.94	0.85	0.38
4. CSIRO Mk3.0	3.08	0.66	0.54
5. MRI CGCM2.3.2a	3.22	0.45	0.78
6. CCCma CGCM3.1 (T47)	3.65	0.83	0.93
7. MIROC 3.2 (medium res.)	4.00	1.05	0.65
8. UKMO HadGEM1	4.45	1.07	0.72
Multi-model mean	3.35	0.80	0.64

3.3.2 HadSM3 experiments

Stuber et al. [2011, manuscript in preparation] carried out a number of idealised aerosol perturbation experiments as well as $2\times CO_2$ and +2% solar constant experiments using HadSM3 in order to investigate mechanisms of tropospheric adjustment. HadSM3 [*Williams et al.*, 2001], the slab ocean configuration of the Hadley Centre Unified Model (v.4.5), includes the direct and semi-direct effects of aerosols, but not the indirect effects. A globally-homogeneous layer of either purely scattering (single scattering albedo = 1) or partially absorbing aerosol was introduced at one of low-cloud level (LC), middle-cloud level (MC), high-cloud level (HC) or a tropopause-following level (UT). For the absorbing aerosol they chose a single scattering albedo of 0.75 to result in warming for the LC case. The mixture of aerosols in the real world has been estimated to have a single scattering albedo of 0.8-0.96 [*Hansen et al.*, 1997]. Their study showed that the surface temperature response to a purely scattering aerosol perturbation is largely independent of the height at which the perturbation is applied, but for absorbing aerosol the response is strongly dependent on the height of the perturbation, with some cases giving surface

warming and others giving surface cooling in agreement with *Hansen et al*. [1997]. The climate was less sensitive to scattering aerosol than CO_2 at all altitudes regardless of whether the standard instantaneous/stratosphere-adjusted forcing or the regression troposphere-adjusted forcing was used. For absorbing aerosol it was not possible to predict the sign of the temperature response using the standard forcing and the climate sensitivity parameter determined from the regression forcing was greater than that for $2\times CO_2$ for all perturbation heights except for the MC case.

The radiative flux and surface air temperature outputs of these $2\times CO_2$, +2% solar constant, HC absorbing aerosol (HCabs), and LC scattering aerosol (LCscat) experiments were used in this study. Although not realistic, these two aerosol experiments were chosen as they give a good range of climate sensitivity parameters and radiative forcing even after allowing for tropospheric adjustments (see Table 3.3) and therefore will provide a good test of how constant the pattern of feedbacks are under different forcing patterns. Despite the aerosol perturbation being applied homogeneously across the world, both the instantaneous forcing and troposphere-adjusted forcing were far from homogeneous. The methods for determining local feedback parameters, equilibrium partial temperature responses and contributions to polar amplification using the regression forcing as described in Section 3.2 were applied. The three-dimensional specific humidity and temperature fields were not available from *Stuber et al.* [2011, manuscript in preparation] and therefore the CMIP3 multi-model mean Planck feedback was used for all HadSM3 forcing mechanisms. The inter-model differences in CMIP3 Planck feedback are very small and therefore using a model-specific Planck feedback parameter would make little difference to the results.

3.4 Results

3.4.1 How well does the linear model of feedback fit?

The goodness of fit was determined using an F-test from the linear regressions. In the global mean, the linear model of feedback generally fits very well for all components (p-value≈1), agreeing with previous work [e.g. *Gregory and Webb*, 2008]. However, for one CMIP3 model in the annual mean and a few models in different seasons the longwave and/or shortwave cloud global mean regressions gave a p-value as low as 0.2. In these cases the feedback parameter was very small so

there is virtually no correlation between radiative flux change and surface temperature change.

The regressions in the polar regions and tropics generally gave good linear fits in the annual mean but in some seasons for some models the tropical shortwave cloud feedback gave a poor linear fit (p-value <0.1). As with the global mean, this again was due to the feedback being very small. When the p-value becomes less than 0.1 this may suggest the linear analysis becomes seriously questionable. However, the error in the feedback in these cases is not large. Where results from these regressions are shown, the associated errors are also shown, where possible, which should give a better indication of the appropriateness of the linear model.

In the zonal mean, it was again found for all feedbacks in all seasons and the annual mean the p-value dropped to ~0.1 when the feedback parameter was very small, i.e. crosses the zero line. This happens more often for cloud feedbacks. It also happens for a few models in some seasons for water vapour plus lapse rate feedback near the equator when the water vapour plus lapse rate and Planck feedbacks completely oppose each other, although generally the longwave clear sky regressions are very good. The regressions on the multi-model mean of the radiative flux and temperature changes were generally better in all seasons than those for individual models because taking a mean of multiple simulations averages out some noise. The standard deviations obtained from the regressions are still small compared to the variations in the feedback parameter across the latitudes and thus I believe the overall patterns of feedback are robust. An assessment was made of a random sample of the residuals in ΔR plotted against the expected ΔRs. These residuals were mostly found to be evenly distributed suggesting the linear model is appropriate. Only in three cases (for surface albedo feedback around 60°S for CSIRO Mk3.0, UKMO HadGEM1 and MIROC 3.2 medres) was there any suggestion of non-linearity. In these cases the surface albedo feedback is reducing slightly as the temperature increases. This also has the effect of giving a non-zero intercept which would not be expected for the Winton shortwave albedo regressions. Figure 3.1 shows the annual mean zonal mean regressions for the UKMO HadGEM1 model (good linear fits) and the MRI CGCM2.3.2a model (worst linear fits) at 60°S (one of the best locations for linear fit) and 30°N (one of the worst locations for linear fit).

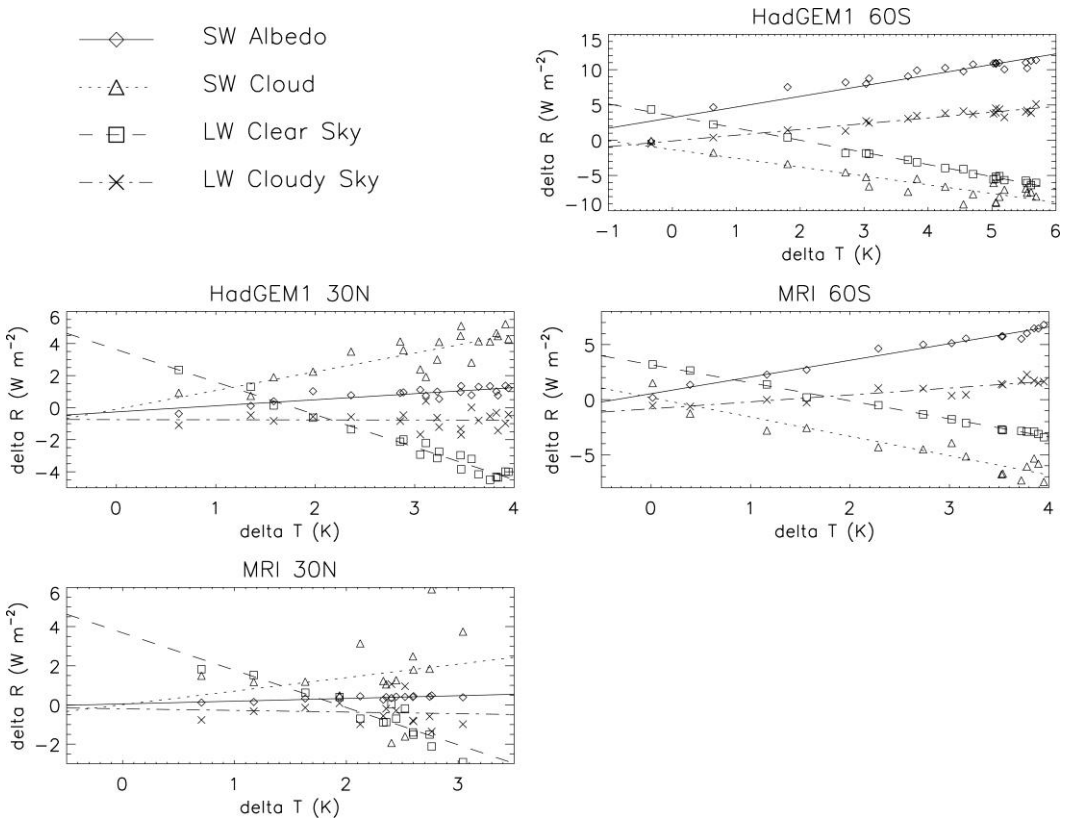

Figure 3.1: Examples of illustrative zonal mean regressions of ΔR against ΔT_s for 2 models at 60°S and 30°N. From Crook et al. [2011].

Performing the regressions in each 10˚×10˚ grid box gave poor linear fits (p-value<0.2) in many locations for the surface albedo, shortwave cloud and longwave cloudy sky (CRF) components and over a few tropical locations for the longwave clear sky component. Given these results I suggest that linear analysis is not applicable to 10˚×10˚ grid boxes but is applicable to zonal means. Therefore further discussions concentrate on results from zonal mean regressions and from polar and tropical regressions, and only for the features where linear fit is good.

3.4.2 Comparison between different forcing definitions

The annual mean forcing determined by regression and the archived stratosphere-adjusted forcing, where available, are shown for each model in Figure 3.2. The regression forcing follows a similar pattern to the stratosphere-adjusted forcing, being positive everywhere with a maximum near the equator and minima at the poles. The stratosphere-adjusted forcing is mostly within plus/minus two

standard deviations of the regression forcing, but differences would be expected due to rapid tropospheric adjustments.

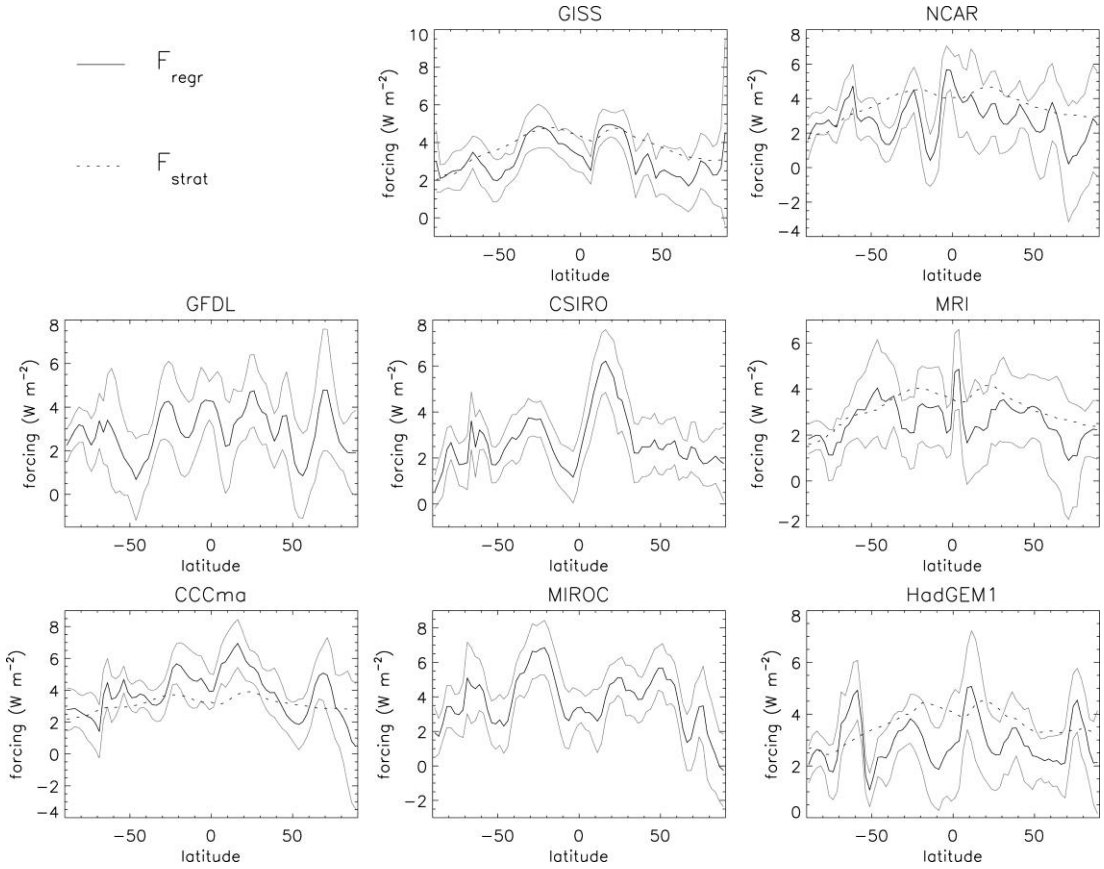

Figure 3.2: Annual mean, zonal mean forcing for CMIP3 models. The solid black lines show the forcing determined from regression and the dotted lines show the archived stratosphere-adjusted forcing where available. The grey lines show ±2σ for the regression forcing. From Crook et al. [2011].

The feedback parameters and the equilibrium partial temperature responses for the 2×CO2 CMIP3 experiments, as calculated from the stratosphere-adjusted forcing (where available) and the mean equilibrium radiative flux and surface temperature changes, showed a similar zonal mean pattern to those calculated by regression. The differences between the two methods are significant in a small number of latitudes, particularly for the cloud related components, but the feedback parameters and equilibrium partial temperature responses from the stratosphere-adjusted forcing are generally within plus/minus two standard deviations of those calculated using F_{regr} (not shown). The global mean regressions give very similar results to those of *Gregory and Webb* [2008] and *Andrews and Forster* [2008] who show there is a small but significant tropospheric adjustment in the global mean

forcing for CO_2. Small differences between the methods in the zonal mean may add up to more significant differences in the global mean (note that errors in the zonal means are greater than in the global mean). Many studies have shown that for aerosols, the difference between the instantaneous/stratosphere-adjusted and troposphere-adjusted forcing is considerable and argue that the rapid tropospheric adjustments should be included within the forcing rather than the feedback, making the climate sensitivity parameter closer to that for $2\times CO_2$ [*Hansen et al.*, 1997; *Hansen et al.*, 2005; *Shine et al.*, 2003; *Lohmann et al.*, 2010]. My own work supports these previous studies in that the zonal mean pattern of feedback parameters for the HadSM3 HCabs experiment, as calculated from the instantaneous forcing (Figure 3.3), was unphysical (e.g. values of around -100 W m^{-2} K^{-1} for the longwave cloudy sky feedback in some latitudes). Therefore, only the results from the regression method are discussed further.

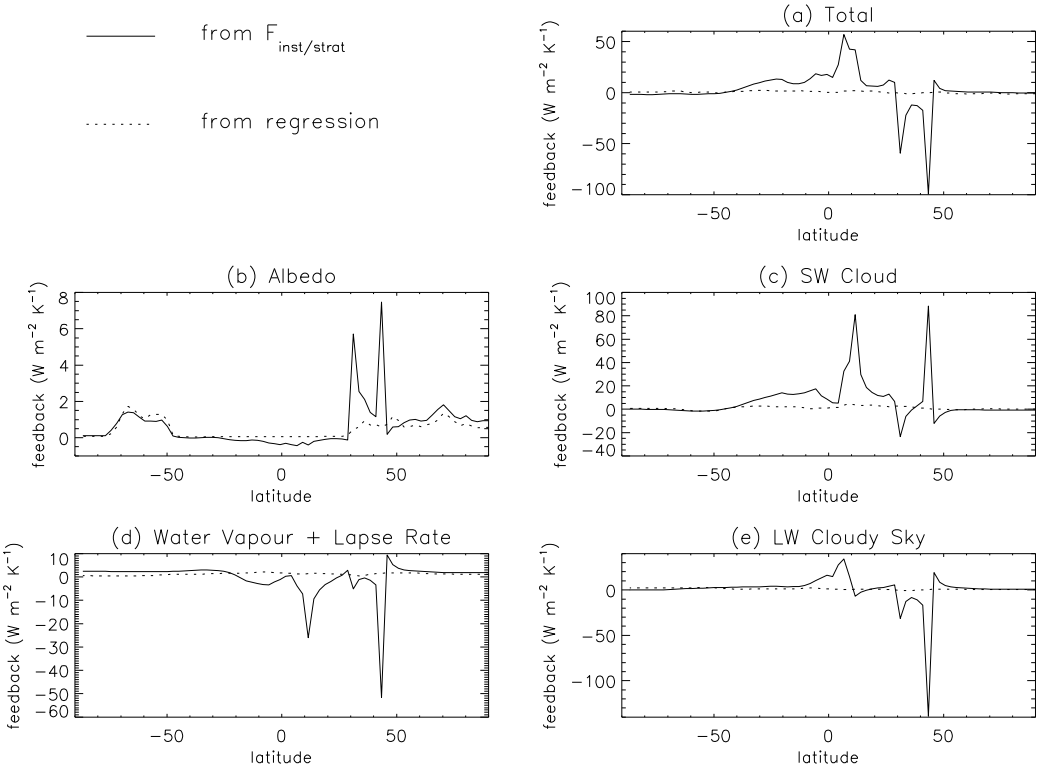

Figure 3.3: Zonal mean feedback patterns for the HCabs experiment using the instantaneous forcing (solid) and from regression (dotted).

3.4.3 Patterns of feedback from 2×CO2 experiments

Figure 3.4 shows the shortwave clear sky feedback, shortwave cloudy sky (CRF) feedback, surface albedo (Winton) feedback and shortwave cloud (Winton) feedback for the NCAR CCSM3.0 model for annual means. The plus/minus two standard deviations in the feedbacks from the regressions are also shown to illustrate the typical errors in the zonal mean feedbacks. This figure shows that clouds provide masking of the surface albedo feedback in the cryosphere regions reducing its strength to about half that of the shortwave clear sky feedback. This is true of all seasons and typical of all the models analysed, although the strength of the masking does vary to some extent. Note that *Qu and Hall* [2006] determined that changes in planetary albedo are about half the change in surface albedo and that this fraction did not vary considerably between the 17 models analysed. The shortwave CRF feedbacks and the Winton feedbacks behave very similarly in tropical regions showing that cloud masking has little effect on this region.

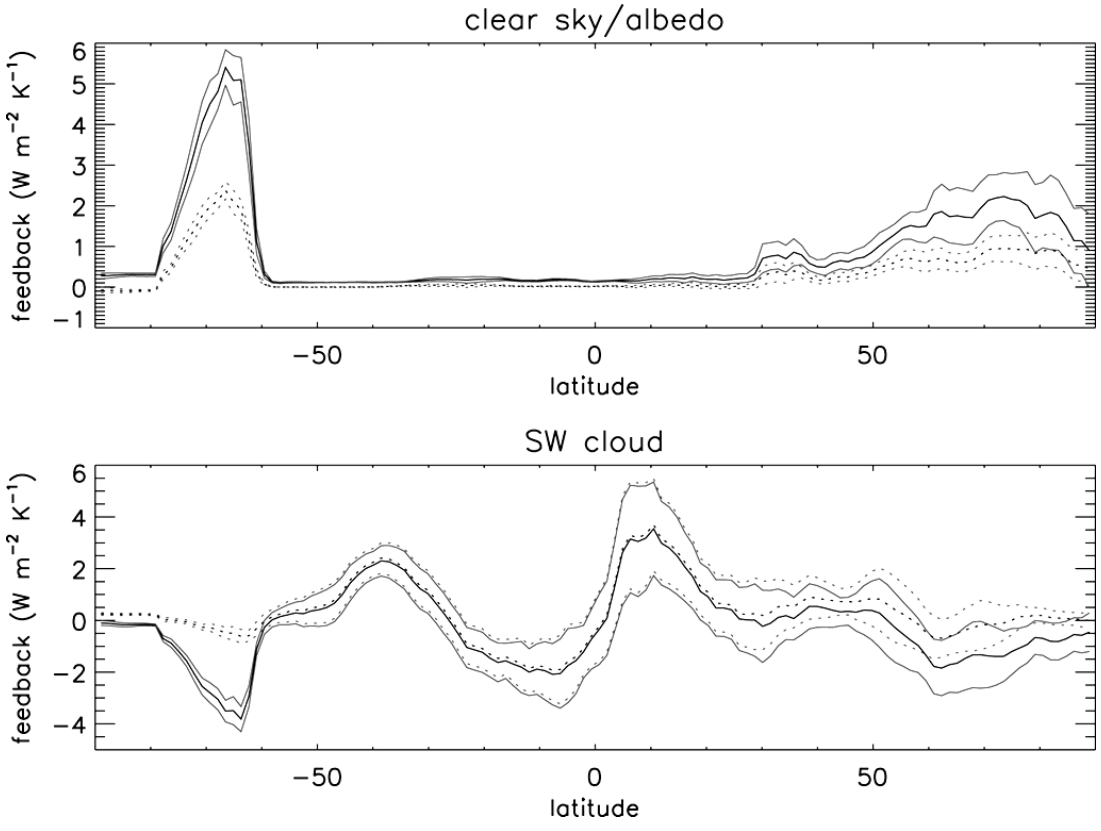

Figure 3.4: Annual mean, zonal mean shortwave feedback parameters for the NCAR CCSM3.0 model forced with 2×CO_2. The solid line uses the CRF method, and the dotted line uses the Winton method. The grey lines indicate ±2σ. From Crook et al. [2011].

The feedback parameters from the zonal mean regressions for annual means and all models are shown in Figure 3.5, and feedback parameters for the multi-model mean zonal mean regressions for seasonal means are shown in Figure 3.6. The multi-model mean feedback patterns show seasonal behaviour typical of most models. The Planck feedback (Figure 3.5a and Figure 3.6a) is negative everywhere and is the most uniform feedback across latitudes, but is slightly more negative in the tropics due to its higher temperatures. It varies seasonally more in higher latitudes where there is greater seasonal variation in temperature.

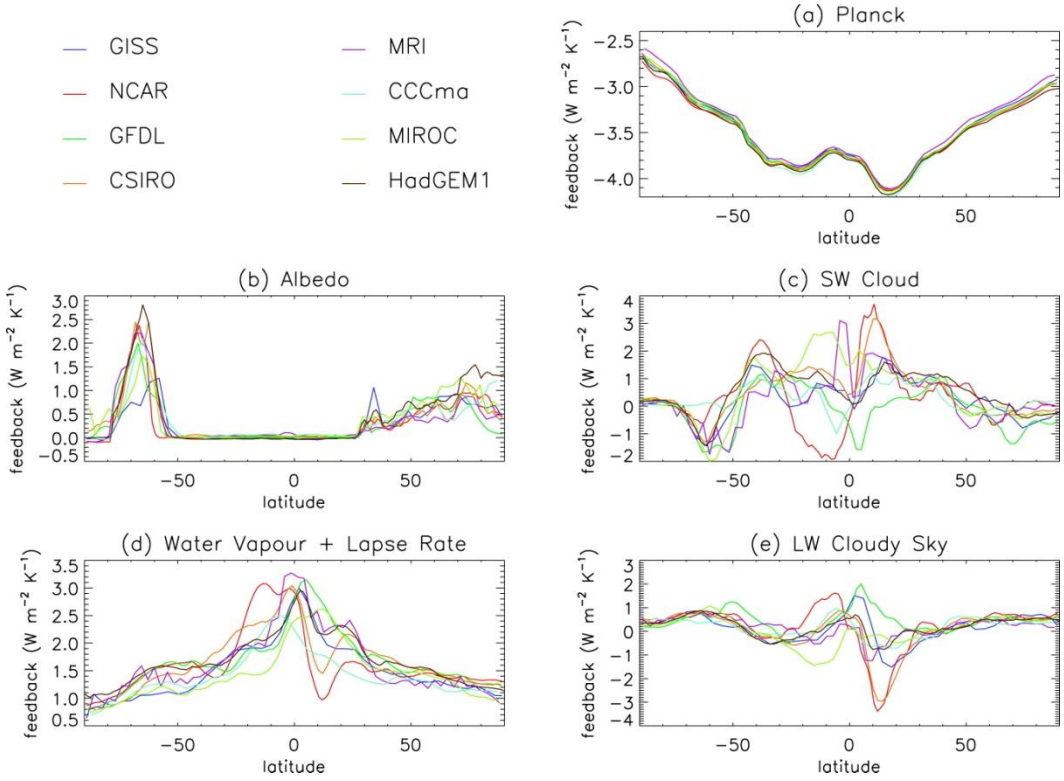

Figure 3.5: Annual mean, zonal mean feedback parameters for the different models forced with 2×CO2. From Crook et al. [2011].

The shortwave feedbacks obviously have no effect poleward of about 65° during the winter when sunlight is absent. The SH sea ice zone shows very strong positive surface albedo feedback in the SH spring and summer, and a much less positive surface albedo feedback in the SH autumn and winter (Figure 3.6b). This peak tends to move poleward through the SH spring and summer, following the northern edge of the sea ice as it retreats poleward and more solar radiation reaches

higher latitudes. The greatest variation between models in the location of this peak (up to 5˚) occurs in the SH spring, whereas the greatest variation in the height (strength of the feedback) of this peak (up to 12 W m^{-2} K^{-1}) occurs in the SH summer (not shown). The surface albedo feedback poleward of 80°S is very small in all seasons. From 50°S to 25°N there is essentially no surface albedo feedback in any season.

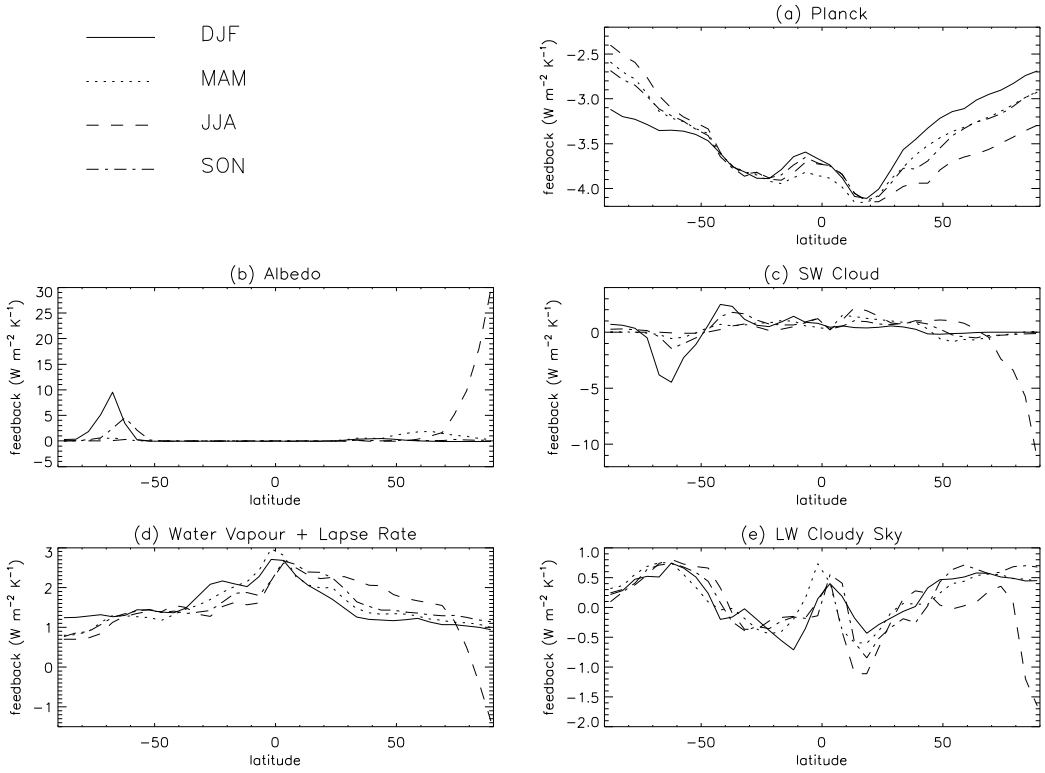

Figure 3.6: 2×CO_2 experiments multi-model mean, zonal mean feedback parameters for each season. From Crook et al. [2011].

In the NH there is positive surface albedo feedback in the annual mean from 25°N to 90°N. This positive feedback is constrained to 25°N to 55°N in the NH winter due to absence of sunlight in high latitudes. The peak centred on 33°N (Figure 3.5b) is due to the Himalaya. In the NH spring the greatest surface albedo feedback is from 45°N to 75°N mainly due to snow over land, whereas during the NH summer the peak narrows and moves poleward. Snow over land has largely melted by the summer but the sea ice melts later in the year. There is very little surface albedo feedback in the NH autumn when snow and ice coverage is small. The eight models behave very differently in the NH summer poleward of 80°N (differences >10 W m^{-2}

K^{-1}) where three models have a surface albedo feedback that becomes negative (not shown). For most of these models the error in the feedback at these high latitudes during summer is quite large and, therefore, these results should be interpreted with caution. The GISS ER model behaves quite differently to other models in having the weakest annual mean surface albedo feedback in the SH sea ice zone but the strongest annual mean surface albedo feedback in the Himalaya (Figure 3.5b). This weak annual mean surface albedo feedback in the SH sea ice zone contributes to it having one of the smaller equilibrium temperature changes and a small SH polar amplification (see Table 3.1).

The shortwave cloud (Winton) feedback (Figure 3.5c and Figure 3.6c) generally shows strong negative feedback co-located with the positive surface albedo feedback. Low cloud tends to increase where sea ice melts leading to the anti-correlation between surface albedo and shortwave cloud feedback. However, the strength of this anti-correlation varies with models, and for CCCma CGCM3.1 (T47) there is no correlation at all (Figure 3.5c). In low and mid latitudes there is considerable difference (up to 4-7 W m^{-2} K^{-1} depending on the season) between models in shortwave cloud (Winton) feedback (not shown), although the errors in the feedback may be up to ±2 W m^{-2} K^{-1} here. This is also true for the longwave cloudy sky feedback (differences up to 5 W m^{-2} K^{-1}) (not shown). The longwave cloudy sky feedback (Figure 3.5e and Figure 3.6e) tends to be anti-correlated with the shortwave cloud (Winton) feedback, although this is much clearer in spring and autumn and is not the case in high NH latitudes in summer. More cloud in general would lead to more shortwave reflection (negative feedback) but more trapping of longwave radiation (positive feedback).

The water vapour plus lapse rate feedback (Figure 3.5d and Figure 3.6d) is generally positive everywhere and tends to be higher in the tropics. However, negative water vapour plus lapse rate feedback is found in summer for MIROC 3.2 and UKMO HadGEM1 around 80°N (not shown) and for the multi-model mean poleward of 80°N, but note that the errors are quite large here. In the tropics there is more inter-model spread (up to 2 W m^{-2} K^{-1}) (not shown). It should be noted that, unlike the shortwave analysis, the methodology used in this study cannot evaluate cloud masking effects in the longwave; if these had been taken into account this feedback strength would have been reduced [*Soden et al.*, 2008]. The lapse rate

feedback has been shown to be negative in the tropics and positive at high latitudes [*Bony et al*., 2006] suggesting that the feedback due to water vapour alone must be particularly high in the tropics. The clear tropical pattern in the NCAR CCSM3.0 model with significantly different feedback strength in each hemisphere is seen in the water vapour plus lapse rate feedback and both cloud feedbacks (Figure 3.5). It is likely that water vapour and cloud amount are positively correlated [*Soden et al*., 2008].

3.4.4 Equilibrium partial temperature responses from 2×CO2 experiments

Not surprisingly, the patterns of equilibrium partial temperature responses (Figure 3.7) for the different feedbacks are similar to the patterns of feedbacks themselves, but high latitude temperature responses are enhanced because the magnitude of the Planck feedback is less at high latitudes (note I am dividing by the Planck feedback to obtain the temperature response, equation 2.13) and the temperature response required to balance the forcing is therefore greater at high latitudes [*Joshi et al*., 2003]. Also the temperature response due to each feedback is affected by the strength of other feedbacks.

The surface albedo feedback gives a positive temperature response which is greatest in high latitudes in spring and summer (Figure 3.7a). The spread of surface albedo feedback equilibrium partial temperature responses between the different models is also greatest for these seasons (up to 12 K for the SH sea ice zone and ~5 K for the NH polar region) (not shown).

The shortwave cloud (Winton) feedback tends to cool the high latitudes and warm the low latitudes with the greatest high latitude cooling occurring in the spring and summer (Figure 3.7b). There is a large inter-model spread of shortwave cloud (Winton) equilibrium partial temperature responses in the tropics in all seasons (~4 K) and in high latitudes in summer (~7 K) (not shown).

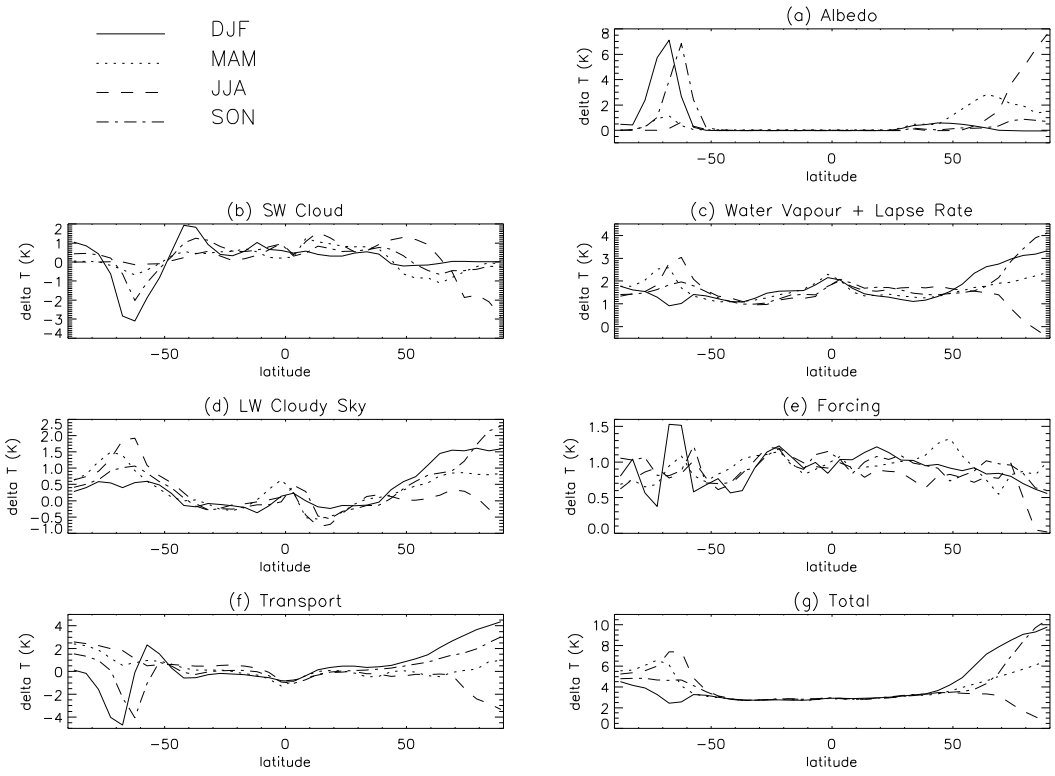

Figure 3.7: 2×CO_2 experiments multi-model mean, zonal mean equilibrium partial temperature responses for each season. From Crook et al. [2011].

The water vapour plus lapse rate feedback tends to warm the NH mid to high latitudes and the SH sea ice zone most in autumn and winter (Figure 3.7c). The inter-model spread in the polar regions in these seasons is ~3 K (not shown). Given that this feedback has not been adjusted for the masking effect of clouds in the longwave, the water vapour plus lapse rate feedback equilibrium partial temperature response would likely be less positive than shown.

The longwave cloudy sky feedback tends to warm the mid to high latitudes, particularly in autumn and winter (Figure 3.7d). The tropics show greatest spread between models (~3 K) for the longwave cloudy sky equilibrium partial temperature response (not shown). With cloud masking effects removed, it is likely that the equilibrium partial temperature response due to longwave cloud effects would be more positive than shown.

The equilibrium partial temperature response due to the forcing is generally more uniform across latitudes (Figure 3.7e) but there is a spread of up to 2 K between models (not shown). Errors in the equilibrium partial temperature response due to the

forcing, shortwave cloud and longwave cloudy sky feedbacks can be up to 1 K (not shown).

In the annual mean when the transport term just includes meridional heat transport, it can be seen that there is decreased transport of heat into the SH sea ice zone, counteracting the strongly positive sea ice albedo feedback (Figure 3.7f). In the SH spring and summer when the albedo feedback is strongest, the transport term, which also includes the seasonal heat storage term, is particularly negative in the SH sea ice zone. The same effect can also be seen in the NH summer. In both hemispheres in autumn and winter, the transport term generally warms the high latitudes. The largest spread in the temperature response due to the transport term between models occurs in the high latitude summers (up to 10 K in the SH and 8 K in the NH) (not shown). Further analysis is required to separate the contributions from heat storage and heat transport in the different seasons. *Lu and Cai* [2009a] found longwave CRF and ocean heat release contributed positively to the seasonal pattern of high latitude warming, but these were secondary to the contribution from their clear sky downward longwave component. They used the surface energy budget to perform their calculations and therefore did not separate the components in the same way as this study; their clear sky downward longwave component included poleward sensible and latent heat transport and the forcing as well as water vapour feedback; their vertical latent and sensible heat fluxes (manifested as lapse rate feedback and included with water vapour feedback here) and ocean heat storage (included with the transport term here) were separated.

The global mean annual mean equilibrium partial temperature responses were calculated from the zonal mean regression results so that the transport term was not lost in the other terms which would be the case if the global mean regression results were used (ΔR goes to zero in the annual global mean at equilibrium). However, the results are not very different from the global mean regression results. The ensemble mean of these equilibrium partial temperature responses for all the models plus/minus two standard deviations and the multi-model mean equilibrium partial temperature responses plus/minus two standard deviations are shown in Table 3.2. The water vapour plus lapse rate feedback was found to contribute most to the inter-model spread of equilibrium partial temperature response. The shortwave cloud (Winton) feedback gives the second greatest inter-model spread. This contrasts with

Dufresne and Bony [2008] who found the temperature contribution from cloud feedback contributed considerably more inter-model spread than any other feedback. Differences may be partly accounted for as they used a stratosphere-adjusted forcing and performed their calculations with AOGCMs. *Andrews and Forster* [2008] also found that use of the regression forcing rather than the stratosphere-adjusted forcing reduced the inter-model spread of cloud feedback. In this study the equilibrium partial temperature response due to the forcing gives the third greatest contribution to inter-model spread.

Table 3.2: $2\times CO_2$ experiments annual mean global mean equilibrium partial temperature responses and partial polar amplifications.

Partial temperature	**global mean $\Delta T_x \pm 2\sigma$ (K)**	**PA_x^{NH} (eqn. 3.3) as % of total ± 2σ**	**PA_x^{SH} (eqn. 3.4) as % of total ± 2σ**
Surface Albedo	0.35 ± 0.26 [a]	55.7 ± 23.7 [a]	115.3 ± 94.0 [a]
	0.35 ± 0.01 [b]	54.6 ± 2.8 [b]	100.9 ± 3.3 [b]
Shortwave Cloud	0.40 ± 0.48 [a]	-50.8 ± 52.5 [a]	-92.8 ± 194.1 [a]
	0.36 ± 0.03 [b]	-45.9 ± 5.5 [b]	-62.4 ± 4.0 [b]
Water vapour plus Lapse rate	1.57 ± 0.57 [a]	19.2 ± 27.3 [a]	-9.2 ± 134.1 [a]
	1.56 ± 0.01 [b]	22.8 ± 2.0 [b]	17.1 ± 2.8 [b]
Longwave cloudy sky	0.12 ± 0.23 [a]	41.9 ± 32.2 [a]	72.7 ± 129.7 [a]
	0.12 ± 0.02 [b]	39.8 ± 2.5 [b]	55.2 ± 2.9 [b]
Forcing	0.91 ± 0.30 [a]	-9.5 ± 19.0 [a]	-5.6 ± 38.0 [a]
	0.95 ± 0.02 [b]	-6.9 ± 7.1 [b]	-3.2 ± 7.4 [b]
Transport	0.01 ± 0.12 [a]	43.5 ± 61.9 [a]	19.6 ± 153.7 [a]
	0.01 [b]	35.7 [b]	-6.7 [b]

a = mean of all models

b = multi-model mean regression results

3.4.5 Polar amplification contributions from 2×CO2 experiments

Both the NH and SH show the greatest warming during their respective winters and the least warming during their respective summers, whereas the tropics show little variation throughout the seasons (Figure 3.7). The partial polar amplifications for all models in each season and the annual mean are shown in

Figure 3.8 and Figure 3.9 for the NH and SH respectively. The error (plus/minus two standard deviations) for each partial polar amplification is also included. In all seasons the transport term consists of contributions from horizontal heat transport and heat storage.

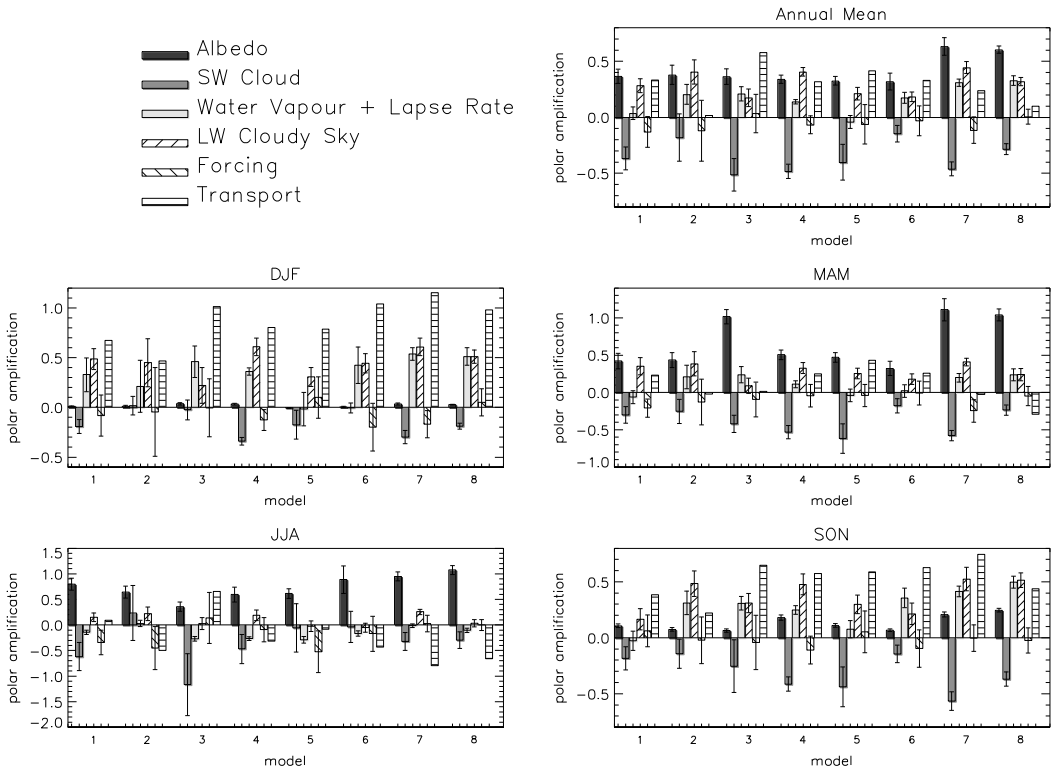

Figure 3.8: NH partial polar amplifications (eqn. 3.3) for each model forced with 2×CO2 for the annual mean and the different seasons. Model numbers are given in Table 3.1. From Crook et al. [2011].

In summer there is virtually no polar amplification especially in the NH despite there being a large warming due to the surface albedo feedback. This is counteracted largely by high latitude cooling due to the transport term and/or shortwave cloud (Winton) feedback. *Lu and Cai* [2009a] also found the large contribution from surface albedo feedback was counteracted by negative CRF in the shortwave. For some models, the water vapour feedback and/or forcing also warm the tropics considerably more than the polar region.

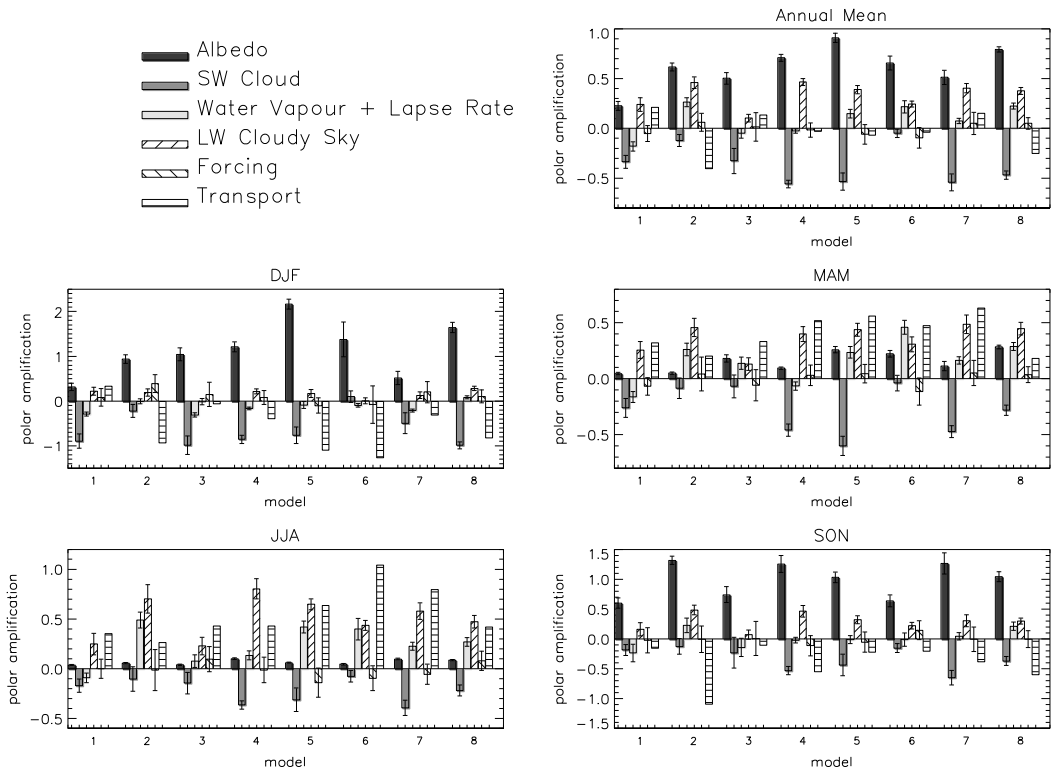

Figure 3.9: SH partial polar amplifications (eqn. 3.4) for each model forced with 2×CO2 for the annual mean and the different seasons. Model numbers are given in Table 3.1. From Crook et al. [2011].

In autumn and winter, the main positive contributors to both the NH and SH polar amplification are the transport term, followed by longwave cloudy sky feedback. For some models, the water vapour plus lapse rate feedback also has a non negligible contribution.

In spring, the main positive contributors to the both the NH and SH polar amplification are the surface albedo feedback, followed by longwave cloudy sky feedback, although some models in the NH have a noteworthy contribution from the transport term and water vapour plus lapse rate feedback.

In all seasons the shortwave cloud (Winton) feedback gives a negative contribution for all models except for NCAR CCSM3.0 which has a positive contribution to the NH polar amplification and CCCma CGCM3.1 (T47) which has a positive contribution to the SH polar amplification in their respective summers. For NCAR CCSM3.0 the partial temperature response due to shortwave cloud (Winton) feedback in summer is negative above 80°N but positive between 60°N and 80°N (not shown), giving an overall positive contribution to the NH polar

amplification. The anti-correlation between albedo and shortwave cloud feedback is strongest where sea ice melts and other factors may play an important part in shortwave cloud feedback over NH high latitude land. It should be noted that the error in the shortwave cloud feedback partial polar amplification for the NCAR CCSM3.0 model is large, suggesting that this partial polar amplification could actually be negative. As mentioned earlier CCCma CGCM3.1 (T47) is unusual in not showing the anti-correlation between surface albedo and shortwave cloud feedbacks in the SH sea ice zone. Further analysis would be required to understand why this might be.

The ensemble mean of the annual mean partial polar amplifications as percentages of the total polar amplification are given in Table 3.2. The annual mean partial polar amplifications as percentages of the total polar amplification for the multi–model mean regression results are also given. These data indicate that the surface albedo feedback gives the greatest contribution in both hemispheres in the annual mean. In the NH the next greatest contribution comes almost equally from the horizontal heat transport and longwave cloudy sky feedback, followed by the contribution from the water vapour plus lapse rate feedback. In the SH the next greatest contribution comes from the longwave cloudy sky feedback. Horizontal heat transport and water vapour plus lapse rate feedback give the next greatest contributions. There is generally more inter-model spread in the annual mean SH polar amplification, but in both hemispheres this spread comes mostly from the contributions from horizontal heat transport and shortwave cloud (Winton) feedback.

3.4.6 Patterns of forcing and feedback from HadSM3 experiments

Both the zonal mean instantaneous and regression forcings were found to be highly inhomogeneous for the HCabs experiment despite a homogeneous aerosol change (Figure 3.10a). The zonal mean regression forcing was found to be more inhomogeneous and considerably reduced compared to the instantaneous forcing resulting in positive forcing in high latitudes and negative forcing in the tropics. Rapid adjustments in clouds, lapse rate and water vapour mixing ratio cause the difference between the regression and instantaneous radiative forcings. Details of these changes are described more fully in *Stuber et al.* [2011, manuscript in preparation]. The regression forcing is virtually identical to the instantaneous forcing

in the shortwave clear sky component, but the other three components show large differences particularly in the cloudy sky components (Figure 3.10b, c, d and e).

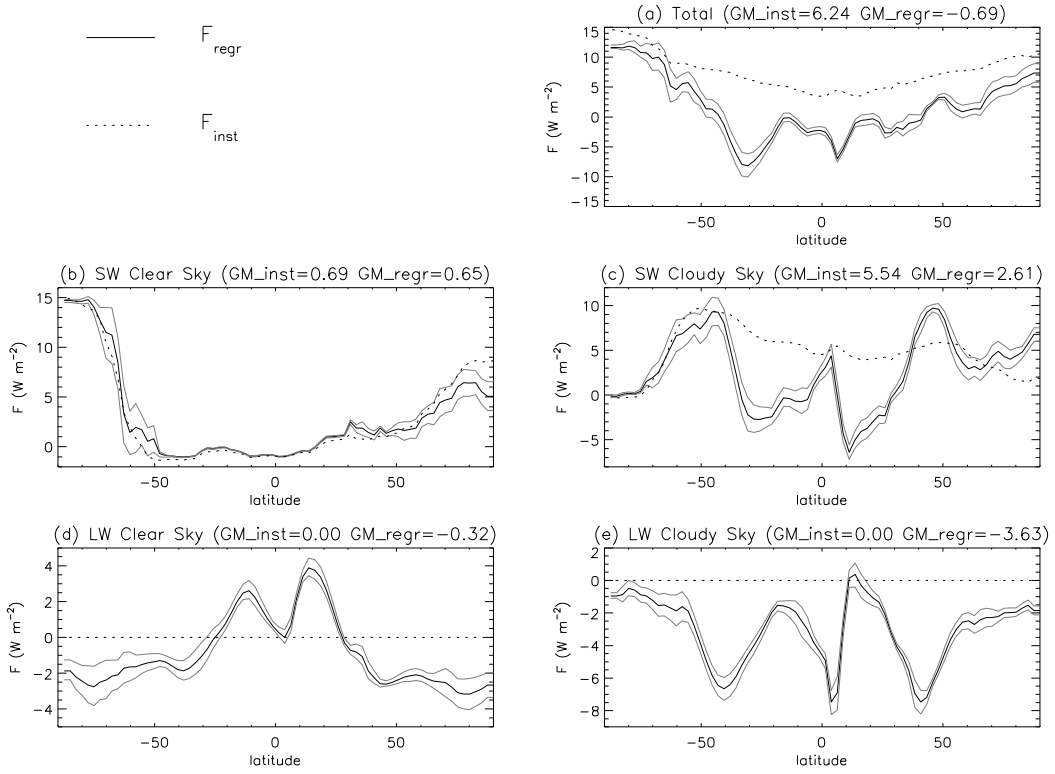

Figure 3.10: Annual mean, zonal mean instantaneous and regression forcing for HadSM3 HCabs experiment. The grey lines show ±2σ for the regression forcing. From Crook et al. [2011].

The high cloud was found to decrease immediately whereas the low and mid cloud increase a little immediately and then increase further throughout the integration. The initial cloud changes result in reducing the shortwave and longwave cloudy sky forcings (Figure 3.10c and e). The further increases in mid and low cloud combine to form the total cloud feedback.

The equilibrium temperature profile response shows a decrease in the lapse rate which is particularly strong in the high latitudes (not shown). In the global mean, this lapse rate decrease is already manifested after two years. This would give a negative forcing in the global mean. The water vapour mixing ratio initially increases in the troposphere (positive forcing) but in the stratosphere it decreases in the tropics (negative forcing) and increases in the high latitudes (positive forcing). The combined effects of lapse rate and water vapour adjustments give rise to the

longwave clear sky component of the regression forcing (Figure 3.10d). Throughout the integration there is a further decrease in stratospheric water vapour in the tropics which would contribute positively to the tropical water vapour plus lapse rate feedback.

The feedbacks from regression show similar patterns for all forcing mechanisms, but the 2×CO_2 and +2% solar forcing have the most similar patterns (Figure 3.11).

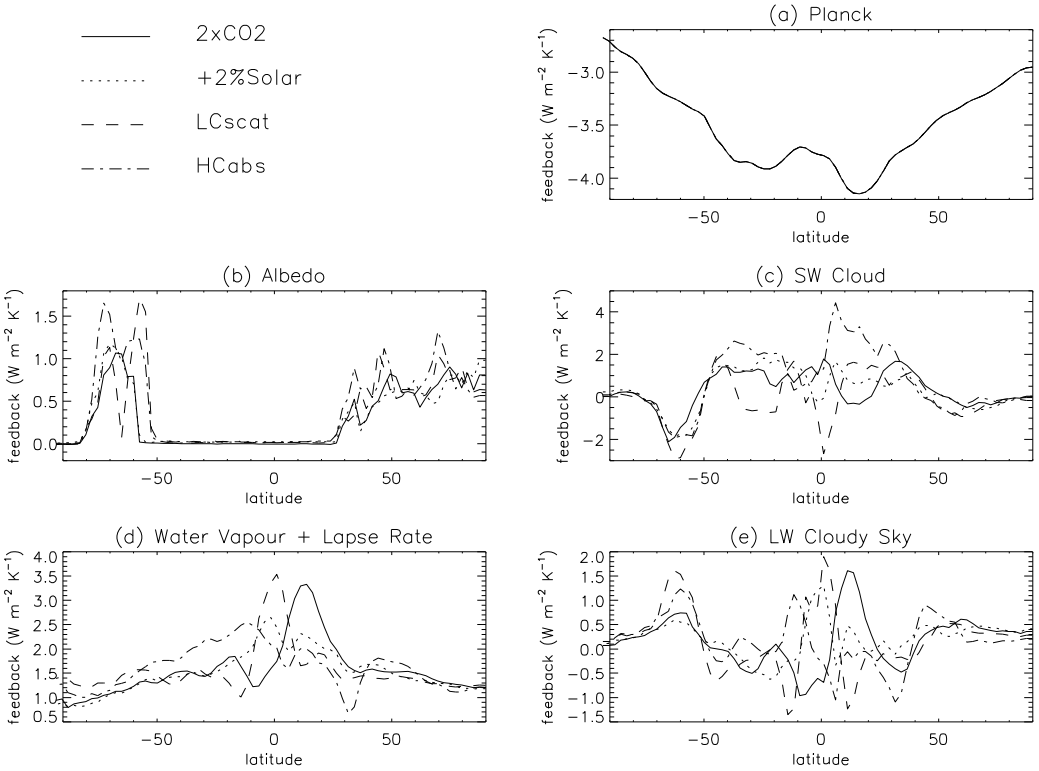

Figure 3.11: HadSM3 annual mean zonal mean feedback patterns for the different forcing mechanisms.

The surface albedo feedback appears stronger for aerosol forcing than 2×CO_2 and +2% solar forcing particularly in the SH and also extends closer to the equator in the SH due to the ice edge being closer to the equator in the colder temperatures of the aerosol-forced simulations. This can also be seen in the temperature response due to the surface albedo feedback (Figure 3.12a). The shortwave cloud (Winton) feedback has a more variable pattern for aerosol forcing in the tropics and is generally more positive for the HCabs experiment and less positive for the LCscat experiment than 2×CO_2 and +2% solar experiments. The water vapour plus lapse rate feedback and the longwave cloudy sky feedback show greatest variation

between forcing mechanisms in the tropics. The longwave cloudy sky feedback is also greater for both aerosol experiments than $2\times CO_2$ and +2% solar experiments in the SH sea ice zone. This is also apparent in the temperature response (Figure 3.12d).

3.4.7 Equilibrium partial temperature responses from HadSM3 experiments

Equilibrium partial temperature responses for the HadSM3 experiments are shown in Figure 3.12. Given that the forcing patterns are different for each experiment one would not expect the temperature responses to be the same. However, the equilibrium temperature response pattern in the HCabs experiment does not match the regression forcing pattern in anyway, with cooling happening almost everywhere and the greatest cooling occurring in high latitudes (Figure 3.12e and g) where the forcing is strongly positive. The equilibrium partial temperature response due to the horizontal heat transport (Figure 3.12f) shows strongly reduced poleward heat transport in the HCabs experiment which counteracts the forcing (Figure 3.12e).

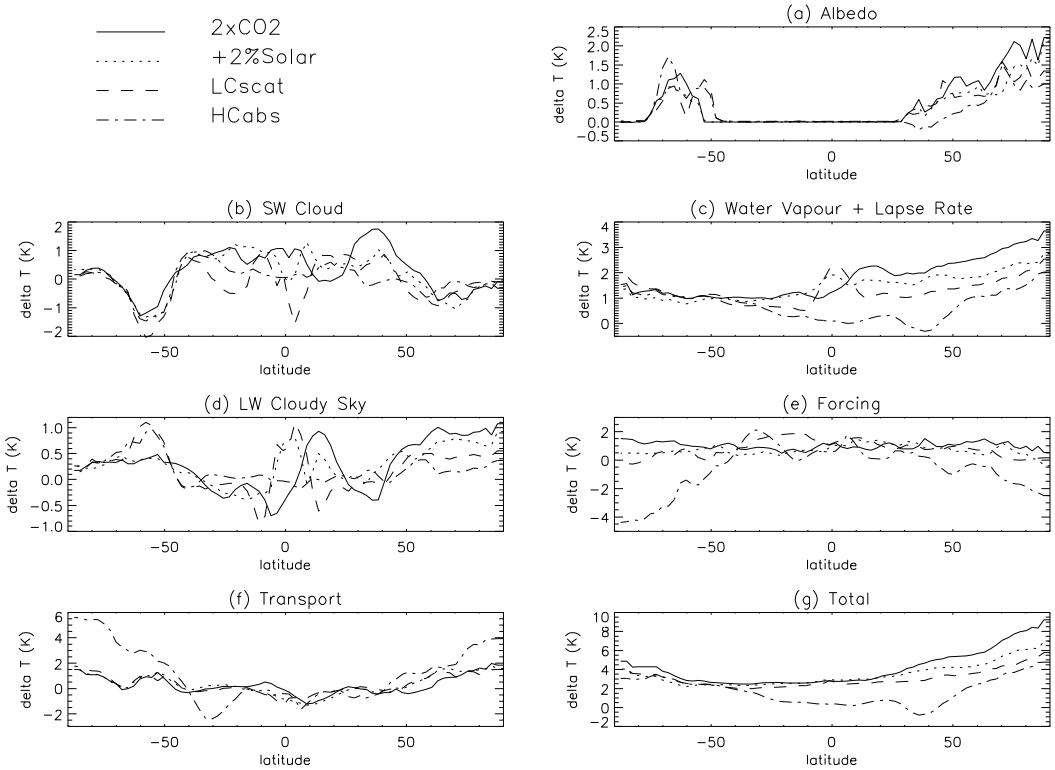

Figure 3.12: Annual mean, zonal mean equilibrium partial temperature responses for HadSM3 experiments. Note that for LCscat and HCabs the temperature responses have been multiplied by -1 for ease of comparison with 2×CO2 and +2% solar. From Crook et al. [2011].

Given that the zonal mean temperature is cooling throughout the integration, this implies the change in horizontal heat transport is manifested early. Analysis found that the Hadley circulation was slowed down causing the rapid decrease of stratospheric water vapour in the tropics.

The global mean equilibrium partial temperature response determined from the zonal means divided by the global mean regression forcing (Table 3.3) gives a measure of the contribution to the global mean climate sensitivity parameter (Figure 3.13).

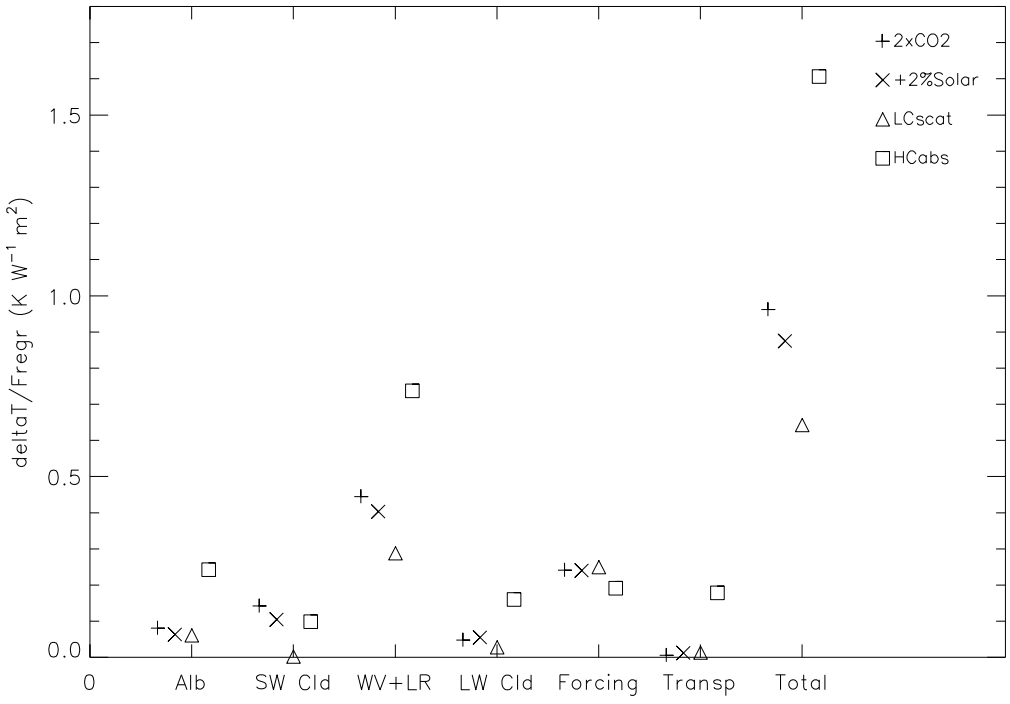

Figure 3.13: Components of the climate sensitivity parameter for HadSM3 experiments. The climate sensitivity parameter is determined as annual mean, global mean equilibrium partial temperature responses (determined from zonal mean regression) divided by the global mean radiative forcing from regression. From Crook et al. [2011].

The HCabs experiment has a higher climate sensitivity parameter due to the water vapour plus lapse rate feedback but also due to the surface albedo feedback, the horizontal heat transport and the longwave cloudy sky feedback. The LCscat

experiment has a lower climate sensitivity parameter because of the shortwave cloud (Winton) and water vapour plus lapse rate feedbacks.

3.4.8 Polar amplification contributions from HadSM3 experiments

The overall polar amplifications for the HadSM3 experiments are given in Table 3.3. The +2% solar and LCscat experiments have similar NH polar amplification and the $2\times CO_2$ experiment has a slightly larger NH polar amplification. In the SH, the polar amplification is most similar for the $2\times CO_2$ and LCscat experiments with the +2% solar experiment having the lowest polar amplification. The HCabs experiment has the largest polar amplification in both hemispheres by far. We do not show the polar amplification contributions from different feedbacks, forcing and horizontal heat transport, but it is clear from Figure 3.12 that in the HCabs experiment the horizontal heat transport plays a far more dominant role than in the other forcing mechanism experiments and the radiative forcing gives a strong negative contribution.

Table 3.3: HadSM3 experiments equilibrium temperature response, regression forcing, climate sensitivity parameter ($\Delta T_{s,eq}/F_{regr}$) and polar amplification.

Forcing mechanism	**global mean ΔT_s at equilibrium (K)**	**Global mean forcing from regression $\pm 2\sigma$ (Wm^{-2})**	**Climate Sensitivity parameter ($KW^{-1}m^2$)**	**Annual mean NH polar amp (eqn. 3.3)**	**Annual mean SH polar amp (eqn. 3.4)**
$2\times CO_2$	3.52	3.66 ± 0.20	0.96	1.11	0.15
+2% Solar	3.08	3.52 ± 0.33	0.87	0.77	-0.05
LCscat	-2.65	-4.13 ± 0.30	0.64	0.69	0.17
HCabs	-1.11	-0.69 ± 0.34	1.61	2.47	2.10

3.5 Conclusions

The eight different CMIP3 models forced with $2\times CO_2$ that were analysed show similar spatial patterns of feedback with similar seasonal behaviour. The greatest inter-model differences are in the pattern of shortwave cloud and longwave cloudy sky feedback in the tropics, in the water vapour plus lapse rate feedback in the tropics, and in the SH sea ice albedo feedback in summer. In this study the greatest inter-model differences in the annual global mean equilibrium temperature response

were found to come from the water vapour plus lapse rate feedback followed by the shortwave cloud feedback, unlike *Dufresne and Bony* [2008] who found the cloud feedback had by far the greatest inter-model differences. Although in the annual mean the greatest contribution to polar amplification is from the albedo feedback, there is a strong coincident negative contribution from shortwave cloud feedback. Considerable positive contributions from the longwave cloudy sky feedback and the transport term occur in autumn and winter. The seasonal transport term includes both horizontal heat transport and heat storage and further study is required to separate these terms. However, *Lu and Cai* [2009a] found the heat storage term to be only a secondary cause of the seasonality of polar amplification, although they do not separate out the heat transport term from longwave clear sky terms. The greatest inter-model spread in the annual mean polar amplification is due to horizontal heat transport and shortwave cloud feedback and therefore a better understanding of these from observations may help constrain models, although due to large internal variability in the polar regions, this may be difficult [*Stott and Jones,* 2009].

Spatial patterns of local climate feedback for a single model forced with four different forcing mechanisms having quite different radiative forcing patterns are quite similar. The equilibrium temperature response to high-level absorbing aerosol shows considerable differences compared to other forcing mechanisms in the contribution from horizontal heat transport and water vapour plus lapse rate feedback as well as from the forcing itself, leading to enhanced polar amplification and a greater climate sensitivity parameter.

Observations of the global mean temperature change and meridional temperature gradient trends over the 20th century cannot be explained by greenhouse gas, solar and ozone forcing alone. *Shindell and Faluvegi* [2009] used the residual to estimate sulphate (reflecting aerosol) and black carbon (absorbing aerosol) forcings over this time period. These estimated forcings are qualitatively consistent with historical emissions. Their calculations required the response per unit forcing for different forcing mechanisms in different regions which they obtained from a single model. Since the mid 1970s the difference between the Arctic and SH extratropics temperature has been increasing. *Shindell and Faluvegi* [2009] suggested that ozone, black carbon and the aerosol indirect effect have had a large impact on Arctic amplification due to their inhomogeneous distribution. Although the absorbing

aerosol experiment in this study was not realistic, it shows that an inhomogeneous distribution of aerosols is not required to produce an inhomogeneous forcing or response, and that the response is strongly dependent on changes in heat transport and the associated amplification of feedbacks. Further work is still required to unravel the complex nature of aerosol forcing, the associated potentially strong semi-direct effects and the considerable changes to poleward heat transport before specific causes of recent Arctic temperature change can be confidently attributed.

4 A Balance Between Radiative Forcing and Climate Feedback in the Modelled 20th Century Temperature Response

4.1 Introduction

Chapters 1 and 2 provided the background to this thesis with Chapter 2 concluding with the aims of this project, splitting the work into three work packages. This chapter describes the second of those work packages, addressing the question "Can the observed and modelled 20th century temperature record be used to constrain total feedback?"

Here the surface temperature response contributions due to long term radiative feedbacks, atmosphere-adjusted forcing, and heat storage/transport were determined for a number of AOGCMs. The linear trends of global mean, Arctic (60°N-90°N) mean and tropical (30°S-30°N) mean surface temperature responses of these models were compared with observations over several time periods to investigate why models do or do not reproduce the observed temperature response patterns. The time periods studied were the whole time period available for all models (1900-1999) and the two particularly strong warming periods (1918-1940 and 1965-1999) seen in the observations. Optimal fingerprinting analyses were also performed on the components of surface temperature response to test the model's forcing, feedback and heat storage responses. This work has been published in *Crook and Forster* [2011].

The observation data, model data and analysis methods are described in Section 4.2, the results are presented in Section 4.3 and conclusions are presented in Section 4.4.

4.2 Data and methods

4.2.1 Data

Observations were taken from the HadCRUT3 data set of 20th century surface temperature anomalies. This consists of land and sea surface temperature anomalies from the 1961-1990 mean on a 5° x 5° grid with no infilling of missing data. This

data set has very similar features to other temperature data sets such as the GISS surface temperature analysis [*Hansen et al.*, 2010]. Uncorrected biases in the instrumental record due to differences in the way sea surface temperatures were measured during the Second World War are partly responsible for the observed rapid cooling around 1945 [*Thompson et al*., 2008]. Correcting for this is expected to only affect temperatures between 1940 and 1960 so trends over the whole period, the pre-1940 period and post-1960 period should not be affected.

The HadCRUT3 data were compared with surface temperature anomalies from simulations of the 20th century climate from CMIP3 AOGCMs. Given that previous studies have shown that both natural and anthropogenic forcings are required to reproduce the warming pattern of the 20th century [*Hegerl et al*., 2007; *Stone et al*., 2009; *Min and Hense,* 2006], only those CMIP3 models which have been forced with both anthropogenic and solar and volcanic forcings [see *Forster and Taylor*, 2006, Table 1] were used. However, the aerosol forcing varies across all models as does whether land use changes have been included. The model responses were split into forcing, feedback and heat storage/transport terms as outlined below.

4.2.2 Determining temperature response contributions

The equilibrium partial temperature responses for the non-Planck feedback, the forcing and the heat transport were calculated using equation 2.13 in the zonal mean. This equation and the linear model of feedback (equations 1.2 and 2.5), from which it is derived, have been shown to hold in the zonal mean as well as the global mean, but tend to break down at smaller spatial scales (see Chapter 3) where there is too much noise in the ΔR and ΔT_s terms. Note that in the zonal mean, equation 2.5 calculates a local feedback parameter, not a local contribution to the global mean feedback parameter that is often used in other studies [e.g. *Boer and Yu*, 2003b]. In this study the local feedback parameter is needed to find the local feedback contribution to the local temperature. Effects on local temperature due to distant forcings are seen in the heat transport (ΔR) term.

In order to use equation 2.13 to break down the 20th century surface temperature response into these components, the total feedback, the Planck feedback and the 20th century forcing are required. The total feedback parameter was determined from simulations forced with a 1% annual increase in CO_2 to the point of

doubling (1pctto2x) where the forcing is known reasonably accurately. Equation 2.5 was used in the zonal mean to obtain the total zonal mean feedback parameter by regressing ΔR-F against ΔT_s over the time when the forcing is changing. The regression method allows for latitudinally-dependent rapid atmospheric adjustments to the forcing [*Gregory et al.*, 2004; *Forster and Taylor*, 2006; *Gregory and Webb*, 2008; *Andrews and Forster*, 2008] that are traditionally included in the feedback term. This has been shown to produce a feedback parameter that is much more independent of the forcing mechanism than using the instantaneous or stratosphere-adjusted forcing and is also more time independent (see Section 1.2.1). For these reasons, my assumption that 1pctto2x feedback parameters can be applied to the 20th century is reasonable [see also *Forster and Taylor*, 2006]. Using the regression method means the 20th century forcing term will also include rapid atmospheric adjustments. I chose to use zonal means because smaller spatial scales show more non-linearities but using larger spatial scales would cause problems because of changing spatial coverage in the observations over the 20th century and different forcing patterns in the 20th century compared to 1pctto2x simulations (see Chapter 3). *Myhre et al*. [1998] showed that the forcing due to CO_2 takes the form:

$$F = \alpha \ln \frac{C}{C_0} \qquad 4.1$$

where C is the current concentration and C_0 is the initial concentration of CO_2 and in this study F and α are functions of latitude. A small number of CMIP3 models provide TOA stratosphere-adjusted forcing for 2×CO_2 (NCAR CCSM3.0, GISS ER, MRI CGCM2.3.2a and IPSL CM4). Equation 4.1 with $\frac{C}{C_0} = 2$ was used to determine α for each of these models and the ensemble mean α was used to determine the forcing for the 1pctto2x scenario. The 1pctto2x forcing in year y is given by

$$F_y = y\alpha \ln(1.01) \qquad 4.2$$

The Edwards Slingo radiation code was used to find the Planck feedback parameter using the method described in Section 3.2.1 for a subset of the models (GFDL CM2.1, NCAR CCSM3.0, GISS EH, UKMO HadGEM1 and MIROC3.2 medres – these were simply the first of the models analysed), although in this case the all-sky fluxes were used. Temperature and humidity profiles for the 1pctto2x case were taken as the 30 year mean after the point of doubling of CO_2 (year 70).

Although calculations were performed for all sky conditions, the model's cloud profile was not included as this would be treated differently in each model's own radiation code. The Planck feedback parameter for these models is very similar and, therefore, the exercise was not repeated for the remaining models. For all models the ensemble mean Planck feedback parameter was used in analysis of 20th century simulations.

Equation 2.5 was then used to determine the 20th century zonal mean forcing in each model using the total zonal mean 1pctto2x feedback parameter and the 20th century total temperature response and TOA net downward radiative flux change. Finally the partial temperature response time series was determined using equation 2.13 in the zonal mean. Surface temperature observations have a considerable amount of missing data, especially during the early part of the 20th century. Given that I am comparing modelled 20th century temperature responses with observations, only the locations with valid observations must be included in the determination of zonal means at each point in time. Therefore interpolation and masking was performed on the total temperature response and TOA net downward radiative flux change before taking zonal means. Note that internal variability will form a part of all three components of temperature response. Some of this variability can be eliminated by taking ensemble means of a number of simulations for each model.

4.2.3 Linear trend comparisons

Linear regression was used to obtain trends for the global mean, Arctic (60°N-90°N) mean and tropical (30°S-30°N) mean surface temperature response over the whole time period available for all models (1900-1999) and over the two particularly strong warming periods (1918-1940 and 1965-1999) seen in the observations. Linear trends were used rather than simple differences between two time periods to reduce the effect of strong or weak responses to the volcanic eruptions of 1902, 1963 and 1991. None of the models has more than 5 simulations for the 20th century and so most models do not provide a good sense of the likely spread of possible trends due to internal variability. Therefore, control data from all CMIP3 models were used to assess whether each model has an adequate representation of the observed warming in these regions in each of these time periods within expected internal variability. This assumes that the control data contains an adequate measure of internal

variability. Models generally reproduce the large scale patterns of seasonal surface temperature variation, temperature extremes, and the dominant extratropical patterns of variability such as annular modes and the Pacific Decadal Oscillation but there still remain problems in adequately representing the El Niño Southern Oscillation and the Madden-Julian Oscillation [*Randall et al.*, 2007]. The control data were divided into sections of the same number of years as each of the three time periods and the same missing data mask as for the observations was applied before determining linear trends of each section.

The model mean trend for the period was added to these control trends and it was checked whether the observed trend fell within two standard deviations (2σ) of the mean. The 20th century results were compared with what might be expected based on the transient climate response (TCR) and Arctic amplification of the 1pctto2x simulations. The TCR was taken as the 20 year mean global mean surface temperature response centred on the point of doubling of CO_2, i.e. year 70, [*Cubasch et al.*, 2001] and the Arctic amplification was taken as the Arctic mean minus tropical mean surface temperature response divided by the global mean surface temperature response for the same 20 year mean. This definition of Arctic amplification was used rather than a simple ratio of Arctic warming to global mean warming because some components of the temperature response may warm the Arctic more than the tropics and others may warm the tropics more than the Arctic (see Section 3.2.3). The TCR and Arctic amplification of the 1pctto2x simulations for all CMIP3 models are shown in Table 4.1. From this it is clear that those models that were analysed under 20th century forcing (marked with asterisks) cover the range of TCR and Arctic amplification of all CMIP3 models. One would not expect the Arctic amplification to be the same in 1pctto2x and 20th century simulations because the forcing in the 20th century is less homogeneous, but those models with high Arctic amplification in 1pctto2x would be expected to have high Arctic amplification in 20th century simulations.

Table 4.1: Surface temperature response of CMIP3 models for 1pctto2x simulations. Models with asterisks have 20th century simulations with both anthropogenic and natural forcing and are used in the subsequent analysis. The multi-model ensemble mean with 2 × standard deviation are also given.

Model	**Transient climate response (K)**	**Arctic amplification (dT_{Arctic}-$dT_{tropics}$)/dT_{global}**
IAP FGOALS	1.22	0.99
NCAR PCM1 *	1.27	1.31
GFDL CM2.1 *	1.43	0.86
GFDL CM2.0 *	1.47	1.04
CSIRO Mk3.0	1.48	0.81
CNRM CM3	1.49	0.24
NCAR CCMS3.0 *	1.50	1.51
GISS ER *	1.55	0.75
INMCM3.0	1.55	0.75
GISS EH *	1.58	0.11
CSIRO Mk3.5	1.74	0.58
MRI CGCM2.3.2a *	1.84	0.88
UKMO HadGEM1 *	1.86	1.39
CCCma CGCM3.1	1.88	0.78
MIUB ECHO G *	1.90	1.03
UKMO HadCM3	1.90	0.85
MIROC3.2 medres *	2.01	1.11
IPSL CM4	2.05	0.92
MPI ECHAM5	2.13	0.90
MIROC3.2 hires *	2.64	1.00
Multi-model mean±2σ	1.72 ± 0.34	0.89 ±0.33

4.2.4 Optimal fingerprint analysis

Details of the optimal fingerprinting technique are given in Appendix 1. This is the first study to apply optimal fingerprinting to patterns of temperature response contributions due to forcing and feedbacks rather than temperature responses due to different forcing mechanisms. Given that the climate models include internal variability and there are only a small number of realisations available of each one, total least squares (TLS) optimal regression was used to allow for noise in the model

data (see Appendix 1, equation A.2). Five year means from 1900 to 1999 were used as all the models chosen cover this time period. The model data and HadCRUT3 dataset were converted to anomalies from the 1900-1999 mean. Control data from as many CMIP3 models as possible were used to provide the estimates of internal variability required by the optimal fingerprint analysis code. These provided two independent sets of 42 segments of non-overlapped control data. One set was required for the "pre-whitening" operator, which is used to produce the optimised fingerprints from the temperature anomaly components, and the second set was required for the model consistency checks [*Allen and Tett*, 1999], allowing the analysis to be performed with up to the first 42 eigenvectors of internal variability (truncation of 42). The analysis was performed on the ensemble mean of all the available runs for each model for 30° latitude band means using truncations 2 to 42 and global means using truncations 2 to 19 (note that the global mean data has a vector size of 20 and therefore only 19 eigenvectors are needed). No assumptions were made on the best number of truncations to use, although it is probably best to use more than 4, but results are presented for a range of truncations. The consistency checks can indicate when the number of truncations is unsuitable. It was not possible to detect all three components of temperature response in one regression. Therefore two components were combined at a time and the regression analysis was performed on $dT_{forcing}$ and $dT_{feedback}$+dT_{heat}, $dT_{feedback}$ and $dT_{forcing}$+dT_{heat}, and dT_{heat} and $dT_{forcing}$+$dT_{feedback}$ so that the regression equations become:

$$dT_{obs} = \left(dT_{forcing} - \nu_{forcing}\right)\beta_{forcing} + \left(dT_{feedback} + dT_{heat} - \nu_{remainder}\right)\beta_{remainder} + \nu_0 \qquad 4.3$$

$$dT_{obs} = \left(dT_{feedback} - \nu_{feedback}\right)\beta_{feedback} + \left(dT_{forcing} + dT_{heat} - \nu_{remainder}\right)\beta_{remainder} + \nu_0 \qquad 4.4$$

and

$$dT_{obs} = \left(dT_{heat} - \nu_{heat}\right)\beta_{heat} + \left(dT_{forcing} + dT_{feedback} - \nu_{remainder}\right)\beta_{remainder} + \nu_0 \qquad 4.5$$

The aim in this analysis was to see if it was possible to distinguish between models through their different contributions to temperature response, but the analysis was also performed for the multi-model mean results.

4.3 Results and discussion

4.3.1 Global mean linear trend comparisons

The linear trends in the global mean temperature response of the models over the 20th century are given in Table 4.2. Using 84 sections of 100 years of control data from all CMIP3 models, the observed trend over the whole time period was found to be within the model ensemble mean ±2σ for all models except MIROC3.2 medres, which has too little warming. NCAR CCSM3 has a warming trend on the upper limit and GISS ER has a warming trend on the lower limit.

The global mean trends over the 20th century are not in the same order as for 1pctto2x (see Table 4.2 and Figure 4.1a). For example, one might expect the high climate sensitivity MIROC3.2 medres model to show one of the greatest warming trends over the 20th century but in fact it shows the least, and NCAR CCSM3.0, a model of low to mid climate sensitivity, shows the greatest warming trend. This is due to the fact that these models have not included the same forcings over the 20th century, varying in whether they include ozone, black carbon, organic carbon, mineral dust, sea salt, land use changes and the indirect effects of sulphate aerosols. *Kiehl* [2007] and *Knutti* [2008] pointed out how surprising it is that models with quite different climate sensitivities and projected future warming, agree so well in simulating 20th century temperature response. They found this was partly caused by the different forcing applied in each model. In fact it is possible that the models may have had parameters tuned to match the observed 20th century surface temperature with their included forcings, and if they included extra forcings they may not capture the 20th century response so effectively with that particularly tuning [*Knutti*, 2008].

Table 4.2: Global mean surface temperature response (total and contributions) for 20th century simulations expressed as a linear trend over the whole time period (fraction of total is given in brackets). For each model these are ensemble means of the number of simulations shown in brackets. The multi-model ensemble mean linear trends with 2 × standard deviation and the observed linear trend with its uncertainty from the linear regression are also given.

Model (no. of simulations included in ensemble mean)	**dT (K)**			
	Total	**Forcing**	**Feedback**	**Heat**
NCAR PCM1 (2)	0.59	0.39 (0.66)	0.35 (0.60)	-0.15 (-0.26)
GFDL CM2.1 (3)	0.56	0.33 (0.59)	0.35 (0.57)	-0.09 (-0.17)
GFDL CM2.0 (3)	0.56	0.33 (0.59)	0.35 (0.61)	-0.12 (-0.22)
NCAR CCSM3.0 (5)	0.87	0.51 (0.58)	0.53 (0.61)	-0.17 (-0.20)
GISS ER (5)	0.49	0.19 (0.30)	0.41 (0.85)	-0.12 (-0.25)
GISS EH (5)	0.51	0.28 (0.55)	0.32 (0.62)	-0.08 (-0.16)
MRI CGCM2.3.2a (5)	0.80	0.38 (0.48)	0.54 (0.68)	-0.13 (-0.16)
UKMO HadGEM1 (1)	0.56	0.30 (0.53)	0.36 (0.65)	-0.10 (-0.18)
MIUB ECHO-G (3)	0.61	0.31 (0.51)	0.37 (0.60)	-0.07 (-0.11)
MIROC3.2 medres (3)	0.43	0.28 (0.66)	0.33 (0.76)	-0.18 (-0.43)
MIROC3.2 hires (1)	0.73	0.38 (0.52)	0.56 (0.77)	-0.22 (-0.29)
Multi-model mean±2σ	0.61 ± 0.27	0.34 ± 0.16	0.41 ± 0.19	-0.13 ± 0.09
Observations±2σ	0.67 ± 0.08	-	-	-

In this analysis those models with the least 20th century warming (GISS ER, GISS EH, and MIROC3.2 medres) have the smallest forcing contribution, whereas NCAR CCSM3.0 has the largest warming and largest forcing contribution. Unlike greenhouse gas forcing, aerosol forcing is far more inhomogeneous and is likely to cause different heat storage/transport contributions to the temperature response. MIROC3.2 hires has a stronger than expected forcing contribution compared to its TCR due to its strong heat storage in the 20th century. Not including MIROC3.2 hires, a weak anti-correlation between $dT_{forcing}$ and TCR of -0.30 (Figure 4.1b) was found. *Knutti* [2008] found a similar anti-correlation between global mean forcing and climate sensitivity. The global mean linear trends in temperature response due to the feedback, expressed as a fraction of the total (Table 4.2), are unsurprisingly more in line with the TCR of the model, although the latitudinal pattern of forcing affects

this. The temperature response contributions due to the forcing and due to the feedback have similar standard deviations between models (Table 4.2) showing the importance of both the differences in the forcing and in the climate sensitivity between models. It should be noted that the forcing contribution includes rapid atmospheric adjustments which can be quite different in different models, and the standard deviation between models in their instantaneous forcing (if that were available) would likely be much smaller.

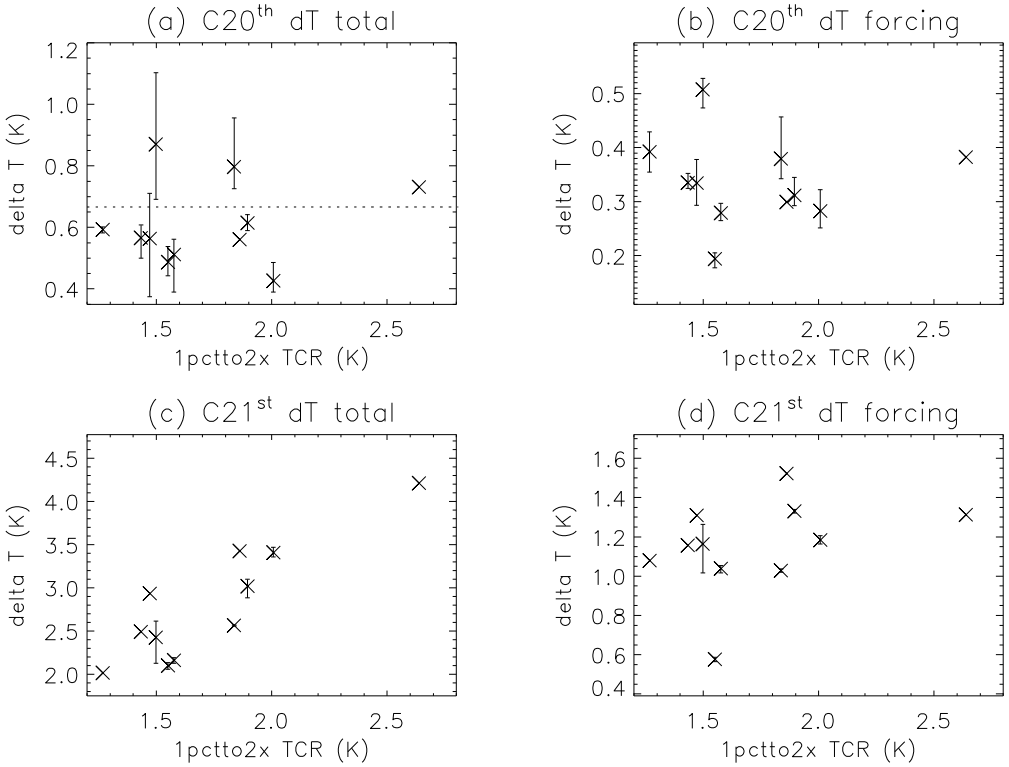

Figure 4.1: Comparison of 20th century and 21st century projected (SRES A1B) global mean warming trends with transient climate response from 1pctto2x experiments – (a) 20th century total global warming trend, (b) 20th century forcing contribution to the global mean warming trend, (c) 21st century total global warming trend, and (d) 21st century forcing contribution to the global mean warming trend. Crosses show the mean trend and vertical error bars show the range of trends of the simulations for each model. The dotted horizontal line shows the 20th century observed global mean warming trend. From Crook and Forster [2011].

Contributions to the temperature response for up to 3 simulations (where available) of each model under the SRES A1B emissions scenario were calculated. In contrast to the 20th century warming, the projected warming for the 21st century is positively correlated with the TCR of the model (Figure 4.1a and c). There are

considerable differences between models in the SRES A1B forcing and there is a weak positive correlation between $dT_{forcing}$ and TCR of 0.36 (Figure 4.1d) that enhances the relationship between temperature response and TCR. The forcing differences were further analysed by examining the linear trends of the shortwave and longwave forcing components (Figure 4.2).

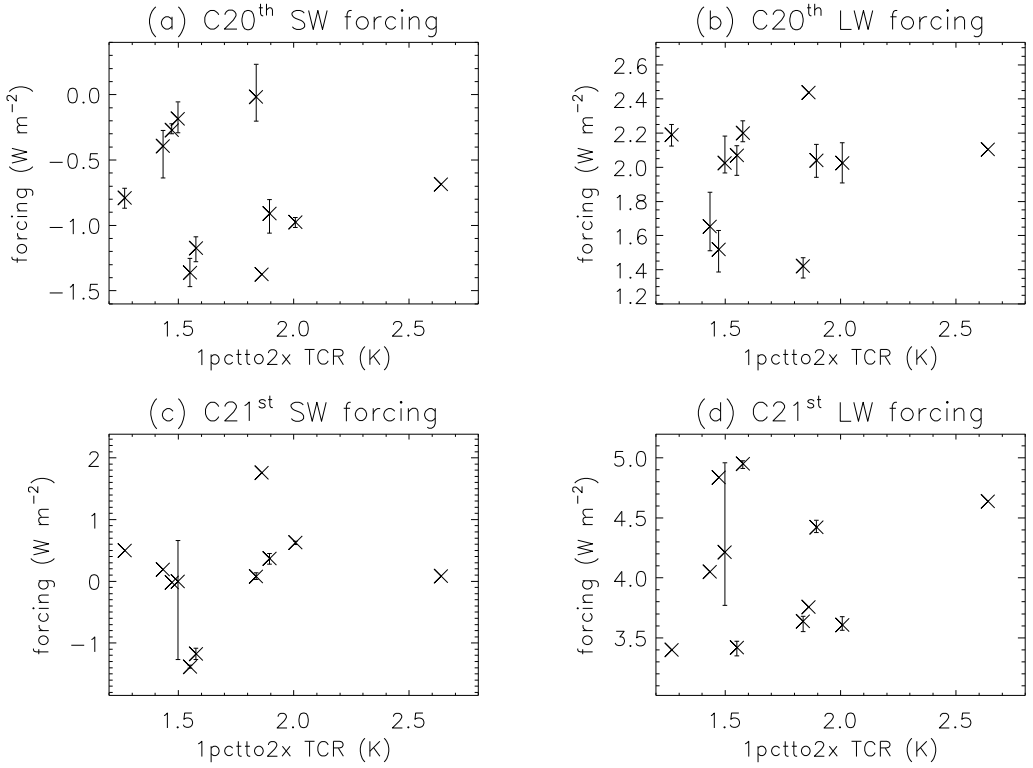

Figure 4.2: Comparison of 20th century and 21st century projected (SRES A1B) global mean forcing component trends with transient climate response from 1pctto2x experiments – (a) 20th century shortwave forcing trend, (b) 20th century longwave forcing trend, (c) 21st century shortwave forcing trend, and (d) 21st century longwave forcing trend. Crosses show the mean trend and vertical error bars show the range of trends of the simulations for each model. From Crook and Forster [2011].

The 20th century shortwave forcing trend is negative in all models, whereas in the 21st century the shortwave forcing trend is positive in some models and negative in others resulting in large differences between models. In the 20th century the shortwave forcing is dominated by volcanic eruptions, although anthropogenic aerosols increase, giving a negative shortwave forcing. However, in the 21st century there are no volcanic eruptions specified and the shortwave forcing should be dominated by decreasing anthropogenic aerosols. The SRES A1B scenario specifies sulphur emissions, but non-sulphate aerosols and whether the indirect effect of

aerosols is included is left to the discretion of the modelling centres. Shortwave forcing is affected by the direct effect of aerosols, but both shortwave and longwave forcings are affected by the rapid tropospheric adjustments (semi-direct effect) to the aerosol forcing and indirect effects to clouds which will be different in each model. The different aerosol forcings cause convergence of modelled temperature response in the 20th century, but divergence in the 21st century.

Attempts to constrain climate sensitivity and future projected warming in multi-model ensembles by weighting models based on their skill in reproducing recent past climate have not been very successful and there is no consensus on how best to obtain model weights [*Weigel et. al.*, 2010]. Climate sensitivity has been constrained using model weighting in perturbed physics parameter ensembles and in energy balance models [*Hegerl et al.*, 2007] to some extent, although the upper limit is still poorly constrained. The climate sensitivity of CMIP3 models typically has a narrower range and lies within these limits. My results show that for CMIP3 models, skill in reproducing 20th century global mean temperature response is unrelated to both TCR and 21st century global mean temperature response because of the differences in aerosol forcing in models. The measure of skill in reproducing 20th century global mean temperature response (and possibly other climate variables) is more a measure of how well the CMIP3 model has been tuned to fit the observations given its included forcing, rather than how well its climate sensitivity matches that of the real world, which helps to explain why constraining climate sensitivity by weighting multi-model ensembles has not been very successful. However, measuring skill in producing the greenhouse gas contribution to the 20th century warming is useful in constraining future warming [*Stott et al.* 2006].

4.3.2 Arctic and tropics trend comparisons

The total response of the models and the contributions in terms of the linear trend in the Arctic and tropics over the whole 20th century are shown in Figure 4.3 and over the two rapid warming periods (1918-1940 and 1965-1999) are shown in Figure 4.4. All three temperature response contributions for both Arctic and tropics vary considerably between models and have the same order of magnitude in their standard deviation (Table 4.3). Relative warming between Arctic and tropics is

highly dependent on the latitudinal distribution of the forcing, which varies between models, and is much less dependent on the Arctic amplification in 1pctto2x.

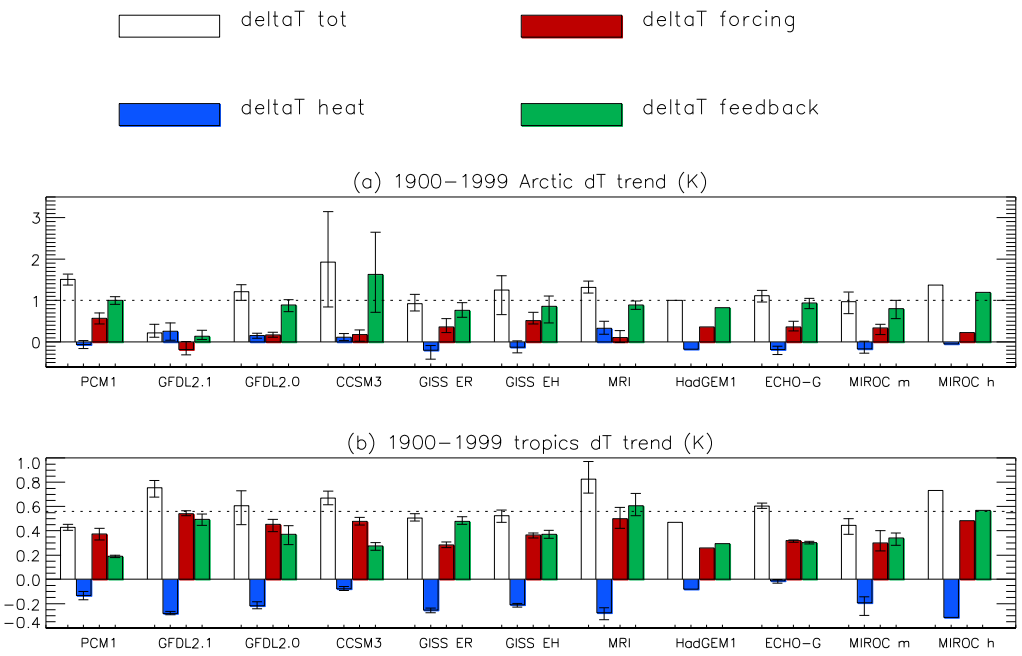

Figure 4.3: Contributions to the modelled temperature response in the Arctic and the tropics over the 1900-1999 period. Vertical error bars show the range of trends from the simulations for each model. The dotted horizontal lines show the observed warming trends for comparison. From Crook and Forster [2011].

Table 4.3: Multi-model ensemble mean (± 2 × standard deviation) surface temperature response (total and contributions) in the Arctic and tropics expressed as a linear trend over the whole 20th century.

dT component	**Arctic (K)**	**Tropics (K)**
dT_{total}	1.16 ± 0.85	0.60 ± 0.27
$dT_{forcing}$	0.27 ± 0.41	0.39 ± 0.20
$dT_{feedback}$	0.90 ± 0.71	0.39 ± 0.26
dT_{heat}	-0.01 ± 0.38	-0.19 ± 0.19

Using 84 sections of 100 years of control data from all CMIP3 models to assess the role of internal variability, the observed 1900-1999 trends in both the Arctic and tropics were found to be within ±2σ for eight of the eleven models.

However, there are three models for which this is not the case and another two models in which the relative warming in the Arctic compared to the tropics is probably unrealistic. I now discuss these five models in detail. Although both NCAR models have plausible 1900-1999 Arctic and tropics trends, the tropical warming for NCAR PCM1 is on the low side and the Arctic warming for NCAR CCSM3.0 is on the high side. There were no simulations that gave a warming less than or equal to the observed trend in the Arctic at the same time as a warming greater than or equal to the observed trend in the tropics, implying that both these models tends to produce too much warming in the Arctic compared to the tropics. For NCAR PCM1 both the forcing and feedback contributions to the temperature response are considerably higher in the Arctic than the tropics leading to this high Arctic amplification. This model also had a high Arctic amplification in 1pctto2x and shows strong Arctic amplification in both early and late warming periods (Figure 4.4). In fact the observed 1965-1999 Arctic trend is outside $\pm 2\sigma$, being considerably lower than the modelled trend. For NCAR CCSM3.0 the high Arctic amplification is due to the high feedback in the Arctic compared to the tropics. This model had the highest Arctic amplification in 1pctto2x. For this model the 1pctto2x feedback parameters were obtained individually for the albedo feedback, shortwave cloud feedback, water vapour plus lapse rate feedback and longwave cloudy sky feedback, and the partial temperature responses due to each of these feedbacks were calculated using the method described in Section 3.2 for both the 1pctto2x run and the 1st run of the 20th century. The percentage contributions to the Arctic amplification from the forcing, heat storage/transport and the individual feedbacks are given in Table 4.4. In both forcing scenarios, the albedo feedback, water vapour plus lapse rate feedback, and longwave cloudy sky feedback provide a similar positive contribution to the Arctic amplification; the shortwave cloud contribution is only weakly negative. I also found a weak negative shortwave cloud contribution for the equivalent slab ocean model forced with $2\times CO_2$, whereas for many other models, there was a strong negative shortwave cloud contribution (see Chapter 3).

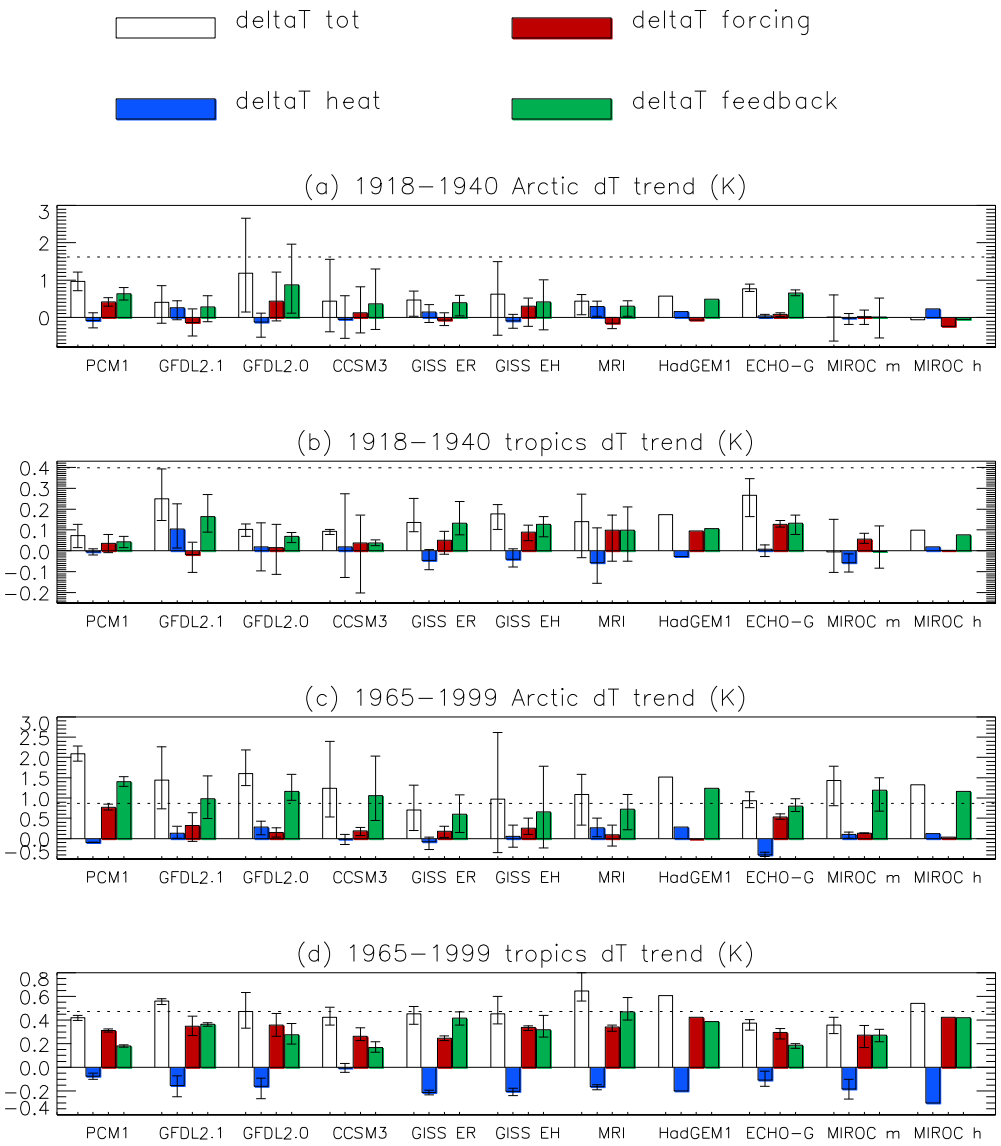

Figure 4.4: Contributions to the modelled temperature response in the Arctic and the tropics during the two warming periods 1918-1940 and 1965-1999. Vertical error bars show the range of trends from the simulations for each model. The dotted horizontal lines show the observed warming trends for comparison.

Table 4.4: Percentage Arctic amplification contributions due to forcing, heat storage/transport, and the different feedbacks for the 1pctto2x and 20th century NCAR CCSM3.0 runs.

Contribution	**1pctto2x**	**20th century run1**
Forcing	-0.23	-0.05
Heat	0.15	-0.05
Surface Albedo	0.38	0.39
Shortwave Cloud	-0.07	-0.07
Water Vapour + Lapse rate	0.43	0.43
Longwave Cloudy Sky	0.34	0.34

The observed 1900-1999 trends in the tropics are outside ±2σ for GFDL CM2.1; the model has too much warming in the tropics. There were no simulations where the warming was greater than or equal to the observed trend in the Arctic at the same time as being less than or equal to the observed trend in the tropics, implying this model produces too little warming in the Arctic compared to the tropics. This model has a strong response to volcanic forcing, particularly to Krakatau in 1983 [*Knutson et al.*, 2006], even without including the aerosol indirect effect. In the tropics, the temperature anomaly recovers only gradually from this cooling effect, with another small cooling presumably due to Santa Maria in 1902, and is still considerably lower than observations in the first decade of the 20th century (Figure 4.5b). This may account for the large 20th century tropical warming trend. In the Arctic, however, although the influence of Krakatau can be seen, the temperature anomaly recovers very rapidly, resulting in an unusually high anomaly at the beginning of the century, and any cooling due to Santa Maria or Katmai (1912) is not enough to bring the anomaly in line with observations at this time (Figure 4.5a). This is the only model which has a negative forcing trend in the Arctic over the whole 20th century. The Arctic forcing contribution shows a gradual decrease from 1920 until the 1970s at which point it shows an increase (Figure 4.5e). *Knutson et al.* [2006] pointed out that this model has particularly large internal variability. Although the rapid warming from the 1890s to 1920 is likely due to recovery from the Krakatau eruption plus internal variability, the subsequent decrease in Arctic forcing until the 1970s is most likely due to negative aerosol forcing outweighing

positive greenhouse gas forcing (note this does not appear to be the case in the tropics).

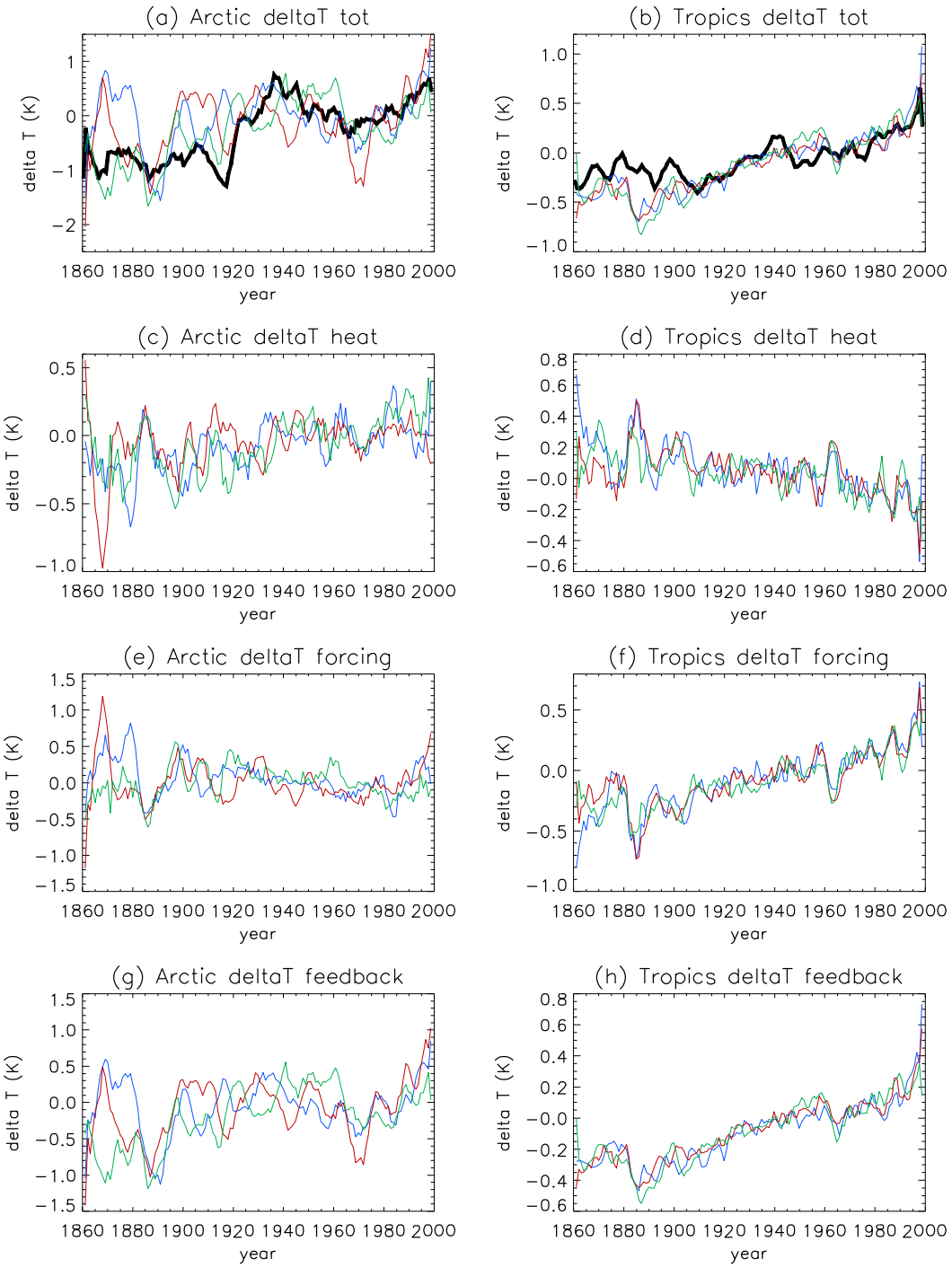

Figure 4.5: Time series of the modelled temperature anomalies and their contributions in the Arctic and the tropics for the GFDL CM2.1 model. The black line is the observed anomaly and the coloured lines are the individual simulations. From Crook and Forster [2011].

The observed 1900-1999 trends in the tropics are outside ±2σ for MRI CGCM2.3.2a; the model has too much warming in the tropics. There were no simulations where the warming was greater than or equal to the observed trend in the Arctic at the same time as being less than or equal to the observed trend in the tropics, implying this model produces too little warming in the Arctic compared to the tropics. The model is cooler in the tropics than observations pre-1910 and then warms quite strongly in the latter part of the 20th century due to strong forcing and feedback contributions. The forcing contribution in the Arctic is very small and warming here is largely caused by heat transport from the tropics.

The observed 1900-1999 trends in the tropics are outside ±2σ for MIROC3.2 hires; the model has too much warming in the tropics. There were no simulations where the warming was greater than or equal to the observed trend in the Arctic at the same time as being less than or equal to the observed trend in the tropics, implying this model produces too little warming in the Arctic compared to the tropics. However, it should be noted that there was only one simulation for this model from which to produce a model mean. The 1918-1940 warming trends in both the Arctic and tropics are too low (Figure 4.4) due to very little forcing; in fact the Arctic cools slightly in the early period. Increasing warming occurs post 1940 in both regions due to strong feedback in the Arctic and strong forcing in the tropics.

4.3.3 Early warming trend comparisons

Figure 4.4 shows that the 1918-1940 warming in both the Arctic and tropics is not well captured by most models. However, the history of warming prior to 1940 followed by cooling, followed by further warming from the 1960s, seen in the observations, and which is much more distinct in the Arctic than the tropics, is found in models to some extent. To ascertain the role of internal variability in the early warming, 366 control sections of 22 years were used with the same missing data mask applied as for the 1918-1940 observations. Probability distribution functions (PDFs) were produced for the Arctic and tropics mean warming trends of all 20th century simulations (Figure 4.6a and b), of all control simulations (Figure 4.6c and d) and of all control simulations plus the multi-model mean warming trend from 20th century simulations (Figure 4.6e and f). This shows that it is exceedingly unlikely that the early warming was due to internal variability alone (both Arctic and tropics

observed trends are outside ±2σ for controls) and that the observed trends are still at the upper end of the 20th century modelled trends which include some forced contribution.

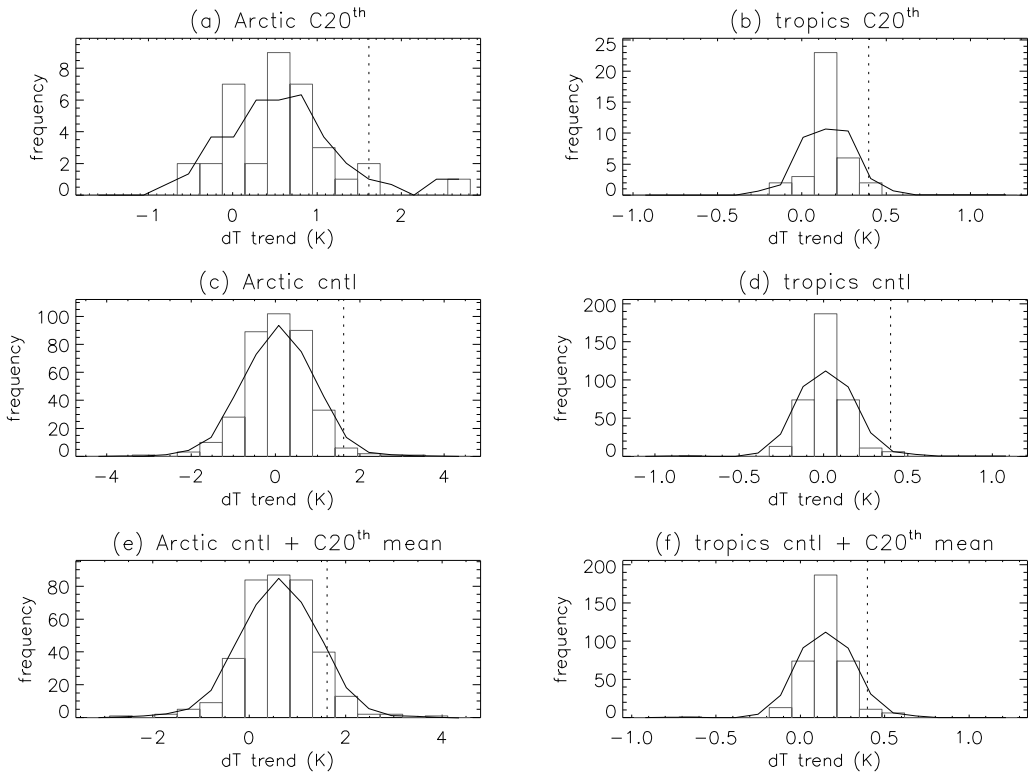

Figure 4.6: PDFs for the Arctic and tropics mean warming trends of (a and b) all 20th century simulations, (c and d) all control simulations, and (e and f) all control simulations plus the 20th century multi-model mean warming trends. The dotted vertical lines show the observed trends. From Crook and Forster [2011].

When comparing the 366 control trends plus the multi-model mean 20th century trend, it is found that the Arctic is just within ±2σ and the tropics is not. Repeating this for each model mean, it is found that only GFDL CM2.1, UKMO HadGEM1 and MIUB ECHO-G have adequate warming in the tropics. Therefore, assuming control runs reproduce multi-decadal internal variability realistically, it is unlikely that internal variability can explain the difference between the multi-model mean 20th century trend and the observed trend in the tropics, and likely that many models are missing some positive forcing or have too much negative forcing here during this time. In the Arctic there is more internal variability than in the tropics and so it cannot be ruled out that internal variability (albeit a large realisation of it) can explain the difference between observations and each model except in the case of

MIROC3.2 medres and MIROC3.2 hires. Certainly in the MIROC3.2 models more positive forcing would be needed to simulate the observed trends.

Wang et al. [2007] suggested Arctic early warming was consistent with internal variability in some but not all CMIP3 models, but they looked at mean anomalies over 1939-1949 rather than looking at trends. They also noted that whereas the observed warming was multi-decadal, the modelled warming was only decadal. Although my results broadly agree with this, I wish to stress that a large warming response due to internal variability is required to match trends in the Arctic. *Delworth and Knutson* [2000] used trends from their older GFDL model and also concluded that only an unusually large realization of internal variability on top of greenhouse gas and sulphate aerosol forcing could have produced the early 20th century warming, although they could not quantify contributions from natural forcing. The more recent study of *Knutson et al*. [2006] on the CMIP3 versions of the GFDL models suggests that the observed early global mean warming can be produced by a combination of anthropogenic forcing and natural forcing, or either anthropogenic forcing or natural forcing only in combination with an unusually strong warming from internal variability, but it should be noted that GFDL CM2.1 was one of only three models with adequate tropical early warming. *Shindell and Faluvegi* [2009] showed that internal variability and a net positive aerosol forcing on top of the greenhouse gas, ozone and natural forcing was required to match 1890-1930 increases in the Arctic minus SH extratropics gradient. They also inferred a net negative aerosol forcing in the tropics over this time.

My results suggest it is likely that many CMIP3 models have too much negative aerosol forcing in the tropics from 1918-1940, and, although eight of the models do include black carbon, it is possible that they do not include enough, or they have too strong an aerosol indirect effect. Another possibility may be that some models do not cool enough in response to the 1883, 1902 and 1912 volcanic eruptions and, therefore, have less to recover from subsequently. Due to lack of observations, the global distribution of aerosol optical depth has to be estimated for these eruptions and this is highly dependent on the circulation patterns at the time of the eruption as well as the amount of SO_2 ejected. Many models use the *Sato et al.* [1993] volcanic dataset where simple assumptions have been made about distributions. The *Ammann et al*. [2003] data set used by the NCAR models attempts

to improve the estimates of aerosol optical depth for the early volcanoes by estimating the spread and decay of the aerosol according to the seasonal stratospheric transport.

Errors in the observed temperature anomalies were not taken into account in my comparisons. Correcting for biases in the instrumental record due to differences in the way sea surface temperatures were measured during the Second World War is expected to only affect temperatures between 1940 and 1960 so our 1918-1940 trends should not be affected. However, to test this, the calculations could be performed just for land grid boxes or with the corrected CRU temperature dataset when it becomes available.

4.3.4 Optimal fingerprint analysis

Detection of components of temperature response proved difficult due to poor signal to noise ratio and degeneracy between components. This was particularly the case for those models with small response to volcanic forcing compared to noise (MRI CGCM2.3.2a, UKMO HadGEM1, MIROC3.2_medres and MIROC3.2 hires) resulting in large uncertainties. Detection was poorer (larger uncertainties) for 30° latitude band means than for global means because the signal to noise is poorer. It was not possible to detect the temperature response due to the feedback ($dT_{feedback}$) and remaining dT ($dT_{forcing}+dT_{heat}$) for any models or the multi-model mean in either global mean or 30° latitude band means as uncertainties were too large. This is not surprising in the global mean as $dT_{feedback}$ is a scaled version of dT_{total} and therefore degenerate with it. In general $dT_{feedback}$ and the remaining dT are also quite similar compared to the noise (particularly in the global mean). Sudden changes in $dT_{forcing}$ from volcanic eruptions are opposed by dT_{heat}, so combining these smoothes the combined response. It was possible to detect $dT_{forcing}$ and the remaining dT ($dT_{feedback}+dT_{heat}$) for many models in both global means and 30° latitude band means (Figure 4.7 shows the global mean results) and to detect dT_{heat} and remaining dT ($dT_{forcing}+dT_{feedback}$) for some models in the global mean (not shown). For these cases most models pass the consistency checks for the majority of truncations, but more confidence should be put in the results of those models which have similar scaling factors across a wide range of truncations. Unfortunately, it was not possible to distinguish scaling factors between models due to large uncertainties. This shows

that it is possible to reproduce the 20th century temperature response pattern in different ways through a balance of forcing and feedback. Nevertheless, these results show that the direct radiative temperature response due to forcings is detectable in the climate record irrespective of the climate feedbacks.

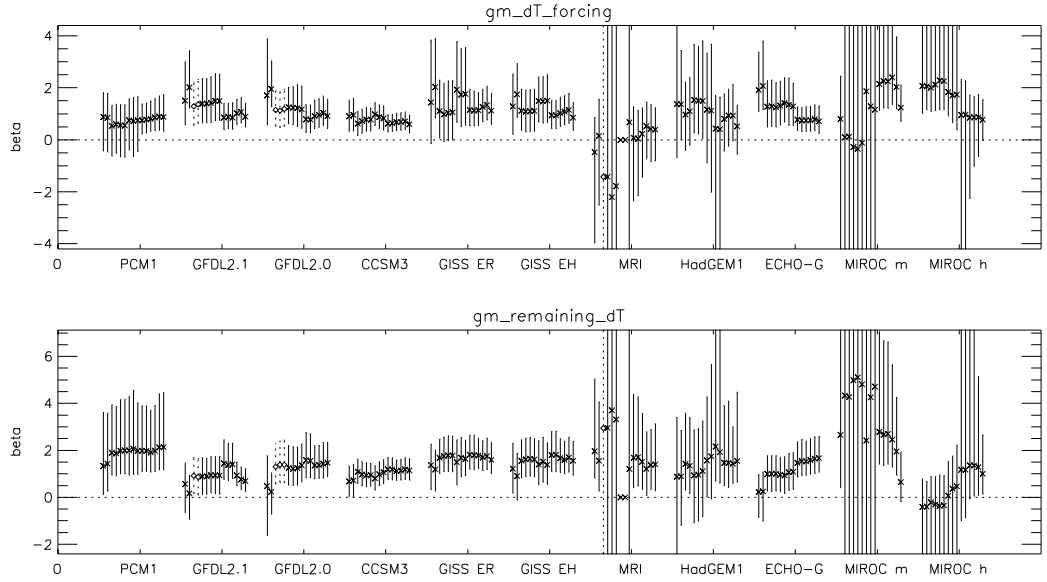

Figure 4.7: Best estimate of scaling factors (× or ◊) and their 5-95% uncertainty estimates (vertical lines) for truncations 5-19 for optimal regression of global mean $dT_{forcing}$ and (dT_{heat} + $dT_{feedback}$). ◊ and dotted vertical lines indicate where the p-value for residual consistency hypothesis testing <0.1 (i.e. where the consistency test fails). From Crook and Forster [2011].

For the multi-model mean the optimal fingerprint analysis was also performed on tropical means and 40°N-60°N means for $dT_{forcing}$ and $dT_{feedback}$+dT_{heat} to see how well different regions performed. I used 40°N-60°N rather than the Arctic because detection was very poor in the Arctic where there is less data and more variability. In both regions and the global mean the scaling factors for the $dT_{forcing}$ contribution were close to one, although in the 40°N-60°N region the uncertainties were larger such that the scaling factors were not inconsistent with zero (the mean scaling factor and their 95% uncertainty ranges over truncations 5-19 for which the consistency test passed were 0.97±0.54 for the global mean, 0.76±0.29 for the tropics and 0.54±2.03 for 40-60°N). An optimal fingerprint analysis of the observed temperature anomaly minus the forcing contribution against the modelled feedback and heat storage/transport contributions was performed by taking away the scaled $dT_{forcing}$

from the observed temperature anomalies. This was the only way to investigate the accuracy of the multi-model mean feedback. The results for these analyses for global means, tropical means and 40°N-60°N means are shown in Figure 4.8. Scaling factors for the dT_{heat} contribution are close to one in all these regions. The feedback contribution tends to be underestimated by the multi-model mean, particularly in the global mean and 40°N-60°N mean where the scaling factor is close to 1.5 suggesting the real world feedback may be greater than the multi-model mean feedback, although the uncertainties are such that the scaling factor is consistent with one.

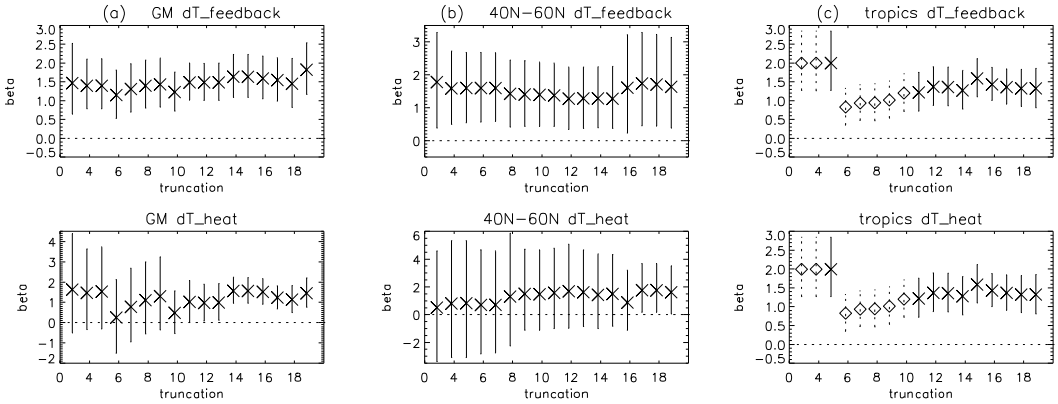

Figure 4.8: Best estimate of scaling factors (× or ◊) and their 5-95% uncertainty estimates (vertical lines) for optimal regression of the multi-model mean $dT_{feedback}$ and dT_{heat} in (a) global mean, (b) 40°N-60°N mean, and (c) tropics mean. ◊ and dotted vertical lines indicate where the p-value for residual consistency hypothesis testing <0.1 (i.e. where the consistency test fails). From Crook and Forster [2011].

4.4 Conclusions

The response of the models over the 20th century in terms of the linear trend in global mean temperature response does not follow the same order as for 1pctto2x due to different 20th century forcing in each model compensating for the climate sensitivity to some extent. Despite being able to detect $dT_{forcing}$ and the remaining dT in most models using optimal fingerprint analysis, it was not possible to distinguish between models due to the large uncertainties in the scaling factors. Both these results highlight the difficulty of constraining climate sensitivity when there is so much uncertainty in 20th century forcing. If 20th century forcing could be better constrained and models run under such a forcing scenario this may lead to a better understanding of which models produce the most accurate response and therefore

could constrain the feedback and hence climate sensitivity. Modelling groups have been adding missing forcings to their models for the CMIP5 experiments, potentially allowing for easier comparison between models. Results from these experiments may shed interesting light on the current understanding of 20th century forcing and feedback.

In contrast to the 20th century, projected global mean warming over the 21st century is much more dependent on the TCR. Whereas differences in aerosol forcing cause convergence of temperature response in the 20th century, differences in the 21st century cause divergence, making it very difficult to constrain climate sensitivity and future predictions of climate change by weighting the CMIP3 models according to their 20th century skill. Better understanding of aerosol forcing is therefore of great importance.

A comparison of modelled and observed warming trends in the Arctic and tropics suggests the tropical warming is too high and Arctic amplification is too low in GFDL CM2.1, MRI CGCM2.3.2a and MIROC3.2 hires due to too little forcing in the Arctic compared to the tropics. The Arctic amplification in NCAR PCM1 and NCAR CCSM3.0 is unrealistically high due to high feedback contributions in the Arctic compared to the tropics in both these models, but also due to a high forcing contribution in NCAR PCM1. It is also evident that few of the models produce the early (1918-1940) warming, particularly in the tropics and that internal variability is unlikely to explain the difference, suggesting many models are missing some positive forcing or have too much negative forcing at this time. Variability is higher in the Arctic and so it is not possible to state the need for more positive forcing here, although a larger positive forcing in the tropics would also cause more warming in the Arctic through increased heat transport from the tropics. The larger positive forcing may be due to more black carbon, a smaller aerosol indirect effect than is currently included in models, or stronger volcanic forcing at the beginning of the 20th century.

Finally, the multi-model mean forcing contribution to the temperature response was quite well detected by optimal fingerprint analysis in global means, 40°N-60°N means and tropical means, but the feedback is lower in these regions than observed temperature anomalies suggest.

5 Comparison of Surface Albedo Feedback in Models and Observations

5.1 Introduction

As described in Chapters 1 and 2, surface albedo feedback has been shown to play an important role in polar amplification, a topic of considerable interest given the rapid decline of Arctic sea ice seen in recent years [*Serreze et al*., 2007]. It has also been suggested that the strength of springtime snow albedo feedback in the USA affects local soil moisture and temperature changes in the summer [*Hall et al*., 2008] and that it will also likely impact summer circulation changes [*Fletcher et al*., 2009]. Although snow and ice albedo feedback have been determined from observations in the NH [*Hall and Qu*, 2006; *Flanner et al*., 2011], there have been no estimates of surface albedo feedback from observations globally, no estimates of zonal patterns of surface albedo feedback from observations, and no estimates of non-cryosphere surface albedo feedback. Although NH snow albedo feedback behaves similarly in the seasonal cycle and under long term climate change in springtime [*Hall and Qu*, 2006], it is unknown whether there is the same potential for estimating long term surface albedo feedback generally using the seasonal cycle. This chapter presents my analysis of surface albedo feedback from satellite observations and models in the seasonal cycle and long term climate change contexts in order to address these shortcomings.

Here estimates of the zonal mean pattern of surface albedo feedback from satellite observation data sets are compared with the zonal mean pattern of surface albedo feedback from a number of AOGCMs for long term climate change as well as from the whole seasonal cycle. *Hall and Qu* [2006] presented the NH extratropical land mean albedo sensitivity to surface temperature for different models and ISCCP observations and show many models have an unrealistic springtime NH snow albedo feedback in the seasonal cycle context (see Sections 2.3.1 and 2.4.2). However, here the actual surface albedo feedback (Y_α) was calculated at all latitudes.

The methods and data used are described in Section 5.2, the results are presented in Section 5.3 and conclusions are presented in Section 5.4.

5.2 Data and methods

Surface albedo feedback was calculated for long term climate change for each season and the annual mean and also from the seasonal cycle by regressing estimates of the change in net downward TOA shortwave flux caused by changes in surface albedo against the coincident change in surface temperature. Monthly surface albedo was calculated from the ratio of upward to downward surface shortwave radiative fluxes for a number of CMIP3 AOGCMs (see Table 5.1).

Observed surface albedo data was taken from three different sources: monthly surface reflectance data from the ISCCP D2 data set, land surface broadband albedo data (MCD43C3) from the MODIS data set, and monthly broadband surface albedo data from the APP-x data set. In the case of the ISCCP data, particularly unusual values were found in 1994 and this year was removed before further processing. In the case of the MODIS data, the 0.05° x 0.05° white-sky albedo was regridded onto a monthly 1° x 1° grid using only data where at least 50% of the grid cell had a quality flag 2 or better as in *Flanner et al*. [2011].

The ISCCP D2 data set covers most of the globe for the period July 1983 to June 2008, the MODIS data set covers much of the land area for the period March 2000 to August 2009, and the APP-x data set covers the polar regions for the period January 1982 to December 2004. For the climate models, data from 1983 to 2009 were taken from the 20c3m and sresa1b experiments of the CMIP3 archive to cover a similar time period to the observations.

In the case of the climate models, the surface temperature data from those climate models were used, whereas for the satellite observations, the surface temperature data from the HadCRUT3 (anomaly time series and absolute climatology) and ERA40/Interim datasets were used. The HadCRUT3 anomaly time series data set consists of land and sea surface temperature anomalies from the 1961-1990 mean on a 5° x 5° grid with no infilling of missing data. It provides temperature anomaly data over the required time period but has much less coverage at high latitudes. The HadCRUT3 absolute data set is an absolute surface temperature climatology based on 1961-1990 with infilling of missing data and is used in the calculation of albedo feedback in the seasonal cycle context where the difference between the temperature in each month is required. The ERA40/Interim

data sets provide a reanalysis product of absolute surface temperature over the required time period giving full spatial coverage on a 2.5° x 2.5° grid. It is preferable to use the HadCRUT3 data rather than the ERA40/Interim reanalysis data in an assessment of observed feedbacks because it is based entirely on observed temperature data and quality controlled for use in climate studies. Unfortunately its data coverage is poor at high latitudes, particularly in the SH, making it difficult to measure surface albedo feedback here. Therefore, observed surface albedo feedback was calculated using both temperature data sets.

Albedo and surface temperature were also taken from the 1pctto2x CMIP3 experiments so that a comparison of surface albedo feedback could be made between the 1983-2009 period and the 70 year period of continuously increasing CO_2 with no aerosol or land use changes. Any drift was removed from the model data using the equivalent control simulation.

To determine surface albedo in the long term climate change context, the Edwards Slingo radiative transfer model (ESRAD) [*Edwards and Slingo*, 1996] was used to estimate net downward TOA shortwave flux, S_α, in each month in each year for the given monthly mean surface albedo time series (from a model or satellite observations). This model uses a 2.5° x 2.5° grid and therefore all albedo and temperature data were interpolated onto this grid before performing feedback calculations. In the case of the 1pctto2x climate model simulations, the decadal means of albedo were used for the first seven decades when the forcing is changing. The radiative transfer model has temperature, cloud and water vapour profiles set to the climatological monthly means based on ISCCP data. Seasonal means and annual means were taken for each year in the time series and a linear regression of zonal mean S_α anomalies against zonal mean surface temperature anomalies was performed to obtain the zonal mean surface albedo feedback pattern for each season and the annual mean.

The seasonal cycle can be used to estimate surface albedo feedback by using S_α and surface temperature anomalies from the annual mean in each month. To determine these S_α anomalies the radiative transfer model was run twice, firstly with climatological means of the surface albedo for each month (seas-cycle) calculated from all the available data (up to 27 years) and secondly using the annual mean surface albedo data in each month (no-seas-cycle). The difference in S_α values

obtained from seas-cycle and no-seas-cycle runs were scaled to remove the effects of different incoming TOA shortwave radiation and atmospheric profile differences between months (i.e. the first two terms of the right hand side of equation 2.10) to give the required S_α anomalies:

$$\Delta S_\alpha^{seas-cycle}(x,m) = \frac{\left[S_\alpha^{seas-cycle}(x,m) - S_\alpha^{no-seas-cycle}(x,m)\right].\overline{S_\alpha^{no-seas-cycle}}(x)}{S_\alpha^{no-seas-cycle}(x,m)} \quad 5.1$$

where x and m refer respectively to space and month dependencies and $\overline{S_\alpha^{no-seas-cycle}}(x)$ is the annual mean of $S_\alpha^{no-seas-cycle}(x,m)$.

A linear regression of zonal mean $\Delta S_\alpha^{seas-cycle}$ values against zonal mean surface temperature climatology anomaly in each month was performed to obtain the zonal mean surface albedo feedback pattern for the seasonal cycle.

In order to compare models and observations the modelled feedbacks were also calculated having applied the same missing data mask to the model albedo as in the observed surface albedo data sets.

For the UKMO HadGEM1 and NCAR CCSM3.0 models, S_α was also calculated using the method of *Winton* [2006b] (see Section 2.2.4) for the 1pctto2x and 1983-2009 experiments so a comparison of the impact on the feedback of different methods as well as different scenarios can be made.

5.3 Results

5.3.1 Impacts of timescales, scenarios and methods on modelled feedback

The feedback patterns for each season and the annual mean are very similar for UKMO HadGEM1 whether the Winton method or ESRAD method is used to obtain S_α and whether the 70 years from the 1pctto2x experiment or the 1983-2009 years of the 20c3m/sresa1b experiments are used (Figure 5.1). However, when only 10 years are used from the 1983-2009 period the feedback patterns are quite different and highly dependent on which 10 year period is chosen, particularly if only land points are used as for MODIS (not shown).

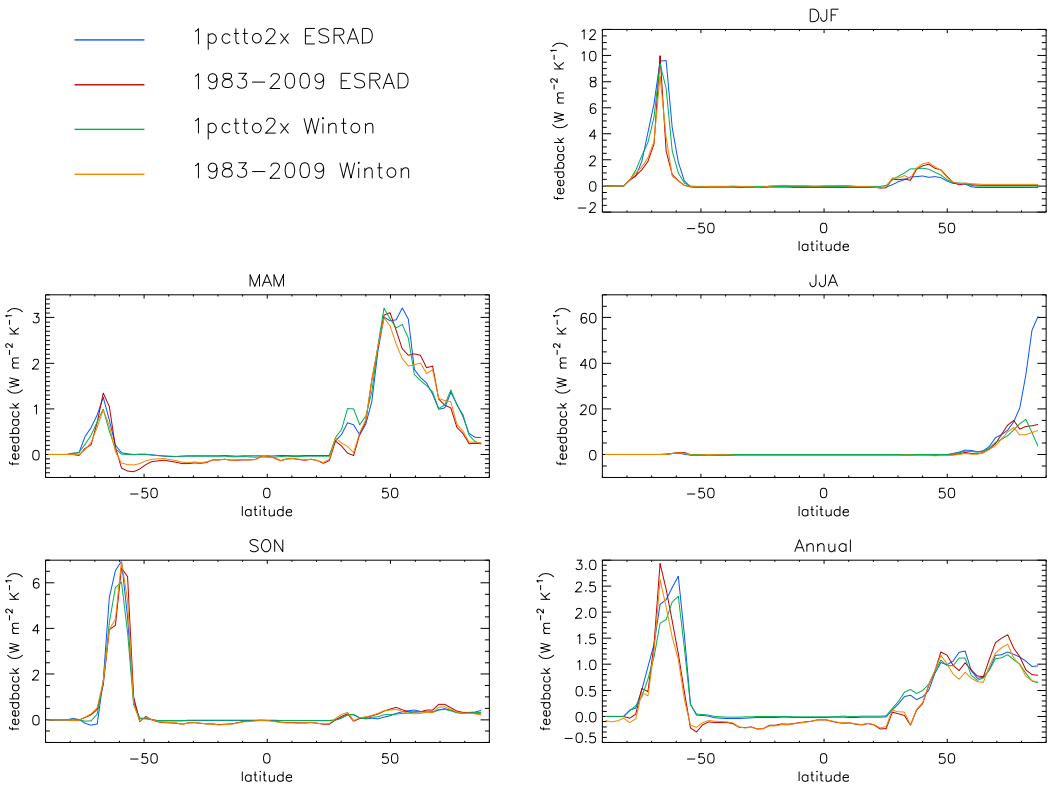

Figure 5.1: Surface albedo feedback patterns in each season and the annual mean for UKMO HadGEM1 using different methods and scenarios.

For NCAR CCSM3.0, the ESRAD method tends to give higher feedback values than the Winton method, presumably because of differences in cloud in ESRAD and NCAR CCSM3.0, but the two different scenarios yield similar feedback patterns (Figure 5.2). For both UKMO HadGEM1 and NCAR CCSM3.0, notable differences occur poleward of 80°N in summer (JJA) for the 1pctto2x experiment using the ESRAD method. This is likely to be caused by cloud amount becoming significantly different from the 20th century cloud amount in the 1pctto2x experiment causing damping of the surface albedo feedback in this region. Using the ESRAD method clouds are fixed at 20th century levels, but using the Winton method an average cloud and water vapour profile over the time period is used.

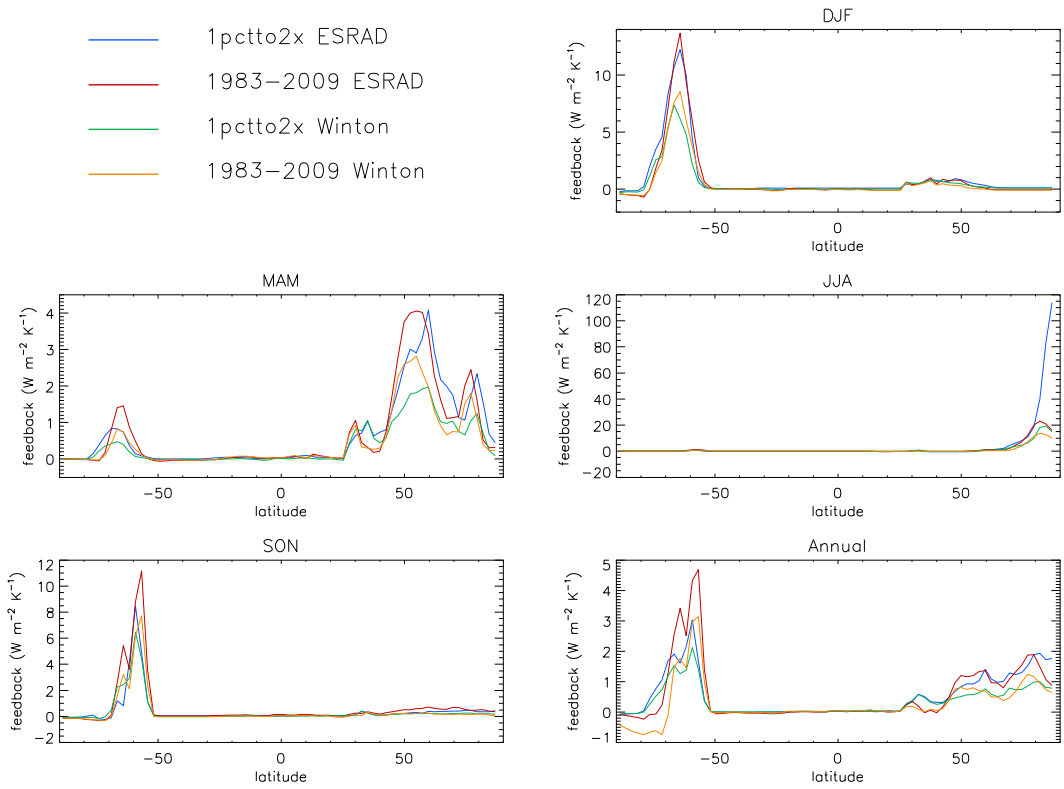

Figure 5.2: Surface albedo feedback patterns in each season and the annual mean for NCAR CCSM3.0 using different methods and scenarios.

All models show similar patterns of annual mean feedback in the 1pctto2x and 1983-2009 experiments using the ESRAD method, with most models showing no feedback between 50°S and 30°N and strong feedback in mid to high latitudes (Figure 5.3) dependent on season. This is despite the fact that seven of the models do include land use changes in their 20c3m experiments which could affect surface albedo, and therefore be seen in the feedback pattern. Note that the GISS ER model does not have data available for the first 70 years of the 1pctto2x experiment so it was not possible to calculate the 1pctto2x surface albedo feedback in this case. The GFDL and MIUB ECHO-G models have higher feedback in the SH sea ice zone in the 1pctto2x case than the 1983-2009 case, whereas for the NCAR models this is the other way round. In the 1983-2009 case the errors from the regression tend to be larger due to a lower signal to noise ratio. *Hall* [2004] found that ice albedo feedback was not the same in the internal variability context as the long term climate change context in a course resolution general circulation model when calculated from 1000 years of control data. This is likely to have an impact on the 1983-2009 feedback

where internal variability plays a larger role, especially in the SH high latitudes where the 1983-2009 temperature trend is small.

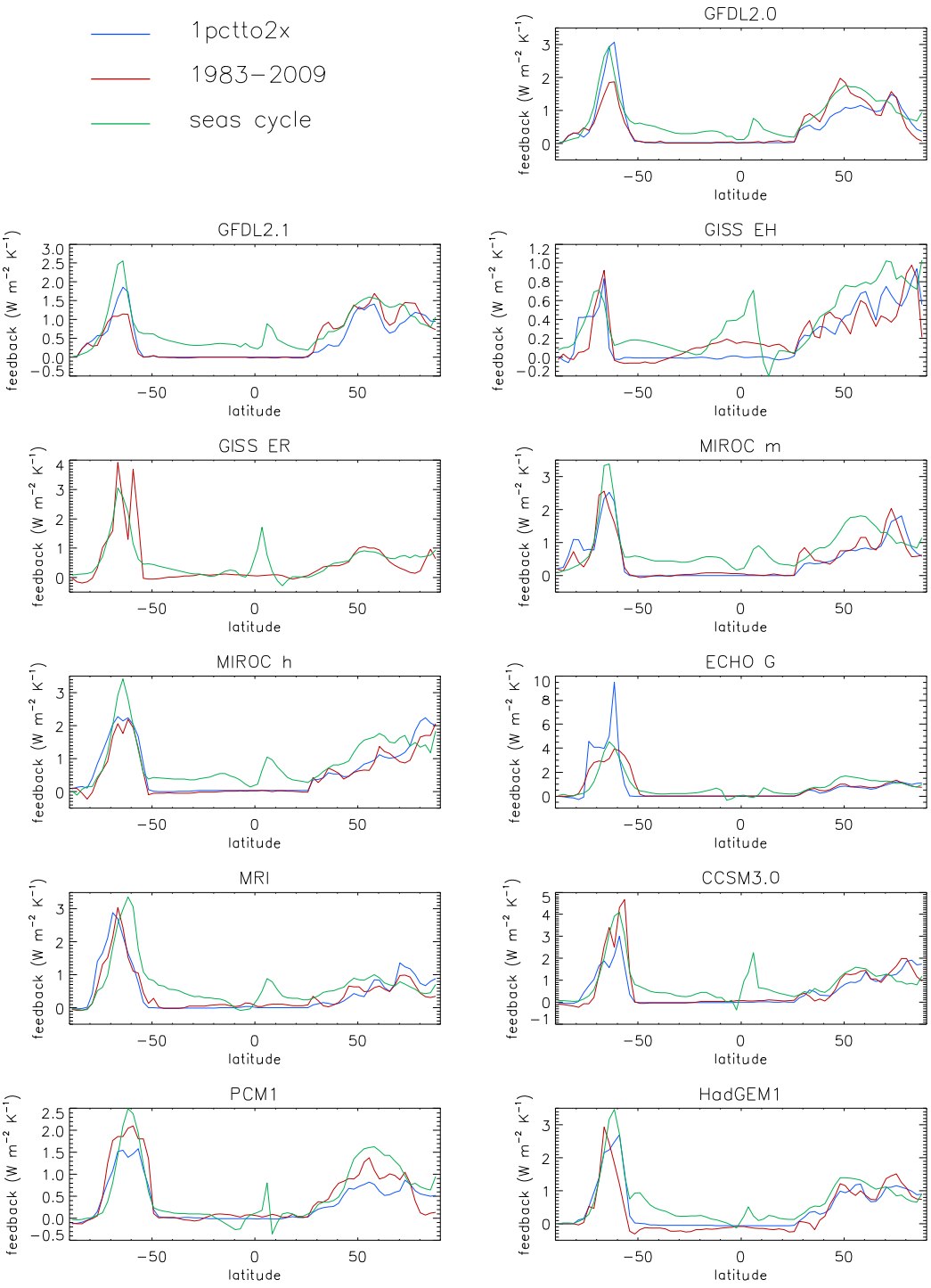

Figure 5.3: Comparison of modelled surface albedo feedback in the long term climate change context for 1pctto2x and 1983-2009 experiments and for the seasonal cycle context.

Despite some deficiencies, these zonal mean results are encouraging, suggesting that it should be possible to obtain a good measure of the long term climate change feedback pattern from 27 years of recent observations. However, if only 10 years of data with the MODIS mask applied are used, the feedback patterns show more variations between latitudes and have larger errors, with large values of feedback in the tropics where zero feedback is seen without the mask applied (not shown). The long term climate change feedback pattern for MODIS albedo data also shows large variations across the tropics (not shown).

The global mean annual mean feedbacks for the 1pctto2x experiment and the 1983-2009 experiment with and without the MODIS mask applied are given in Table 5.1.

Table 5.1: Modelled global mean annual mean surface albedo feedback as determined from 1pctto2x experiment and 1983-2009 data (with and without MODIS mask) using the ESRAD method.

Model	**Global mean annual mean feedback in the long term climate change context (W m^{-2} K^{-1}). The error is quoted as ± 2 standard deviations as determined from the linear regressions.**		
	1pctto2x	**1983-2009**	**1983-2009 MODIS mask**
GFDL CM2.0	0.37±0.08	0.61±0.12	-2.65±6.31
GFDL CM2.1	0.29±0.08	0.35±0.08	-1.51±4.05
GISS EH	0.11±0.06	0.18±0.08	-9.56±13.32
GISS ER	-	0.23±0.10	-8.63±5.34
MIROC3.2 hires	0.47±0.02	0.43±0.08	-1.47±.60
MIROC3.2 medres	0.33±0.04	0.38±0.10	-5.69±3.58
MIUB ECHO G	0.27±0.04	0.68±0.18	-1.92±7.71
MRI CGCM2.3.2a	0.32±0.04	0.18±0.12	2.45±6.27
NCAR CCSM3.0	0.47±0.04	0.59±0.12	-4.44±3.98
NCAR PCM1	0.30±0.04	0.47±0.20	-7.21±4.06
UKMO HadGEM1	0.40±0.02	0.32±0.14	-4.65±3.70

There is a reasonable agreement and correlation between 1pctto2x and 1983-2009 feedbacks, although for some models the difference is quite considerable. Although feedbacks may be acting similarly at the zonal scale, the different zonal patterns of temperature change in these two scenarios can make the global mean feedbacks quite different. The feedback for the 1983-2009 scenario with the MODIS mask applied (actually only using 10 years of data) is quite different with no correlation and has large errors. This result and the equivalent zonal mean result suggest it is not possible to measure the long term climate change feedback using only 10 years of observations, such as is available with MODIS.

5.3.2 Comparison of modelled feedback in the long term climate change and seasonal cycle contexts

The seasonal cycle of surface albedo was found to be very similar for all models regardless of whether the 1pctto2x experiment or 1983-2009 model data was used, or in fact if a 10 year subset of the 1983-2009 model data was used. Therefore, the feedback in the seasonal cycle context was only calculated using the 1983-2009 model data. Figure 5.3 compares the annual mean feedback in the long term climate change context with the feedback in the seasonal cycle context for all the models. Models show good agreement between the pattern of feedback in the long term climate change and seasonal cycle contexts, although the low to mid-latitude feedback tends to be greater than zero in the seasonal cycle context. Whether this higher feedback comes from the land or sea is model dependent, although higher feedback near the equator is usually due to the land (not shown). Changes in primary productivity or soil moisture may affect feedback for land in the seasonal cycle in a different way to the long term climate change context. The dependence of ocean albedo on solar zenith angle may affect feedback for the sea in the seasonal cycle but would not have an effect in the long term climate change context. The regressions for the seasonal cycle tended to show hysteresis in low to mid latitudes, and at 50°N $\Delta S_{\alpha}^{seas-cycle}$ showed non-linearity (a decreasing trend) with temperature for all models. It is likely that in this region the temperature change in the seasonal cycle is so great that snow completely melts in the summer whereas in the annual mean climate change context snow does not completely disappear. These results suggest using the seasonal cycle to measure surface albedo feedback should give a

reasonable measure of the feedback in the long term climate change context, and that 10 years is just enough time to obtain an adequate seasonal cycle of surface albedo.

5.3.3 Comparison of long term climate change surface albedo feedback from observations and models

The long term climate change surface albedo feedback was determined for ISCCP albedo data using the two temperature data sets (Figure 5.4). The feedback patterns are in reasonable agreement apart from at high latitudes, and particularly in the SH, where they can even disagree in sign. This is where the HadCRUT3 data set has particularly poor coverage. Unlike the NH, the 1983-2008 temperature trends in the SH high latitudes are small, meaning that the feedback measured is more dependent on internal variability than forced change and can be influenced strongly by one or two years with extreme values. Although both data sets show a decreasing temperature trend over the time period around 60ºS where the albedo is also decreasing, there is no discernable trend and large interannual variability around 75ºS.

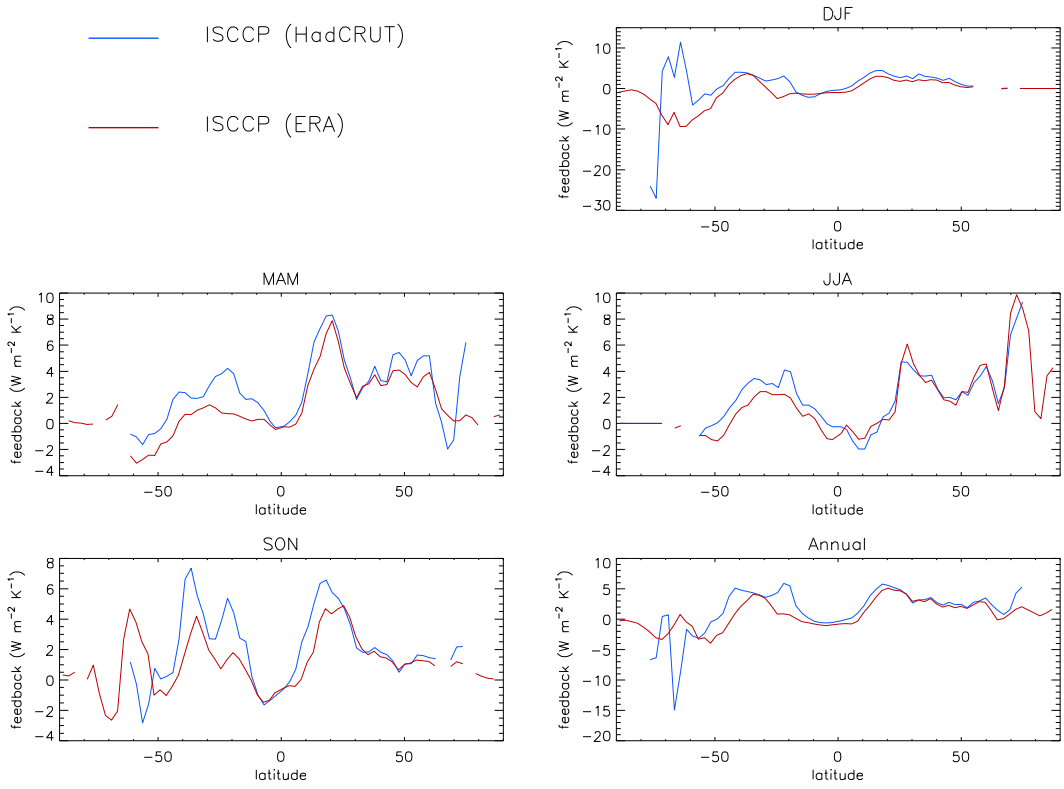

Figure 5.4: Comparison of ISCCP surface albedo feedback in the long term climate change context using HadCRUT3 and ERA40/Interim temperature data.

Both feedback patterns show distinct features of high feedback in mid-latitudes in both hemispheres and generally a negative feedback in the SH high latitudes unlike models (Figure 5.5). A breakdown of the ISCCP surface albedo feedback into contributions from land and sea revealed that the SH mid-latitude peak was due to sea, and the NH mid-latitude peaks and SH high latitude peaks were due to both land and sea with all continents appearing to contribute (not shown).

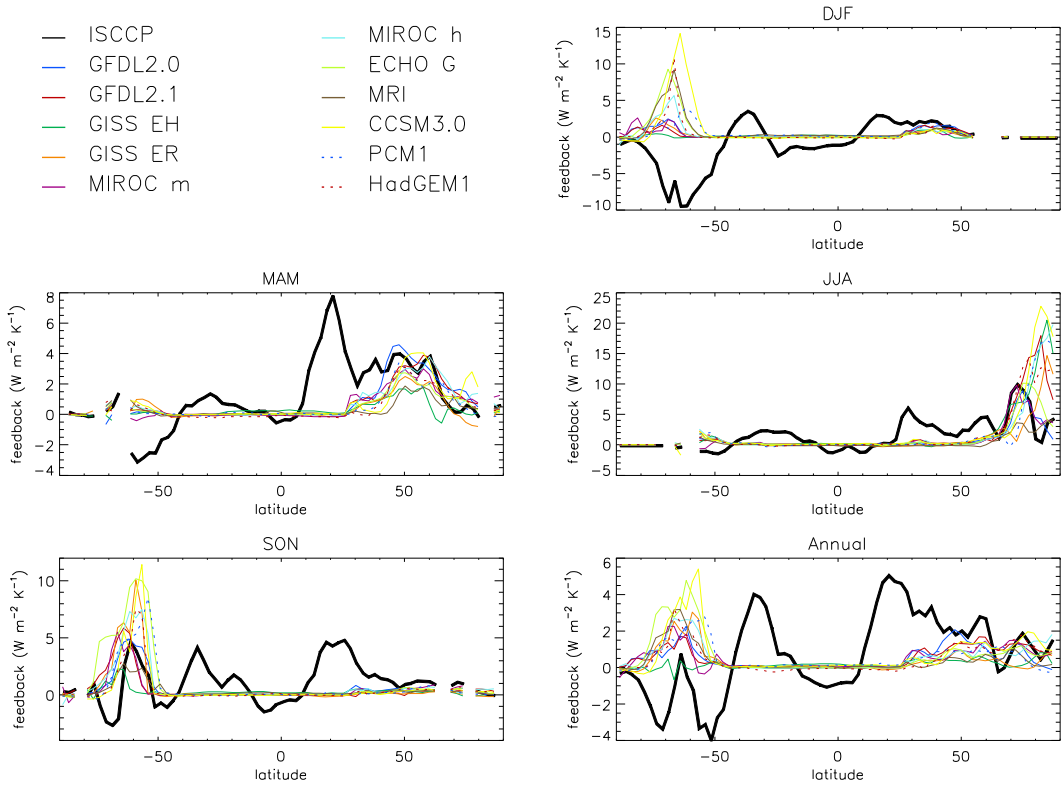

Figure 5.5: Comparison of ISCCP and modelled surface albedo feedback in the long term climate change context. ISCCP feedback is determined using ERA40/Interim temperature. Models have had the ISCCP albedo missing data mask applied before determining the feedback.

It is not clear how much vegetation feedbacks (not represented in the CMIP3 climate models) or land use change (only in seven of the models) have contributed to changes in albedo or whether some of these changes are spurious features of the ISCCP data. However, it is surprising that the sea can have so much influence in regions where there is no sea-ice and this could be a spurious feature of ISCCP data related to cloud cover. Further investigation outside the scope of this thesis would be required to understand the causes of these ISCCP features and whether models are missing important processes. Unfortunately, APP-x albedo only covers high latitudes

so cannot be used to confirm the low to mid-latitude ISCCP feedback, and MODIS albedo does not have a long enough time period to estimate the feedback due to land in the long term climate change context.

The long term climate change surface albedo feedback was determined for APP-x albedo data using only ERA40/Interim data because of the lack of high latitude spatial coverage in HadCRUT3 data. The APP-x feedback is negative in SH high latitudes in DJF, MAM, and in the annual mean (Figure 5.6), like the ISCCP feedback. There is little change in albedo or temperature in this region and feedback can be strongly influenced by one or two extreme values, as for ISCCP. The annual mean NH mid to high latitude feedback is greater than for ISCCP and models. Most models have higher feedback in the Arctic in summer than ISCCP or APP-x feedback. It is possible that this is due to difficulties of measuring surface albedo of sea ice under cloudy conditions, rather than models over predicting the melting of Arctic sea ice.

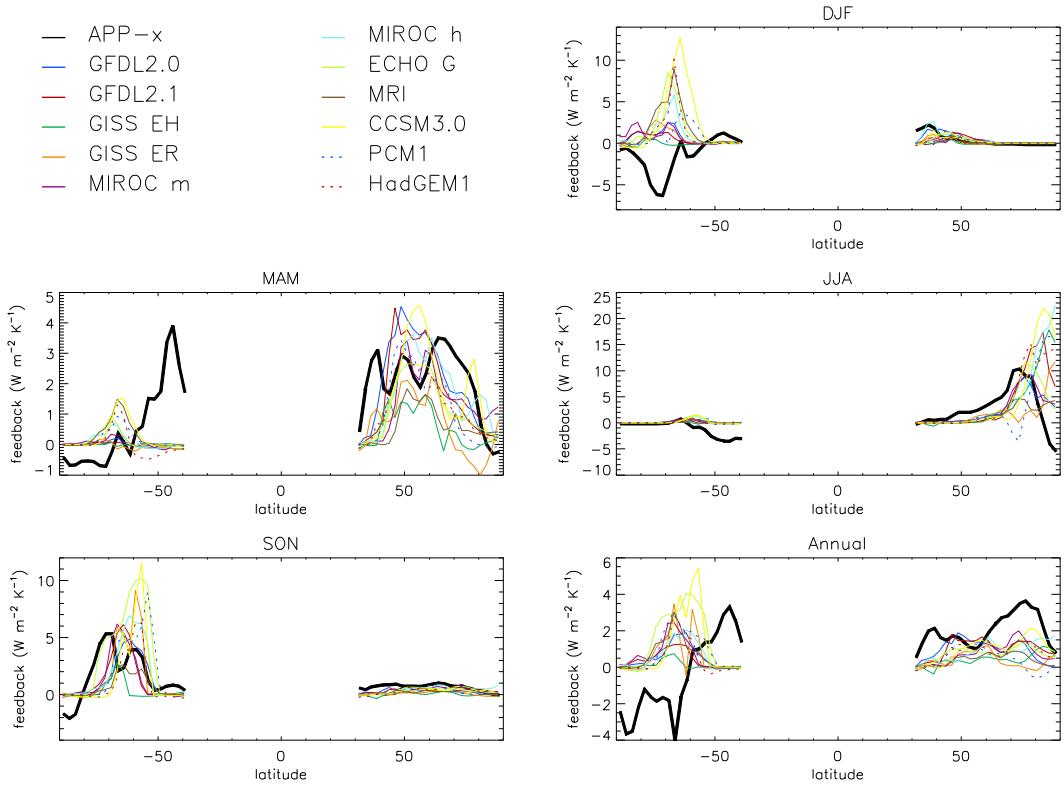

Figure 5.6: Comparison of APP-x and modelled surface albedo feedback in the long term climate change context. Models have had the APP-x albedo missing data mask applied before determining the feedback.

5.3.4 Comparison of seasonal cycle surface albedo feedback between models and observations

The surface albedo feedback in the seasonal cycle context for models and observations are shown in Figure 5.7. Unlike in the long term climate change context, both ISCCP and APP-x show strong positive feedback in the SH sea ice zone in the seasonal cycle context. Compared to the ISCCP feedback, models tend to have lower feedback at high latitudes and do not show the negative peaks in the tropics. A breakdown of the ISCCP feedback into contributions from land and sea revealed that these negative tropical peaks were entirely due to sea and could be spurious features caused by cloud. With the ISCCP contribution from the tropical sea removed, models and ISCCP seasonal cycle feedbacks are quite similar. The APP-x feedback around 60°S is less than that for ISCCP and similar to models apart from GISS EH which has a particularly low feedback here. However, several models have a higher feedback than APP-x in NH high latitudes.

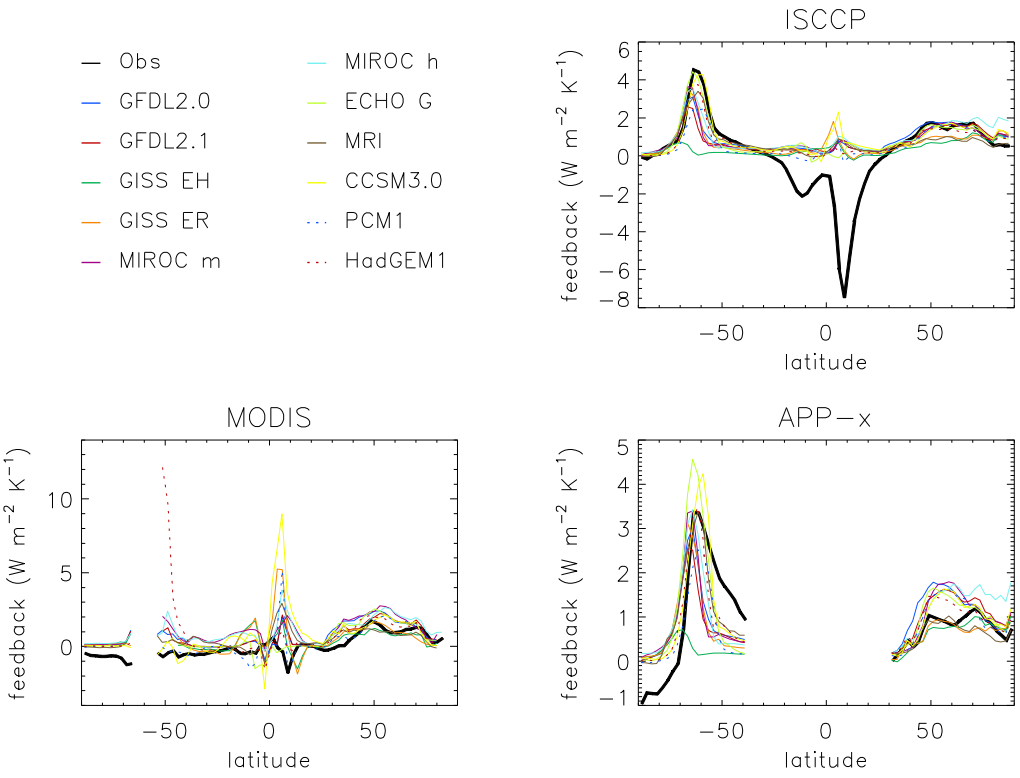

Figure 5.7: Comparison of observed and modelled surface albedo feedback in the seasonal cycle context. Models have had the equivalent observed albedo missing data mask applied before determining the feedback.

When the MODIS mask is applied, the seasonal cycle feedback is large for some models around 50°S. The feedback here is due to snow albedo in Patagonia (this high feedback is not seen when all the sea points around this latitude, which have virtually zero albedo feedback, are also included). Several models have a much greater seasonal cycle in albedo in Patagonia than MODIS and ISCCP data suggest is the case. This may be due to difficulties of representing mountainous regions in models. Although models show little change in albedo in the Antarctic continent in the seasonal cycle, both MODIS and APP-x do have significant change. The global mean surface albedo feedback can be estimated directly in the long term climate change context either by performing the regressions in the global mean or by taking the global mean of the temperature weighted zonal mean feedback pattern. However, in the seasonal cycle, the NH is warm while the SH is cold and vice versa so it makes no sense to use global mean regressions in this case. An estimate of the global mean annual mean long term climate change feedback from the seasonal cycle can be calculated by taking the global mean of the zonal mean seasonal cycle feedback pattern weighted by the zonal mean temperature change pattern of long term climate change:

$$Y_\alpha = \overline{Y_\alpha(x).\frac{\Delta T(x)}{\overline{\Delta T}}} \qquad 5.2$$

where overbar indicates the global mean, *x* indicates the dependency on latitude and $\Delta T(x)$ is the zonal mean temperature change pattern of long term climate change. The temperature change over the 1983-2009 period is quite small so the temperature change over a longer period (1958-2009) from the ERA40/Interim data was used. The results are dependent on the time frame taken but the temperature scaling is applied to both models and observations so a direct comparison can be made. Figure 5.8 shows a scatter plot of the global mean feedback from the long term climate change context against the global mean feedback as estimated from the seasonal cycle for all models with different missing data masks applied to match the observations. The horizontal and vertical bars indicate the ± 2 standard deviation (σ) error determined from the regressions. Although there is some correlation in the global mean feedback between the seasonal cycle and long term climate change contexts, the seasonal cycle has a larger feedback originating from the larger low to mid latitude feedback seen in Figure 5.3. Also shown in Figure 5.8 (as vertical lines

and shading for the ± 2σ confidence limits) are the global mean feedbacks as estimated from the seasonal cycle for each satellite data set. When the spurious tropical sea feedback is removed from the ISCCP data it is clear that models and observations are in good agreement, but for other satellite data sets the agreement is less good, with all models overestimating the feedback. The reasons for these differences have been highlighted in the zonal mean results. As in *Hall and Qu* [2006], the feedback for several models fall outside the observed estimate, but it should be noted that the shading only indicates the error estimate from the regressions and does not include estimates of errors in the measurements themselves.

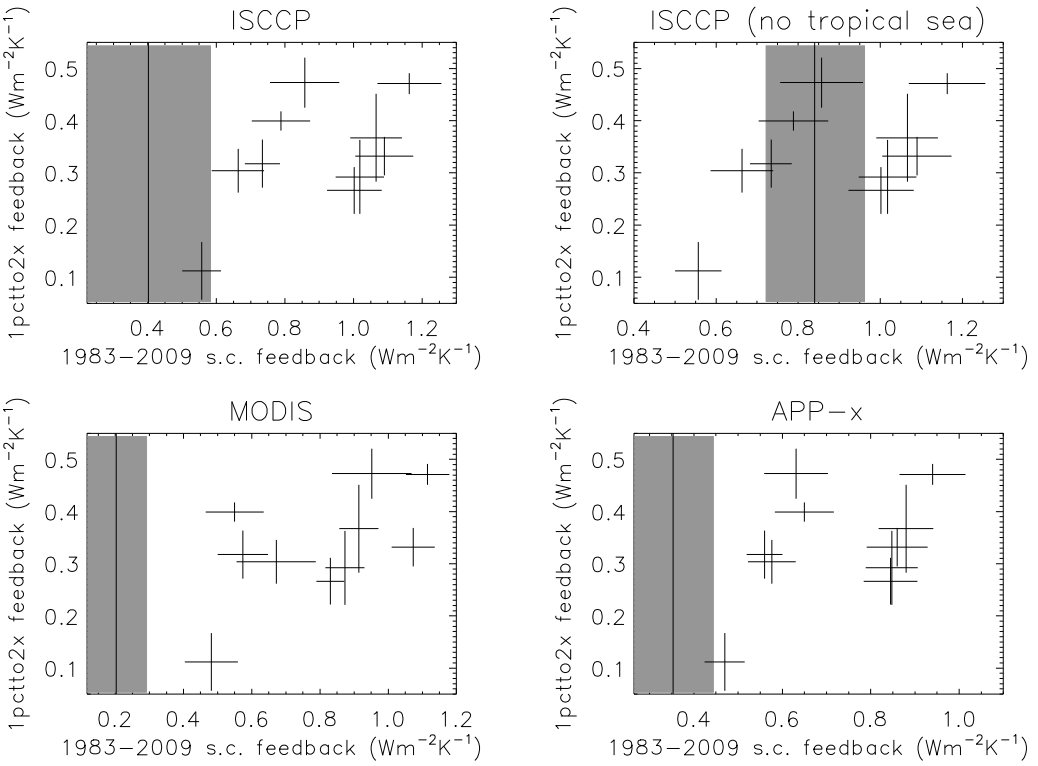

Figure 5.8: Scatter plot of global mean surface albedo feedback from the 1pctto2x long term climate change context vs. the seasonal cycle context for all models. Feedback as estimated from the seasonal cycle context for the indicated satellite data set is shown as a vertical line.

5.4 Conclusions

These results have shown that it should be possible to obtain a good measure of the long term climate change feedback pattern from 27 years of recent

observations, but it is not possible to measure the long term climate change feedback pattern using only 10 years of observations, particularly if data only for land points is used such as is available with MODIS. Using the seasonal cycle to measure surface albedo feedback should give a reasonable measure of the feedback in the long term climate change context. It was found that 10 years is just about enough time to obtain an adequate seasonal cycle of surface albedo, at least from models. Adjustments to the seasonal cycle feedback could be made to bring it more into line with the long term climate change feedback, for example removing the impact of solar zenith angle on sea albedo which affects the feedback in the seasonal cycle context but not in the long term climate change context.

Long term climate change feedback determined from ISCCP data suggests there have been large changes in the albedo of both land and sea in regions outside the cryosphere. Some of these may be due to land use change or vegetation feedbacks but large feedbacks from the sea in these regions are more likely to be due to spurious features related to measuring albedo under different cloud conditions. It is difficult to measure long term climate change feedback from observations in the SH high latitudes because the temperature change has been small in this region resulting in a poor signal to noise ratio. The observed annual mean NH mid to high latitude feedback is likely to be greater than that for models, although this is clearer for APP-x than ISCCP. However, most models have higher feedback in the Arctic in summer. *Stroeve et al.* [2007] suggested climate models underestimate recent Arctic sea ice decline, particularly in September, and *Winton* [2011] showed that several climate models have underestimated recent observed sensitivity of annual mean Arctic sea ice coverage to temperature and this is unlikely to be due to internal variability. *Flanner et al.* [2011] also found the observed annual mean NH snow and sea ice albedo feedback to be considerably higher than models. The use of snow and ice data for which there is a longer record in some regions, may give a more accurate result than surface albedo which can be difficult to estimate from satellite measurements where there is cloud cover.

In the seasonal cycle, models also show some significant differences to observations in certain regions, particularly compared to MODIS in Patagonia and near the equator, although this may be enhanced due to the short time frame over which the seasonal cycle was determined. APP-x and ISCCP also show some

significant disagreements making it difficult to infer conclusions about models under or overestimating surface albedo feedback in the seasonal cycle context compared to observations.

These results highlight the need for accurate measures of surface albedo in order to constrain surface albedo feedback. Where satellite data sets agree, comparisons can be made with models and improvements to models made. For example, a better understanding of the model and observation discrepancies in the seasonal cycle could lead to model improvements. Further investigation is also required to ascertain the accuracy of non-cryosphere surface albedo changes seen in ISCCP.

6 Conclusions and Recommendations for Further Research

6.1 Conclusions

As outlined in Chapter 1 the overall aim of this project is to gain a better understanding of climate feedbacks in terms of their zonal patterns through the use of observations and models. Specific aims were outlined in Section 2.6. My analysis of spatial patterns of local climate feedbacks and equilibrium partial temperature responses from slab ocean GCMs (see Chapter 3) showed that the linear model of feedback works well for zonal means but noise becomes more of an issue at smaller spatial scales. It also showed that, for a climate model forced with absorbing aerosol, allowing rapid atmospheric adjustment to the radiative forcing by using the regression method to obtain climate feedbacks gives a realistic pattern of feedbacks, whereas using the standard definition of radiative forcing gives an unphysical pattern of feedback. These same techniques were applied to my analyses of AOGCMs and 20^{th} century observations discussed in Chapters 4 and 5.

The first aim of the project, to compare zonal mean feedback patterns in different models and for different forcing mechanisms, and to determine how the different feedbacks contribute to polar amplification, is covered in detail in Chapter 3. Spatial patterns of local climate feedback and equilibrium partial temperature responses were determined from eight slab ocean GCMs forced by doubling CO_2. The analysis was extended to other forcing mechanisms with the UK Met Office HadSM3 model. This study showed that, in agreement with previous studies, the greatest inter-model differences are in the tropical cloud feedbacks, although tropical water vapour plus lapse rate feedback and SH sea ice albedo feedback in summer also show considerable inter-model differences. The greatest inter-model spread in the global mean equilibrium temperature response was found to come from the water vapour plus lapse rate feedback, not clouds, disagreeing with a previous study. This was most likely because this study allowed tropospheric adjustment to be included in the forcing rather than the feedback. Although the surface albedo feedback was found to contribute most in the annual mean to polar amplification, its effect is significantly ameliorated by shortwave cloud feedback. In different seasons the

relative importance of the contributions varies considerably, with longwave cloudy sky feedback and horizontal heat transport plus ocean heat release playing a major role during winter and autumn when polar amplification is greatest. The greatest inter-model spread in annual mean polar amplification was found to be caused by variations in horizontal heat transport and shortwave cloud feedback. Spatial patterns of local climate feedback for HadSM3 forced with $2\times CO_2$, +2% solar, low-level scattering aerosol and high-level absorbing aerosol are more similar than those for different models forced with $2\times CO_2$. However, the equilibrium temperature response to high-level absorbing aerosol shows considerably enhanced polar amplification compared to the other forcing mechanisms, largely due to differences in horizontal heat transport and water vapour plus lapse rate feedback, with the forcing itself acting to reduce amplification. Such variations in high latitude response between models and forcing mechanisms make it difficult to infer specific causes of recent Arctic temperature change.

The second aim of the project, to use a break down of the temperature response of 20th century AOGCM simulations into components due to radiative forcing, climate feedback and heat storage/transport to understand how well climate models reproduce the observed 20th century temperature record, is discussed in detail in Chapter 4. Despite large differences between models' feedback strength, they generally reproduce the temperature response well but for different reasons in each model. This study showed that the differences in forcing and heat storage/transport give rise to a considerable part of the inter-model variability in global, Arctic and tropical mean temperature responses over the 20th century. Projected future warming trends are much more dependent on a model's feedback strength, suggesting that constraining future climate change by weighting these models based on their 20th century reproductive skill is not possible. Although it was not possible to constrain the observed global mean climate feedback strength, it was still possible to make suggestions of why some models may not be reproducing Arctic and tropical temperature responses well. The tropical 20th century warming was found to be too large and Arctic amplification unrealistically low in the GFDL CM2.1, MRI CGCM232a and MIROC3.2 hires models due to unrealistic forcing distributions. The Arctic amplification in both NCAR models was found to be unrealistically high due to high feedback contributions in the Arctic compared to the tropics. Few models

reproduce the strong observed warming trend from 1918 to 1940. The simulated trend was found to be too low, particularly in the tropics, even allowing for internal variability, suggesting there is too little positive forcing or too much negative forcing in the models at this time. An optimal fingerprint analysis showed that over the whole of the 20th century, the feedback strength is likely to be underestimated by the multi-model mean.

The third aim of the project, to compare the behaviour of modelled and observed surface albedo feedback in the seasonal cycle and long term climate change contexts is discussed in detail in Chapter 5. Zonal patterns of surface albedo feedback were determined from AOGCMs and observations. This study showed that it should be possible to obtain a good measure of the long term climate change surface albedo feedback pattern from 27 years of recent observations, but using only 10 years of observations is not, particularly if data only for land points are used. ISCCP data shows large changes in the albedo of both land and sea in regions outside the cryosphere, unlike models. Land use change or vegetation feedbacks and difficulties of measuring albedo under different cloud conditions may be to blame. The small observed temperature changes in the SH high latitudes make it difficult to measure long term climate change feedback here. The observed annual mean NH mid to high latitude feedback was found to be greater than that for models in agreement with other studies. Models suggest the surface albedo feedback pattern in the seasonal cycle context is similar to that in the long term climate change context, although positive feedback in low to mid latitudes in the seasonal cycle context makes the global mean seasonal cycle feedback larger than that for long term climate change. Models show some significant differences in the seasonal cycle to observations in Patagonia and near the equator. Different satellite data sets also show some significant disagreements making it difficult to infer conclusions about the ability of models to represent surface albedo feedback.

All three parts of this project have shown benefits of feedback analysis at the zonal mean rather than just the global mean scale, allowing a better understanding of where models may be deficient or disagree significantly, and pointing towards areas for further research.

6.2 Recommendations for further research

Although the first aim of the project has been covered fully, the second and third aims are limited to some extent by lack of good spatial and temporal coverage of observations, and by temperature changes in some regions that have poor forced signal to noise ratios. Continued monitoring of the climate system to produce temporally consistent data sets with good spatial coverage over the next few decades as the climate continues to warm is essential for better comparisons with climate models.

Both the studies in Chapters 3 and 4 highlight the need to better understand 20th century forcing in order to attribute causes to 20th century warming and to measure climate feedback. A similar analysis to that described in Chapter 4 of the CMIP5 model data, where models should contain more similar forcings than they did for CMIP3, will be revealing. Greater understanding of the semi-direct and indirect effects of aerosols is also required. This is currently underway with the Cosmics Leaving Outdoor Droplets (CLOUD) laboratory project which is being used to understand the role of aerosol species and cosmic rays in cloud formation [*Kirkby et al.*, 2011]. Complex aerosol chemistry models can be coupled with climate models to compare modelled and observed region specific aerosol particle size and number concentration to improve understanding of aerosol behaviour. Simplifying this complex aerosol behaviour enough to be included in GCMs and Earth System models run over decades, and the ability to run such models at a higher resolution than has been possible until very recently will then allow improvements to the representation of modelled aerosol and cloud processes in climate change studies [*Carslaw et al*., 2010].

Chapter 5 highlighted the need for accurate measures of surface albedo in order to constrain surface albedo feedback. For the cryosphere regions, the use of snow and ice data, for which there is a longer record in some regions, may give a more accurate result than surface albedo which can be difficult to estimate from satellite measurements where there is cloud cover. Further investigation is also required to ascertain the accuracy of non-cryosphere surface albedo changes seen in ISCCP by comparison with land based measurements where these exist. Where satellite data sets agree, comparisons can be made with models and improvements to models made. For example, a better understanding of the model and observation

discrepancies in the seasonal cycle of surface albedo could lead to model improvements. *Wang et al*. [2006] compared surface albedo from ISCCP with IPCC AR4 models in the North America, Canada and Canadian Arctic region. They found larger interannual variations and a larger decreasing 1984-1999 trend in ISCCP surface albedo than in models suggesting improvements to albedo parameterisations are required in models in this region. Similar studies in other regions and for other feedback variables will aid model improvements to feedback behaviour providing the observed feedback variables are accurate and consistent over time.

References

Allen, M.R., and P.A. Stott (2003), Estimating signal amplitudes in optimal fingerprinting, part I: theory. *Climate Dyn.*, *21*, 477-491.

Allen, M.R., and S.F.B. Tett (1999), Checking for model consistency in optimal fingerprinting, *Climate Dyn.*, *15*, 419-434.

Alexeev, V.A., P.L. Langen, and J.R. Bates (2005), Polar amplification of surface warming on an aquaplanet in "ghost forcing" experiments without sea ice feedbacks, *Climate Dyn.*, *24*, 655-666.

Ammann, C.M., G.A. Meehl, W.M. Washington, and C.S. Zender (2003), A monthly and latitudinally varying volcanic forcing dataset in simulations of 20th century climate, *Geophys. Res. Lett.*, *30* (12), 1657, doi:10.1029/2003GL016875.

Andrews T., and P.M. Forster (2008), CO_2 forcing induces semi-direct effects with consequences for climate feedback interpretations, *Geophys. Res. Lett.*, *35*, L04802.

Arblaster, J.M., and G.A. Meehl (2006), Contributions of external forcings to the Southern Annular Mode trends, *J. Climate*, *19*, 2896-2905.

Barnett, T. P., D. W. Pierce, and R. Schnur (2001), Detection of anthropogenic climate change in the world's oceans, *Science*, *292*, 270–274.

Boé, J., A. Hall, and X. Qu (2009), September sea-ice cover in the Arctic Ocean projected to vanish by 2100, *Nat. Geosci.*, *2*, 341-343, doi: 10.1038/NGEO467.

Boer, G. J., and B. Yu (2003a), Climate sensitivity and climate state, *Climate Dyn.*, *21*, 167-176.

Boer, G. J., and B. Yu (2003b), Climate sensitivity and response, *Climate Dyn.*, *20*, 415-429.

Bony S. and co-authors. (2006), How well do we understand and evaluate climate change feedback processes?, *J. Climate*, *19*, 3445-3482.

Brohan, P., J.J. Kennedy, I. Harris, S.F.B. Tett, and P.D. Jones (2006), Uncertainty estimates in regional and global observed temperature changes: a new dataset from 1850, *J. Geophys. Res.*, *111*, D12106, doi:10.1029/2005JD006548.

Cai, M. (2006), Dynamical greenhouse-plus feedback and polar warming amplification, Part I: A dry radiative-transportive climate model, *Climate Dyn.*, *26*, 661–675.

Cai, W, and T. Cowan (2007), Trends in southern hemisphere circulation in IPCC AR4 models over 1950-99: Ozone depletion versus greenhouse forcing, *J. Climate*, *20*, 681-693.

Cai, M., and J. Lu (2007), Dynamical greenhouse-plus feedback and polar warming amplification, Part II: meridional and vertical asymmetries of the global warming, *Climate Dyn.*, *29*, 375–391.

Carslaw, K.S., O. Boucher, D.V. Spracklen, G.W. Mann, J.G.L. Rae, S. Woodward, and M. Kulmala (2010), A review of natural aerosol interactions and feedbacks within the Earth system, *Atmos. Chem. Phys.*, *10*, 1701–1737

Cess, R.D., and co-authors (1990), Intercomparison and interpretation of climate feedback processes in 19 atmospheric general circulation models, *J. Geophys. Res.*, *95* (D10), 16601–16615.

Cess, R.D, and co-authors (1996), Cloud feedback in atmospheric general circulation models: An update, *J. Geophys. Res*., *101*, 12791–12794.

Chapman, W.L., and J.E Walsh (2007), A synthesis of Antarctic temperatures, *J. Climate*, *20*, 4096-4117.

Clement, A.C., R. Burgman, and J.R. Norris (2009), Observational and model evidence for positive low-level cloud feedback, *Science*, *325*, 460-464.

Colman, R. (2002), Geographical contributions to global climate sensitivity in a general circulation model, *Global Planet. Change*, *32*, 211-243.

Colman, R. (2003), A comparison of climate feedbacks in general circulation models, *Climate Dyn.*, *20*, 865–873.

Comiso, J.C., C.L. Parkinson, R. Gersten, and L. Stock (2008), Accelerated decline in the Arctic sea ice cover, *Geophys. Res. Lett*., *35*, L01703.

Crook, J.A., and P.M. Forster (2011), A balance between radiative forcing and climate feedback in the modeled 20th century temperature response, *J. Geophys. Res.*, *116*, D17108, doi:10.1029/2011JD015924.

Crook, J.A., P.M. Forster, and N.Stuber (2011), Spatial patterns of modeled climate feedback and contributions to temperature response and polar amplification. *J. Climate*, *24* (14), 3575-3592, doi: 10.1175/2011JCLI3863.1.

Cubasch, U., and co-authors (2001), Projections of future climate changes. In: *Climate Change 2001: The Scientific Basis. Contribution of Working Group I to the Third Assessment Report of the Intergovernmental Panel on Climate Change* [Houghton, J.T., *et al*. (Eds.)]. Cambridge University Press, Cambridge, United Kingdom and New York, NY, USA.

Curry, J.A, J.L. Schramm, D.K. Perovich, and J.O. Pinto (2001), Applications of SHEBA/FIRE data to evaluation of snow/ice albedo parameterizations, *J. Geophys. Res*., *106* (D14), 15345-15355.

Dee, D. P., and co-authors (2011), The ERA-Interim reanalysis: configuration and performance of the data assimilation system. *Quart. J. Royal Meteorol. Soc.*, *137*, 553-597.

Delworth, T. L., and T. R. Knutson (2000), Simulation of early 20th century global warming, *Science*, *287*, 2246– 2250.

Dessler, A.E. (2010), A determination of the cloud feedback from climate variations over the past decade, *Science*, *330*, 1523-1527.

Dessler, A.E., and S. Wong (2009), Estimates of the water vapor climate feedback during El Niño –Southern Oscillation, *J. Climate*, *22*, 6404-6412.

Dessler, A.E, Z. Zhang, and P. Yang (2008), Water-vapor climate feedback inferred from climate fluctuations, 2003–2008, *Geophys. Res. Lett*., *35*, L20704, doi:10.1029/2008GL035333.

Dufresne, J-L, and S. Bony (2008), An assessment of the primary sources of spread of global warming estimates from coupled atmosphere–ocean models, *J. Climate, 21*, 5135–5144, doi: 10.1175/2008JCLI2239.1.

Edwards, J. M., and A. Slingo, (1996), Studies with a flexible new radiation code. I: Choosing a configuration for a large-scale model. *Quart. J. Royal Meteorol. Soc., 122*, 689–720.

Flanner, M.G., C.S. Zender, J.T. Randerson, and P.J. Rasch (2007), Present-day climate forcing and response from black carbon in snow, *J. Geophys. Res.*, *112* (D11), D11202.

Flanner, M.G., K.M. Shell, M. Barlage, D.K. Perovic, and M.A Tschudi (2011), Radiative forcing and albedo feedback from the northern hemisphere cryosphere between 1979 and 2008, *Nat. Geosci.*, *4*, 151-155.

Fletcher, C., P. Kushner, A. Hall, and X. Qu (2009), Circulation responses to snow albedo feedback in climate change, *Geophys. Res. Lett.*, *36*, L09702, doi:10.1029/2009GL038011.

Forster, P.M., and M. Collins (2004), Quantifying the water vapour feedback associated with post-Pinatubo global cooling, *Climate Dyn.*, *23*, 207-214.

Forster, P.M., and J. Gregory (2006), The climate sensitivity and its components diagnosed from Earth Radiation Budget data**,** *J. Climate*, *19*, 39-52.

Forster, P.M., and K.E. Taylor (2006), Climate forcings and climate sensitivities diagnosed from coupled climate model integrations, *J. Climate*, *19*, 6181-6194.

Forster, P.M., M. Blackburn, R. Glover, and K.P. Shine (2000), An examination of climate sensitivity for idealised climate change experiments in an intermediate general circulation model, *Climate Dyn.*, *16*, 833-849.

Forster, P., and co-authors (2007), Changes in Atmospheric Constituents and in Radiative Forcing. In: *Climate Change 2007: The Physical Science Basis. Contribution of Working Group I to the Fourth Assessment Report of the Intergovernmental Panel on Climate Change* [Solomon, S. et al. (eds.)]. Cambridge University Press, Cambridge, United Kingdom and New York, NY, USA.

Gillett, N.P., and D.W.J. Thompson (2003), Simulation of recent southern hemisphere climate change. *Science, 302*, 273-275.

Gillett N.P., R.J. Allan, T.J. Ansell (2005), Detection of external influence on sea level pressure with a multimodel ensemble, *Geophys. Res. Lett.*, *32*, L19714.

Graversen, R.G., and M. Wang (2009), Polar amplification in a coupled climate model with locked albedo, *Climate Dyn*., *33* (5), 629-643, doi: 10.1007/s00382-009-0535-6.

Graversen, R.G., T. Mauritsen, M. Tjernström, E. Källen, and G. Svensson (2008), Vertical structure of recent Arctic warming, *Nature, 54*, 53-56.

Gregory, J., and M. Webb (2008), Tropospheric adjustment induces a cloud component in CO_2 forcing, *J. Climate*, *28*, 58-71.

Gregory, J., W. J. Ingram, M. A. Palmer, G. S. Jones, P. A. Stott, R. B. Thorpe, J. A. Lowe, T. C. Johns, and K. D. Williams (2004), A new method for diagnosing radiative forcing and climate sensitivity, *Geophys. Res. Lett.*, *31***,** L03205.

Hall, A. (2004), The role of surface albedo feedback in climate, *J. Climate*, *17*, 1550-1568.

Hall, A., and S. Manabe (1999), The role of water vapor feedback in unperturbed climate variability and global warming, *J. Climate*, *12*, 2327-2346.

Hall, A., and X. Qu (2006), Using the current seasonal cycle to constrain snow albedo feedback in future climate change, *Geophys. Res. Lett*., *30*, L03502.

Hall, A., X. Qu, and J.D. Neelin (2008), Improving predictions of summer climate change in the US, *Geophys. Res. Lett.*, *35*, L01702, doi:10.1029/2007GL032012.

Hallegatte, S, A. Lahellec, and J. Grandpiex (2006), An elicitation of the dynamic nature of water vapor feedback in climate change using a 1D model, *J. Atmos Sci*., *63*, 1878–1894.

Hansen, J., M. Sato, and R. Ruedy (1997), Radiative forcing and climate response, *J. Geophys. Res.*, *102*, 6831-6864.

Hansen, J., and co-authors (2005), Efficacy of climate forcings, *J. Geophys. Res*., *110*, D18104.

Hansen, J., and L. Nazarenko (2004), Soot climate forcing via snow and ice albedos, *PNAS*, *101*, 423-428.

Hansen, J., and co-authors (2007), Dangerous human-made interference with climate: a GISS modelE study, *Atmos. Chem. Phys*., ***7***, 2287-2312.

Hansen, J., R. Ruedy, Mki. Sato, and K. Lo (2010), Global surface temperature change, *Rev. Geophys., 48*, RG4004, doi:10.1029/2010RG000345.

Hasselmann, K. (1979), On the signal-to-noise problem in atmospheric response studies. In Shwan (Ed.) *Meteorology of Tropical Oceans*. Royal Meteorological Society, London, UK, pp 251-259.

Hasselmann, K (1997), On multifingerprint detection and attribution of time dependent climate change. *Climate Dyn., 13*, 601-611.

Hegerl, G. C., T. J. Crowley, S. K. Baum, K.-Y. Kim, and W. T. Hyde (2003), Detection of volcanic, solar and greenhouse gas signals in paleoreconstructions of northern hemispheric temperature, *Geophys. Res. Lett*., *30* (5), 1242, doi:10.1029/2002GL016635.

Hegerl, G.C., and co-authors (2007), Understanding and attributing climate change. In: *Climate Change 2007: The Physical Science Basis. Contribution of Working Group I to the Fourth Assessment Report of the Intergovernmental Panel on Climate Change* [Solomon, S., et al. (eds.)]. Cambridge University Press, Cambridge, United Kingdom and New York, NY, USA.

Holland, M.M., and C.M. Bitz (2003), Polar amplification of climate change in coupled models, *Climate Dyn., 21*, 221-232.

Jansen, E., and co-authors (2007), Palaeoclimate. In: *Climate Change 2007: The Physical Science Basis. Contribution of Working Group I to the Fourth Assessment Report of the Intergovernmental Panel on Climate Change* [Solomon, S., et al. (eds.)]. Cambridge University Press, Cambridge, United Kingdom and New York, NY, USA.

Jones, P.D., M. New, D.E. Parker, S. Martin, and I.G. Rigor (1999), Surface air temperature and its variations over the last 150 years, *Rev. Geophys., 37,* 173-199.

Jones G.S., S.F.B. Tett, P.A. Stott (2003), Causes of atmospheric temperature change 1960-2000: A combined attribution analysis, *Geophys. Res. Lett., 30,* (5), 1228, doi:10.1029/2002GL016377.

Joshi, M., K. Shine, M. Ponater, N. Stuber, R. Sausen, and L. Li (2003), A comparison of climate response to different radiative forcings in three general circulation models: Towards an improved metric of climate change, *Climate Dyn., 20*, 843– 854.

Kiehl, J.T. (2007), Twentieth century climate model response and climate sensitivity, *Geophys. Res. Lett., 34*, L22710, doi:10.1029/2007GL031383.

Kirkby, J., and co-authors (2011), Role of sulphuric acid, ammonia and galactic cosmic rays in atmospheric aerosol nucleation, *Nature, 476*, 429-433. doi:10.1038/nature10343.

Knutson, T.R., and co-authors (2006), Assessment of twentieth-century regional surface temperature trends using the GFDL CM2 coupled models, *J. Climate, 19,* 1624-1650.

Knutti, R. (2008), Why are climate models reproducing the observed global surface warming so well?, *Geophys. Res. Lett., 35*, L18704, doi:10.1029/2008GL034932.

Le Treut, H., R. Somerville, U. Cubasch, Y. Ding, C. Mauritzen, A. Mokssit, T. Peterson, and M. Prather (2007), Historical overview of climate change. In: *Climate Change 2007: The Physical Science Basis. Contribution of Working Group I to the*

Fourth Assessment Report of the Intergovernmental Panel on Climate Change [Solomon, S.,et al., (eds.)]. Cambridge University Press, Cambridge, United Kingdom and New York, NY, USA.

Lindzen, R. S., M.-D. Chou, and A. Y. Hou (2001), Does the Earth have an adaptive infrared iris?, *Bull. Amer. Meteorol. Soc*., *82*, 417– 432.

Lohmann, U., and co-authors (2010), Total aerosol effect: Radiative forcing or radiative flux perturbation? *Atmos. Chem. Phys*., *10*, 3235–3246.

Lu, J., and M. Cai (2009a), Seasonality of polar surface warming amplification in climate simulations, *Geophys. Res. Lett.*, *36*, L16704, doi:10.1029/2009GL040133.

Lu, J., and M. Cai (2009b), A new framework for isolating individual feedback processes in coupled general circulation climate models. Part I: formulation, *Climate Dyn*., *32*, 873-885.

Mann, M.E. (2009), Defining dangerous anthropogenic interference, *PNAS*, *106*, 4065-4066.

Meehl, G.A. W.M. Washington, C.M. Ammann, J.M. Arblaster, T.M.L. Wigley, and C. Tebaldi (2004), Combinations of natural and anthropogenic forcings in twentieth-century climate, *J. Climate*, *17*, 3721-3727.

Meehl, G.A. and co-authors (2007a), Global climate projections. In: *Climate Change 2007: The Physical Science Basis. Contribution of Working Group I to the Fourth Assessment Report of the Intergovernmental Panel on Climate Change* [Solomon, S., et al. (eds.)]. Cambridge University Press, Cambridge, United Kingdom and New York, NY, USA.

Meehl, G. A., C. Covey, T. Delworth, M. Latif, B. McAvaney, J. F. B. Mitchell, R. J. Stouffer, and K. E. Taylor (2007b), The WCRP CMIP3 multi-model dataset: A new era in climate change research, *Bull. Amer. Meteorol. Soc*., *88*, 1383-1394.

Min, S.-K., and A. Hense (2006), A Bayesian assessment of climate change using multimodel ensembles. Part I: Global mean surface temperature. *J. Climate, 19***,** 3237–3256.

Murphy, D.M., S. Solomon, R.W. Portmann, K.H. Rosenlof, P.M. Forster, and T. Wong (2009), An observationally based energy balance for the Earth since 1950, *J. Geophys. Res*., *114*, D17107, doi:10.1029/2009JD012105.

Myhre, G., E. J. Highwood, K. P. Shine, and F. Stordal (1998), New estimates of radiative forcing due to well mixed greenhouse gases, *Geophys. Res. Lett.*, *25***,** 2715–2718.

Nakicenovic, N. and R. Swart (2000), IPCC Special Report on Emissions Scenarios, Cambridge University Press, UK.

National Snow and Ice Data Centre (2011), http://nsidc.org/arcticseaicenews/, August 2011.

Nozawa, T., T. Nagashima, H. Shiogama, and S. A. Crooks (2005), Detecting natural influence on surface air temperature change in the early twentieth century, *Geophys. Res. Lett*., *32*, L20719, doi:10.1029/2005GL023540.

Qu, X., and A. Hall (2006), Assessing snow albedo feedback in simulated climate change, *J. Climate, 19*, 2617–2630.

Qu, X., and A. Hall (2007), What controls the strength of snow albedo feedback?, *J. Climate*, *20*, 3971-3981.

Ramaswamy, V., and co-authors (2001), Radiative forcing of climate change. In: *Climate Change 2001: The Scientific Basis. Contribution of Working Group I to the Third Assessment Report of the Intergovernmental Panel on Climate Change* [Houghton, J.T., et al. (eds.)]. Cambridge University Press, Cambridge, United Kingdom and New York, NY, USA, pp.349–416.

Randall, D.A., and co-authors (2007), Climate models and their evaluation. In: *Climate Change 2007: The Physical Science Basis. Contribution of Working Group I to the Fourth Assessment Report of the Intergovernmental Panel on Climate Change* S. Solomon *et al*. (Eds.), Cambridge University Press, Cambridge, United Kingdom and New York, NY, USA.

Rap, A., P. M. Forster, A. Jones, O. Boucher, J. M. Haywood, and R. R. De Leon (2010), Parameterisation of contrails in the UK Met Office climate model, *J. Geophys. Res*., *115*, D10205, doi:10.1029/2009JD012443.

Ridley, J., J.M. Gregory, P. Haybrechts, and J. Lowe (2010), Thresholds for irreversible decline of the Greenland ice sheet, *Climate Dyn*., *35*, 1065-1073.

Sato, M., J.E. Hansen, M.P. McCormick, and J.B. Pollack (1993), Stratospheric aerosol optical depths, 1850-1990, *J. Geophys. Res*., *98* (D12), 22987-22994.

Screen J.A., and I. Simmonds (2010), The central role of diminishing sea ice in recent Arctic temperature amplification, *Nature*, *464*, 1334-1337.

Schiffer, R.A., and W.B. Rossow (1983), The International Satellite Cloud Climatology Project (ISCCP) The First Project of the World Climate Research Program, *Bull. Amer. Meteorol. Soc.*, *64*, 779-784.

Senior, C. A., and J. Mitchell (2000), The time-dependence of climate sensitivity, *Geophys. Res. Lett*., *27*, 2685-2689.

Serreze M.C., M.M. Holland, and J. Stroeve (2007), Perspectives on the Arctic's shrinking sea-ice, *Science, 315* (5818), 1533–1536.

Shindell, D.T. and G.A. Schmidt (2004), Southern hemisphere climate response to ozone changes and greenhouse gas increases, *Geophys. Res. Lett., 31*, L18209.

Shindell, D., and G. Faluvegi (2009), Climate response to regional radiative forcing during the twentieth century, *Nat. Geosci.*, *2*, 294-300.

Shine, K.P., J. Cook, E.J. Highwood and M.M. Joshi (2003), An alternative to radiative forcing for estimating the relative importance of climate change mechanisms, *Geophys. Res. Lett*., *30* (20), 2047.

Soden B.J. and I.M. Held (2006), An assessment of climate feedbacks in coupled ocean-atmosphere models, *J. Climate*, *19*, 3354-3360.

Soden, B.J., R.T. Wetherald, G.L. Stenchikov and A. Robock (2002), Global cooling after the eruption of Mount Pinatubo: A test of climate feedback by water vapour, *Science, 296*, 727-730.

Soden, B.J, A. J. Broccoli, and R.S. Hemler (2004), On the use of cloud forcing to estimate cloud feedback, *J. Climate*, *17*, 3661-3665.

Soden, B.J., I.M. Held, R. Colman, K.M. Shell, J.T. Kiehl, and C.A. Shields (2008), Quantifying climate feedbacks using radiative kernels, *J. Clim*ate, *21*, 3504–3520.

Spencer, R.W., W.D. Braswell, J.R. Christy, and H. Hnilo (2007), Cloud and radiation budget changes associated with tropical intraseasonal oscillations, *Geophys. Res. Lett*., *34*, L15707, doi:10.1029/2007GL029698.

Stone, D.A., M. R. Allen, P. A. Stott, P. Pall, S-K. Min, T. Nozawa, and S. Yukimoto (2009), The Detection and attribution of human influence on climate, *Annu. Rev. Environ. Resour*., *34*, 1–16.

Stott, P. A., and G. S. Jones (2009), Variability of high latitude amplification of anthropogenic warming, *Geophys. Res. Lett*., *36*, L10701, doi:10.1029/2009GL037698.

Stott P.A., S.F.B. Tett, G.S. Jones, M.R. Allen, J.F.B. Mitchell, and G.J. Jenkins (2000), External control of 20th century temperature by natural and anthropogenic forcings, *Science*, *290*, 2133–37.

Stott, P.A., M.R. Allen, and G.S Jones (2003), Estimating signal amplitudes in optimal fingerprinting. Part II: application to general circulation models, *Climate Dyn*., *21*, 493-500.

Stott, P.A., J.F.B. Mitchell, M.R. Allen, T.L. Delworth, J.M. Gregory, G.A. Meehl, and B.D. Santer (2006), Observational Constraints on Past Attributable Warming and Predictions of Future Global Warming, *J. Climate*, *19*, 3055-3069.

Stephens, G.L. (2005), Cloud feedbacks in the climate system: A critical review, *J. Climate*., *18*, 237– 273.

Stroeve, J., M. M. Holland, W. Meier, T. Scambos, and M Serreze (2007), Arctic sea ice decline: Faster than forecast, *Geophys. Res. Lett.*, *34*, L09501.

Thompson, D.W.J., and J.M. Wallace (1998), The Arctic Oscillation signature in the wintertime geopotential height and temperature fields, *Geophys. Res. Lett.*, *9*, 1297-1300.

Thompson, D.W.J. and Solomon, S. (2002), Interpretation of recent southern hemisphere climate, *Science, 296*, 895-899.

Thompson, D.W.J, J.J. Kennedy, J.M. Wallace, and P.D. Jones (2008), A large discontinuity in the mid-twentieth century in observed global-mean surface temperature, *Nature*, *453*, 646-649, doi:10.1038/nature06982.

Trenberth, K.E., and co-authors (2007), Observations: Surface and atmospheric climate change. In: *Climate Change 2007: The Physical Science Basis*. Contribution of Working Group I to the Fourth Assessment Report of the Intergovernmental Panel on Climate Change [Solomon, S. et al. (eds.)]. Cambridge University Press, Cambridge, United Kingdom and New York, NY, USA.

Uppala, S., and co-authors (2005), The ERA-40 re-analysis. *Quart. J. Royal Meteorol. Soc.*, *131*, 2961-3012.

Vavrus, S. (2004), The impact of cloud feedback on Arctic climate under greenhouse forcing, *J. Climate*, *17*, 603-615.

Wang, X. and J. Key (2005a), Arctic surface, cloud, and radiation properties based on the AVHRR Polar Pathfinder data set. Part I: Spatial and temporal characteristics, *J. Climate*, *18* (14), 2558-2574.

Wang, X. and J. Key (2005b), Arctic surface, cloud, and radiation properties based on the AVHRR Polar Pathfinder data set. Part II: Recent trends, *J. Climate*, *18*(14), 2575-2593.

Wang, S., A.P. Trischenko, K.V. Khlopenkov, and A. Davidson (2006), Comparison of International Panel on Climate Change Fourth Assessment Report climate model simulations of surface albedo with satellite products over northern latitudes, *J. Geophys. Res*., *111*, D21108.

Wang, M., J.E. Overland, V. Kattsov, J.E. Walsh, X. Zhang, and T. Pavlova (2007), Intrinsic versus forced variation in coupled climate model simulations over the Arctic during the twentieth century, *J. Climate*, *20*, 1093-1107, doi:10.1175/JCLI4043.1.

Weigel, A.P., R. Knutti, M.A. Liniger, and C. Appenzeller (2010), Risks of Model Weighting in Multimodel Climate Projections, *J. Climate*, *23*, 4175-4191, doi: 10.1175/2010JCLI3594.1.

Wetherald R.T. and S. Manabe (1988), Cloud feedback processes in a general circulation model, *J. Atmos. Sci*., *45*, 1397–1415.

Williams, K. D., C. A. Senior, and J. F. B. Mitchell (2001), Transient climate change in the Hadley Centre models: The role of physical processes, *J. Climate*, *14*, 2659–2674.

Williams K.D., W.J. Ingram, and J.M. Gregory (2008), Time variation of effective climate sensitivity in GCMs, *J. Climate*., *21*, 5076-5090.

Winton, M. (2005), Simple optical models for diagnosing surface-atmosphere shortwave interaction, *J. Climate*, *18*, 3796-3805.

Winton, M. (2006a), Amplified Arctic climate change: What does surface albedo feedback have to do with it?, *Geophys Res Lett*., *33*, L03701, doi:10.1029/2005GL025244.

Winton, M. (2006b), Surface albedo feedback estimates for the AR4 climate models, *J. Climate*., *19*, 359-365.

Winton, M. (2011), Do climate models underestimate the sensitivity of northern hemisphere sea ice cover?, *J. Climate*, *24* (15), 3924-3934.

Yang, F., A. Kumar, W. Wang, H. Juang, and M. Kanamitsu (2001), Snow-albedo feedback and seasonal climate variability over North America. *J. Climate, 14***,** 4245–4248.

Zhang, M. H., J. J. Hack, J. T. Kiehland, and R. D. Cess (1994), Diagnostic study of climate feedback processes in atmospheric general circulation models. *J. Geophys. Res., 99***,** 5525–5537.

Zhang X.B., F.W. Zwiers, G.C. Hegerl, F.H. Lambert, N.P. Gillett, S. Soloman, P.A. Stott, and T. Nozawa (2007), Detection of human influence on twentieth-century precipitation trends, *Nature*, *448*, 461–66.

Appendix 1 – Optimal Fingerprinting

Optimal fingerprinting is generalised multivariate regression adapted to the detection of climate change [*Hasselmann*, 1979, 1997; *Allen and Tett*, 1999; *Allen and Stott*, 2003] and has been used in the attribution of change to externally forced climate change signals. The ordinary least squares (OLS) regression model has the matrix form:

$$y = \mathbf{X}\beta + \nu \qquad \text{A.1}$$

where vector y is a filtered version of the observed record, matrix **X** contains the estimated response patterns (signals) that are under investigation, β is a vector of scaling factors that adjusts the amplitudes of those patterns and ν represents internal climate variability. If the scaling factor for a specific forcing mechanism is found to be significantly greater than zero, then a detectable influence due to that forcing mechanism has been found.

Vector ν is usually assumed to be a Gaussian random vector but the noise in the raw climate data is generally far from white, so a "pre-whitening" operator (determined from the covariance matrix of an estimate of ν) is applied to transform **X** and y before the regression algorithm is applied. This rotates **X** and y perpendicular to the noise, improving the signal-to-noise ratio, and allows a better unbiased estimation of the scaling factors [*Allen and Stott*, 2003]. An estimate of ν is usually obtained from long unforced control AOGCM simulations because the instrumental record is too short to provide a reliable estimate and may be affected by external forcing. The estimated residuals, ν, can be checked for consistency (i.e. that they are within the expected range of internal variability) by hypothesis testing with estimates of internal variability that are independent of those estimates used to produce the "pre-whitening" operator [*Allen and Tett*, 1999]. This provides confirmation of the validity of the regression model.

The OLS form of the linear regression equation assumes no noise in **X**. However, in practice general circulation models, which include internal variability, are often used and the number of such model simulations used to form an ensemble mean of **X** is often quite small, meaning there will be sampling uncertainty. In this

case it is better to use a total least squares (TLS) form of the regression equation which allows for noise in both the modelled and observed signals [*Stott et al.*, 2003]:

$$y = \sum_i (x_i - \nu_i)\beta_i + \nu_0 \qquad \text{A.2}$$

The y and **X** may be a simple time series or may also include spatial patterns. Attribution has been performed on a variety of climate variables such as surface and free tropopause temperatures [*Stott et al.*, 2000; *Jones et al.*, 2003], sea level pressure [*Gillett et al.*, 2005], latitudinal patterns of large-scale precipitation change [*Zhang et al.*, 2007], and ocean heat content patterns [*Barnett et al.*, 2001].